Master's thesis

NTNU
Norwegian University of Science and Technology
Faculty of Engineering
Department of Civil and Environmental Engineering

Sebastian Kaasa
Ludvig Grytbakk Tronsaune

Bottom-Fixed Steel Jacket Substructures for the IEA-15-MW 240 Reference Wind Turbine in the Southern North Sea II

Master's thesis in Civil and Environmental Engineering
Supervisor: Arild Holm Clausen
Co-supervisor: Håkon S. Andersen (Dr.techn. Olav Olsen AS)
June 2022

NTNU
Norwegian University of
Science and Technology

Sebastian Kaasa
Ludvig Grytbakk Tronsaune

Bottom-Fixed Steel Jacket Substructures for the IEA-15-MW 240 Reference Wind Turbine in the Southern North Sea II

Master's thesis in Civil and Environmental Engineering
Supervisor: Arild Holm Clausen
Co-supervisor: Håkon S. Andersen (Dr.techn. Olav Olsen AS)
June 2022

Norwegian University of Science and Technology
Faculty of Engineering
Department of Civil and Environmental Engineering

NTNU

Kunnskap for en bedre verden

Department of Structural Engineering
Faculty of Engineering
NTNU – Norwegian University of Science and Technology

ACCESSIBILITY
Open

MASTER THESIS 2022

SUBJECT AREA: Structural Engineering	DATE: 11.06.2022	NO. OF PAGES: 94 + 36

TITLE:
Bottom-Fixed Steel Jacket Substructures for the IEA-15-MW-240 Reference Wind Turbine in the Southern North Sea II

Bunnfaste Ståljacket Understell for IEA-15-MW-240 Referanse Vindturbinen i Sørlige Nordsjø II

BY:

Ludvig Grytbakk Tronsaune

Sebastian Kaasa

SUMMARY:
Offshore wind energy is a quickly emerging market in the renewable energy sector. In 2020, the Norwegian oil- and energy department opened for concession applications for the instalment of 3000 MW of wind energy in the offshore wind field Southern North Sea II, located 140 km off the coast of Norway. With depths of 53-72 m, both bottom-fixed and floating substructures are viable options.

This thesis is a study on two different bottom-fixed jacket concepts: a straight-legged jacket and a skew-legged jacket. The jackets were designed for the new 15-MW Reference Wind Turbine proposed by NREL and based on water depths of 60 m. The study includes a quasi-static ultimate limit state (ULS) analysis, a natural frequency analysis, and a time-domain fatigue limit state (FLS) analysis. Various modules in the DNV software package Sesam, such as GeniE, Wajac, Framework, and Sesam Wind Manager, were used in the design. In addition, another DNV software named Bladed was used along with a concept model of the 15-MW turbine to assess realistic turbine loads and to provide a time series simulation of the turbine-jacket system. This time series was used in the FLS analysis.

With the benefit of being a better option for standardization, the performance of the straight-legged jacket was compared to a skew-legged counterpart. The two jackets were designed with comparability and standardization in mind. Through the study, it was shown that the skew-legged jacket performed better on almost all counts. However, many simplifications had to be made, and more detailed analyses must be performed to assess the true potential of the jacket substructures for the 15-MW RWT. The report, therefore, finishes off with suggestions for further work.

The assignment was proposed by Dr. Techn. Olav Olsen AS, who also provided valuable assistance throughout the study.

RESPONSIBLE TEACHER: Professor Arild Holm Clausen

SUPERVISOR(S): Håkon S. Andersen (Dr. Techn. Olav Olsen AS)

CARRIED OUT AT: Norwegian University of Science and Technology

Institutt for konstruksjonsteknikk
Fakultet for ingeniørvitenskap
NTNU – Norges teknisk-naturvitenskapelige universitet

TILGJENGELIGHET
Åpen

MASTEROPPGAVE 2022

FAGOMRÅDE: Konstruksjonsteknikk	DATO: 11.06.2022	ANTALL SIDER: 94 + 36

TITTEL:

Bunnfaste Ståljacket Understell for IEA-15-MW-240 Referanse Vindturbinen i Sørlige Nordsjø II

Bottom-Fixed Steel Jacket Substructures for the IEA-15-MW-240 Reference Wind Turbine in the Southern North Sea II

UTFØRT AV:

Ludvig Grytbakk Tronsaune

Sebastian Kaasa

SAMMENDRAG:
Offshore vindenergi er et raskt voksende marked innenfor den fornybare energisektoren. I 2020 vedtok Norges olje- og energidepartement at det skulle bli åpnet for konsesjonssøknader til installasjon av 3000 MW havvind i området Sørlige Nordsjø II, som ligger 140 km utenfor Norges kyst. Med vanndybder på 53-72 m er både bunnfaste og flytende turbiner aktuelle løsninger.

I denne avhandlingen har det blitt gjennomført en studie på to ulike konsepter for bunnfaste ståljackets: en skråbeint og en rettbeint. Jacketene ble designet for den nye 15-MW referanseturbinen som er utgitt av NREL og det har blitt gått ut ifra en vanndybde på 60 m. Studiet inneholder en kvasi-statisk analyse i bruddgrensetilstand (ULS), en egenfrekvensanalyse, og en tidsserieanalyse i utmattingsrensetilstand (FLS) av de to jacketene. Ulike moduler i DNV sin programvarepakke Sesam har blitt brukt til design og utforming. Noen eksempler er GeniE, Wajac, Framework og Sesam Wind Manager. I tillegg har programmet Bladed, også laget av DNV, blitt brukt sammen med en konseptmodell av 15-MW turbinen for å fastsette realistiske turbinlaster, og for å fremskaffe en responstidsserie av turbin-jacket systemet som kunne brukes i en FLS analyse.

En rettbeint jacket vil være fordelaktig med tanke på standardisering, noe som kan bli et viktig tiltak når nye store vindparker skal etableres. I denne studien har dermed ytelsen og virkemåten til en rettbeint konseptjacket blitt sammenlignet med en tilsvarende skråbeint jacket. Begge jacketene ble utformet med standardisering og sammenlignbarhet som grunnlag. Det ble vist at den skråbeinte jacketen presterer bedre på nesten alle punkter som testes. Det måtte likevel gjøres mange antakelser. En mer detaljert analyse vil dermed være nødvendig for å fastsette det virkelige potensialet til jacketene til bruk som understell for 15-MW referanseturbinen. Rapporten avslutter dermed med noen forslag til videre arbeid.

Oppgaven ble foreslått av og utformet i samarbeid med Dr. Techn. Olav Olsen AS, som også bistod med verdifull hjelp gjennom studiet.

FAGLÆRER: Professor Arild Holm Clausen

VEILEDER(E): Håkon S. Andersen (Dr. Techn. Olav Olsen AS)

UTFØRT VED: Norges teknisk-naturvitenskapelige universitet

NORGES TEKNISK-NATURVITENSKAPELIGE UNIVERSITET
INSTITUTT FOR KONSTRUKSJONSTEKNIKK

MASTEROPPGAVE 2022

Sebastian Kaasa og Ludvig Grytbakk Tronsaune

Design av stålunderstell til vindturbin

(Design of steel substructure for bottom-fixed offshore wind turbine)

Dr. techn. Olav Olsen AS er for tiden involvert i et konseptutviklingsprosjekt for bunnfaste 15-MW offshore vindturbiner. Et aktuelt konsept, som kan benyttes for vanndybder i konsesjonsfeltet Sørlige Nordsjø 2, består av et fagverksunderstell med fire søyler.

Masteroppgaven er knyttet opp mot dette utviklingsprosjektet. Det er en lang rekke aktuelle problemstillinger for et slikt stålunderstell: Design av knutepunkt, utmatting, dynamisk last fra selve vindturbinen, bølgekrefter osv. Masteroppgaven vil ta for seg et utvalg av disse.

Innholdet i masteroppgaven kan f.eks være:

- Litteraturstudium: Last og respons på lignende konstruksjonstyper
- Presentasjon av valgt(e) case for stålunderstell
- Globalanalyse for valgte lasttilstander
- Analyse av lokal respons, f.eks utmatting eller design av knutepunkt
- Rapportering: Presentasjon av data og resultater

Oppgaven er foreslått av og utføres i samarbeid med Dr. techn. Olav Olsen AS.

Etter samråd med veiledere kan kandidatene konsentrere sitt arbeide til spesielle deler av oppgaven, eller trekke inn andre aspekter.

Besvarelsen skal ha form som en forskningsrapport hvor det legges stor vekt på en klar og oversiktlig presentasjonsform, og den organiseres i henhold til gjeldende retningslinjer.

Veiledere: Arild Holm Clausen, Institutt for konstruksjonsteknikk
Håkon S. Andersen, Dr. techn. Olav Olsen AS

Besvarelsen skal leveres innen 11. juni 2022.

NTNU, 14. januar 2022

Arild Holm Clausen
Faglærer

Preface

This thesis is the delivery for TKT4950 Structural Engineering. It is the final project of the five-year master's programme in Civil and Environmental Engineering from August 2017 until June 2022. The thesis was conducted from January until mid-June 2022. We chose this project as it granted us the opportunity to learn new topics within maritime engineering and to provide fascinating insight into the topic of renewable energy. The problem description provided by our supervisor Arild Holm Clausen gave us the freedom to focus on fields within maritime and structural engineering that we found engaging.

This project has been challenging at times; the issues within maritime engineering were relatively unfamiliar. As a result, learning new software, producing models, and running simulations have been time-consuming. Therefore, we are particularly grateful for the valuable insight and support provided by our supervisor from Dr. techn. Olav Olsen, Håkon S. Andersen. In addition, we are grateful for the technical discussions and advice provided on short notice on many occasions.

We would also like to thank our supervisor Professor Arild Holm Clausen, from the Department of Structural Engineering at the Norwegian University of Science and Technology, for guidance with the report.

Finally, we would like to thank DNV for the courtesy of providing chargeless use of necessary software and answering technical questions at standstill times during the course of this thesis.

Contents

Nomenclature

Abbreviations

ALS Accidental Limit State

BIM Building Information Modeling

CAD Computer Aided Design

CHS Circular Hollow Sections

CW Cut-out Wind Conditions

DNV Det Norske Veritas

DOF Degree of Freedom

DTU Technical University of Denmark

EU European Union

EW Extreme Wind Conditions

FEA Finite Element Analysis

FEM Finite Element Method

FLS Fatigue Limit State

GW Gigawatt

HAT Highest Astronomical Tide

HSWL Highest Still Water Level

LAT Lowest Astronomical Tide

LSWL Lowest Still Water Level

MDOF Multi Degree of Freedom

MSL Mean Surface Level

MW Megawatt

NORSOK Norsk Sokkels Konkurranseposisjon

NREL National Renewable Energy Laboratory

OWT Offshore Wind Turbine

PSD Power Spectral Density

PSM Partial Safety Method

RNA Rotor-Nacelle-Assembly

RW Rated Wind Conditions

RWT Reference Wind Turbine

SCF Stress Concentration Factor

SLS Servicability Limit State

TLP Tension-Leg-Platform

TP Transition Piece

ULS Ultimate Limit State

UMaine University of Maine

Symbols

β The Frequency Ratio

$\Delta\omega_D$ Contant Amplitude Fatigue Limit Stress Range

$\Delta\omega_L$ Cut-Off Limit Stress Range

$\Delta\sigma$ Stress Range

Δ Change/Difference

$\eta(x,t)$ Wave Profile

η Utilization Factor

γ_{fi} Load Factor

γ_{mi} Material Factor

λ Wavelength

ω Eigenfrequency

ω_{load} Frequency of an Exeternal Load

ρ Density

σ	Stress
$\mathbf{C}$	System Damping Matrix
$\mathbf{C}_{ae}$	System Aerodynamic Damping Matrix
$\mathbf{f}(t)$	System Load Vector
$\mathbf{K}$	System Stiffness Matrix
$\mathbf{K}_{ae}$	System Aerodynamic Stiffness Matrix
$\mathbf{M}$	System Mass Matrix
$\mathbf{v}$	Eigenvector
ξ	Critical Damping Ratio
C_D	Drag Coefficient Wave Loads
C_M	Mass Coefficient Wave Loads
D	Fatigue Damage
d	Water Depth
F_x	Point Load Along Global x-Axis
F_y	Point Load Along Global y-Axis
F_z	Point Load Along Global z-Axis
H_s	Significant Wave Height
I_u	Turbulence Intensity Factor
k	Wave Number
M_x	Moment About Global x-Axis
M_y	Moment About Global y-Axis
M_z	Moment About Global z-Axis
N	Number of Cycles
R_d	Design Resistance
R_{ki}	Characteristic Resistance
S_d	Design Load Effect
S_u	Power Spectrum Wind
S_J	JONSWAP Wave Spectrum

S_{PM} Pierson-Moskowitz Wave Spectrum

S_{uu} Cross Spectrum Wind

T_P Spectral Peak Period

T_R Return Period

U Wind Speed

U_0 Reference Wind Speed

U_R Ursell's Number

1 Introduction

1.1 Motivation

The strict international climate commitments compel wind power actors to explore and develop new technologies and methodologies. EU has set an objective to install 60 GW of offshore wind power before the start of 2030 and 300 GW before 2050 [1]. On June 12th, 2020, the oil- and energy department (OED) in Norway adopted that Southern North Sea II and Utsira North were to open for concession applications for the installment of offshore wind energy in 2021. The purpose is to contribute to EU's climate goals, to lower prices and reduce variations in the electricity market and ultimately make the annual energy prices independent of coal- and gas prices [2]. Southern North Sea II is a favorable area for wind production due to its environmental conditions and geographical location [3]. As seen in Figure 1.1, Southern North Sea II is located southwest of Norway and borders Denmark's economic interest zone. This location enables efficient electricity transportation through cables to Denmark, Great Britain, and Germany. The planned installment of wind power production in Southern North Sea II is 3 GW, which corresponds to 15% of the total production capacity, from a pure area assessment [1].

Offshore wind production has been an increasing area of interest in the past couple of decades as opposed to onshore production. First of all, offshore wind parks benefit from higher and more stable wind speeds, as there is no local topology affecting the wind flow at sea. This yields increased predictability and reliability of the production conditions. Secondly, onshore wind turbines have been a topic of political opposition due to their infliction on local ecosystems, noise, and aesthetic appearance, all favoring development of offshore wind power. However, new challenges arise when establishing wind parks further from shore; the cost of installment and maintenance increases with the water depths and the hazardous environmental conditions. Solutions regarding the support structures for offshore wind turbines (OWTs) are highly dependent on the water depths on the installation sites. Rammed monopiles have been the dominating choice as a support structure for OWTs to date. However, it is only deemed favorable for water depths of 5-20 meters [4]. Southern North Sea II, the site in question, has an average water depth of 60 meters, which entails that a monopile substructure would attract significant moments and

Figure 1.1: The Location of the concession field Southern North Sea II, illustrating the adjacent economic zones [3].

shear forces at the seabed. This would require a large design cross-section for the monopile leading to an expensive fabrication and installment process. In addition, the technological growth of wind turbines is aiming for higher capacity, which forces the industry actors towards larger-sized turbines.

Larger wind turbines lead to increased self-weight and surface area affected by wind loads. To comply with these changes, the suitable choice of substructure is under investigation by the structural engineering community. The choice needs to take the commercial aspect into account, both the cost of installing and the cost of fabrication vs. the performance of the wind turbine structure in the site-specific environmental conditions. This thesis will cover a concept study of steel jacket substructures for wind turbines proposed by Dr. Techn. Olav Olsen AS. The goal of Olav Olsen for the study is to prepare and position themselves in the wind power market ahead of the projects in the concession field Southern North Sea II. This thesis aims to investigate the design of two proposed steel jackets and optimize the choice of cross-sections with respect to environmental loads and fatigue. The open-source reference wind turbine IEA-Wind 15-MW [5] will be utilized as a basis for calculations of aeroelastic loads.

1.2 Problem Description

This thesis aims to aid in the concept study conducted by Dr. Techn. Olav Olsen on bottom-fixed steel jacket substructures for wind turbines in the Southern North Sea

II. There are many well-developed solutions to date for smaller jackets. However, as the jackets are scaled up to keep pace with larger turbines at increased water depths, several unresolved issues need to be addressed. These include design performance in terms of strength, longevity, standardization, installation, economy, and environmental footprint.

This paper compares a straight-legged jacket proposed by Olav Olsen to a skew-legged design. The comparison was based on the structural performance of the two solutions as a substructure for a 15-MW turbine. The main objective was to assess the potential of the straight-legged solution and obtain a viable preliminary design that could be used in later studies. The work was conducted in the following order:

1. Determination of structural- and environmental conditions/load effects
2. Creation and calibration of a FEM-model
3. Assessment of the structure's natural frequencies and ultimate limit state performance
4. Structure optimization based on the ultimate limit state
5. Performance assessment in the fatigue limit state
6. Comparison and presentation of results

The structure performance was characterized by several factors established through several finite element analyses (FEAs). The FEAs were carried out in Sesam, an offshore software package developed by Det Norske Veritas (DNV).

In the ULS, the goal was to determine the maximum load-bearing capacity of the structure in terms of strength and stability. This included code checking of the structural members according to relevant design codes. In addition, an eigenvalue analysis was performed to assess the system's natural frequencies. Based on these two analyses, the structure was optimized, and only the final optimized setup was presented in the report.

In the FLS, the focus was on the structure's capacity in terms of fatigue. This included lifetime analysis of members and joints based on the time-variant load effects from waves and wind. The optimized structures from the earlier ULS analyses were utilized, and the goal was to assess the fatigue performance of the two jackets.

1.3 Scope

This thesis was written as a concept study for a new concession field for wind power production in the Southern North Sea II. A direct consequence of designing structures in

such areas is that no site-specific measurements are available. The work conducted in this report was thus carried out without access to any data sets for the environmental and soil conditions. As mitigation for this, the stability of the structure was assessed by assuming bottom-fixed boundary conditions for the jacket's legs, and many of the loads had to be assumed or based on design codes and statistical analyses.

The work was focused on the structures undercarriage, the steel jacket. The FEM model was established without the rotor-nacelle-assembly and a detailed transition piece. Instead, the transition piece was assigned stiffness and mass, resembling a proposed solution provided by Olav Olsen.

The most improbable design events were not evaluated, i.e., the events covered by, accidental limit state (ALS), such as earthquakes, collisions, fire, and explosions. Serviceability limit state (SLS) was also not considered.

1.4 Design Codes and Recommended Practice

Several standards have been used as a foundation for the steel jacket design. The majority of the standards are developed by DNV. The rest are made from a collaboration initiative between several organizations called *Norsk Sokkels Konkurranseposisjon* (NORSOK).

DNV-RP-C205: deals with environmental conditions and loads and includes definitions on well-supported theories [6].

DNV-RP-C203: covers a detailed description of the effects of fatigue on offshore steel structures and provides guidelines for recommended practice [7].

DNV-ST-0126: covers support structures for wind turbines and provides principles for design, construction, transportation, installation, and inspection [8].

DNV-ST-0437: covers loads and site conditions for wind turbines and provides technical requirements, principals, and guidance [9].

NORSOK N-003:2017 covers actions and action effects, specifically on the Norwegian continental shelf [10].

NORSOK N-004:2013 covers the design of offshore steel structures and includes guidelines and requirements for design and documentation [11].

1.5 Software

Sesam-GeniE

GeniE is a tool in the Sesam package for modeling and analyzing offshore structures and is developed by DNV based on the finite element method (FEM). The software is compatible with the maritime conditions relevant for offshore structures during their lifecycle. Wajac and Sestra were utilized during this thesis through GeniE, which are Sesam modules for calculations of wave loads and structural analysis, respectively. GeniE version V8.3-04 was used.

Bladed

Bladed is an integrated software package for aeroelastic simulations of wind turbines, also developed by DNV. The software is a computer-aided engineering tool that builds wind turbine models, runs calculations, and processes the results. Bladed was utilized to assess the dynamic loads from the wind turbine in light of fatigue damage in the jacket structure.

Sesam-Framework

The Framework module is an interactive post-processor for code checks and fatigue calculations. The input loads are compatible with the results from a hydrodynamic analysis in Wajac and an aeroelastic analysis in Bladed.

Sesam Wind Manager

Sesam Wind Manager is a software used for time-domain fatigue analysis and ultimate strength analysis of fixed beam structures. It was utilized to set up and manage multiple runs with varying environmental conditions to assess time-domain fatigue.

1.6 Outline of Thesis

Chapter 2: introduces the 15-MW reference wind turbine used as a basis for the thesis along with some of the most important parameters in terms of substructure design. In addition, the chapter provides a brief introduction to different types of substructures that are applicable today or will be in the future.

Chapter 3: provides a theoretical basis for the principles of structural analysis. This includes a description of the limit states, dynamic analysis, and fatigue with an emphasis on offshore structures.

Chapter 4: provides the theoretical approach for determining load actions from wind and marine conditions, that are relevant for marine structures. The theory is mostly based on the design codes RP-C205 [6] and ST-0437 [9] developed by DNV.

Chapter 5: describes the modeling process of the jackets in Sesam. The choice of geometry, cross-section, material, applied loads, and model assumptions are presented in detail.

Chapter 6: presents the results from the dynamic analysis, including the power spectral densities of the exciting loads and a discussion of the findings, based on the modeling described in Chapter 5.

Chapter 7: presents the results from the ultimate limit state analysis of the two jackets, based on the modeling described in Chapter 5.

Chapter 8: describes the modeling choices for the fatigue limit state analysis. It encompasses the statistical model utilized for determining probable sea states in the Southern North Sea II.

Chapter 9: presents the results from the fatigue analysis, based on the implementation presented in Chapter 8.

Chapter 10: the solution methods, assumptions, and results are further discussed.

Chapter 11: provides conclusions from the findings discovered during the work of this thesis and suggestions for further work.

2 | Offshore Wind Turbines

2.1 IEA-15-MW Reference Wind Turbine

In the preliminary design, research, and engineering of new wind turbine technology, the industry often takes inspiration from reference wind turbines (RWTs). RWTs are open-access and represent a possible setup for an actual turbine serving as a benchmark to estimate costs and evaluate performance. One of the benefits of using the open-access RWT as a design basis is that it opens up for collaboration between companies without jeopardizing their competitive advantage [5].

A technical report released in March 2020 proposed a 15-Megawatt RWT for offshore energy production. The name of the report is *Definition of the IEA Wind 15-Megawatt Offshore Reference Wind Turbine* [5], and it was developed from a collaboration between the National Renewable Energy Laboratory (NREL), the Technical University of Denmark (DTU), and the University of Maine (UMaine). The report provides a detailed description of the turbine and addresses tower geometry, rotor and generator performance, amongst other things. The reported parameters are based on numerical analyses performed in several different softwares. The report assessed a monopile substructure, but most concepts and values are also applicable for jacket substructures. Therefore, the RWT from the NREL report was used as the basis for the jacket analysis.

The RWT with a monopile substructure is illustrated in Figure 2.1. Some of the key parameters in terms of substructure design are listed in Table 2.1. For the jacket substructure proposed by Olav Olsen, the distance between mean sea level (MSL) and the transition piece is 20 m, as opposed to 15 m for the monopile suggested by the NREL report. The different substructure alternatives are discussed in further detail in Section 2.2.

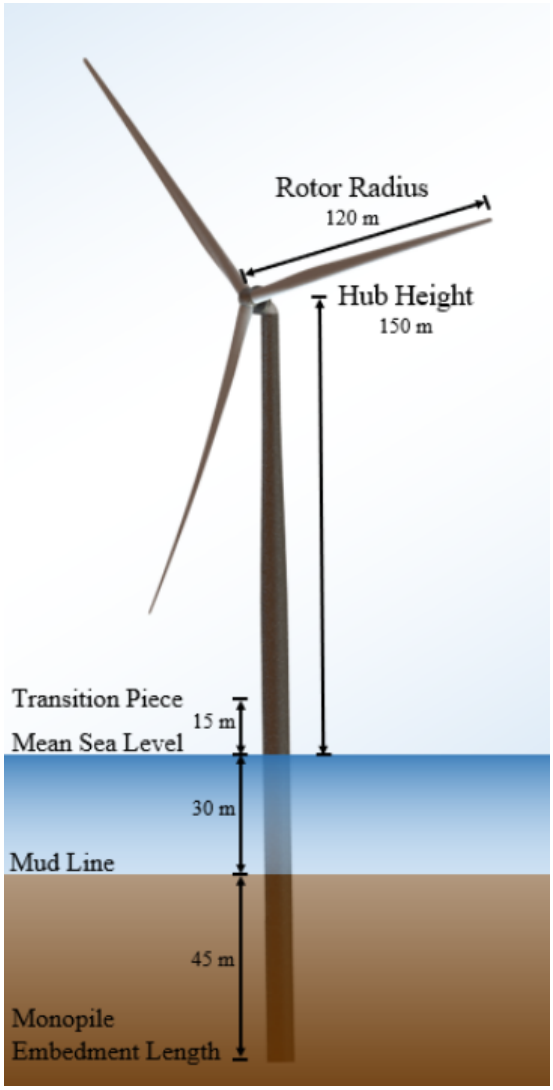

Figure 2.1: IEA-15-MW RWT with a monopile substructure [5].

Parameter	**Units**	**Value**
Power rating	MW	15
Rotor diameter	m	240
Hub height above MSL	m	150
Transition piece height above MSL (monopile)	m	15
Transition piece height above MSL (jacket)	m	20
Tower mass	$tonnes$	860
Rotor-nacelle-assembly mass	$tonnes$	1017
Blade mass	$tonnes$	65
Maximum thrust (rated wind speed)	MN	2.50
Maximum torque	MNm	20
First eigenfrequency	Hz	0.170

Table 2.1: Key parameters for the IEA-15-MW RWT [5].

2.2 Substructures

The substructure for offshore wind turbines (OWTs) is the submerged support structure connected underneath the turbine tower. Usually, this connection is made via a transition piece. As illustrated in Figure 2.2, there are roughly speaking two main types of substructures that both offer numerous different solutions. The first is a bottom-fixed support structure such as monopiles, tripods, steel jackets, and gravity-based foundations. The second is a floating support structure including tension-leg-platforms, spar-buoys, and semi-submersibles.

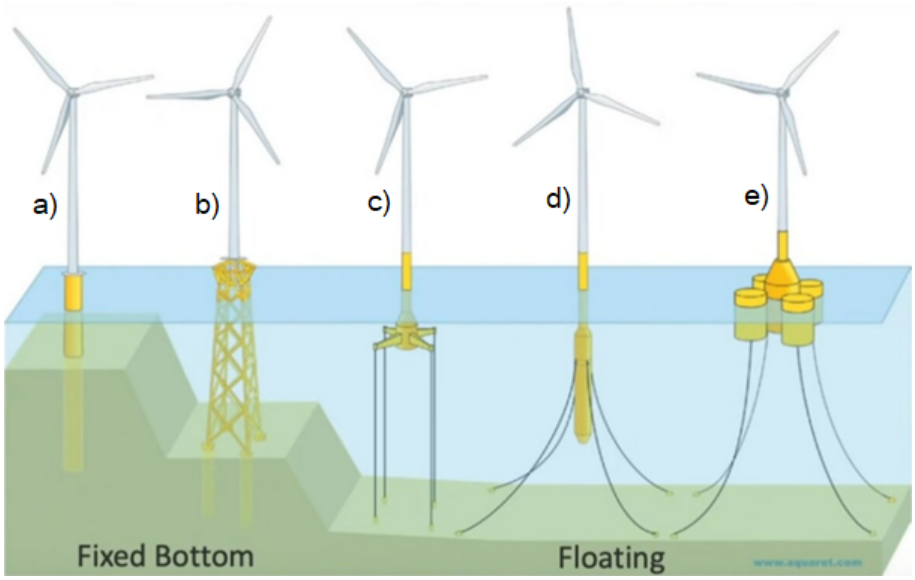

Figure 2.2: (a) monopile (b) steel jacket (c) tension-leg-platform (d) spar-buoy (e) semi-submersible [12].

The choice of substructure depends on various technical, economic, and commercial aspects, and it is not always the best and most effective solution that is most widely used. A comparison of the 2010 and 2019 distribution of substructures is displayed in Figure 2.3. As of 2019, the majority of OWTs connected to the European power grid had a monopile substructure, whereas the second most used was steel jackets [13]. These substructures have increased their relative share much at the cost of gravity-based support structures. Floating substructures account for only a tiny fraction, showing that this technology is still in the developing stage. This might change in the future if wind farms are transitioned to deeper water regions.

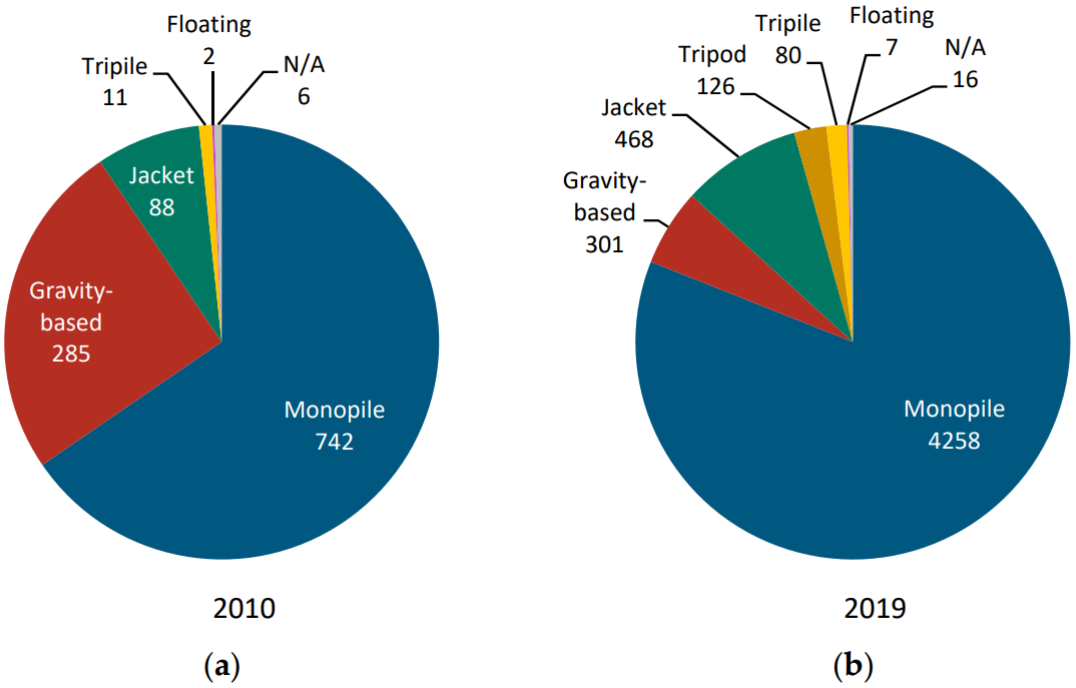

Figure 2.3: Distribution of substructures in Europe in (a) 2010 and (b) 2019 [13].

2.2.1 Monopile

Monopiles consists of a single hollow steel tube piled into the seabed. There are several reasons why monopiles are the most used substructure in Europe today. First of all, the design is arguably quite simple compared to other solutions, and the installation process is relatively straightforward. The seabed does not require any preparation. The monopile is simply transported to the site and piled directly into the seabed [13].

With a monopile substructure, the loads from the turbine are transferred from the tower to the monopile via a transition piece. Lateral loads are transferred to the foundations primarily by shear forces and moments. Due to this behavior, monopiles are most suitable for smaller turbines in shallow water with depths up to 30 meters [13]. In more intermediate water depths, the cost of this solution will increase rapidly along with the increased required diameter, thickness, and embedment length of the pile. As the demand for larger turbines located in deeper water increases, the dominance of the monopile as a substructure might be challenged by other solutions in the future, like jackets and floating substructures [13].

2.2.2 Steel Jacket

Steel jackets are space frames consisting of tubular profiles with welded joints. The behavior resembles a truss, but due to the welded connections, the joints will be relatively stiff. Jackets are versatile and can be shaped to accommodate the conditions. They can

be three- and four-legged with either vertical or skew legs. The frame is often braced in the horizontal and vertical directions. Profiles can be differentiated to improve the structure's efficiency and reduce costs.

Compared to monopiles, the jacket substructure is better suited for more intermediate water depths up to 50-60 m. There are several reasons for this. In contrast to monopiles, some of the global overturning moments due to horizontal loads from the turbine will be transferred into the soil as axial moment pairs. This is advantageous, especially when dealing with weak soil. The large internal moment arm will also give a much stiffer substructure resulting in smaller deflection at the tower top and a smaller eigenperiod. Another competitive advantage in favor of the steel jacket is that it is favorable to monopiles regarding scour and ship collisions, as it has more ways to redistribute loads [14].

2.2.3 Foundation Structures for Steel Jackets

There are several alternative foundation solutions for a bottom-fixed jacket. Some examples for Norwegian seas are gravity-based foundations, suction buckets, and piles. All these solutions offer different advantages and disadvantages regarding cost, water depths, installation work, and interaction with the soil. The three solutions are illustrated in Figure 2.4 for a three-legged jacket.

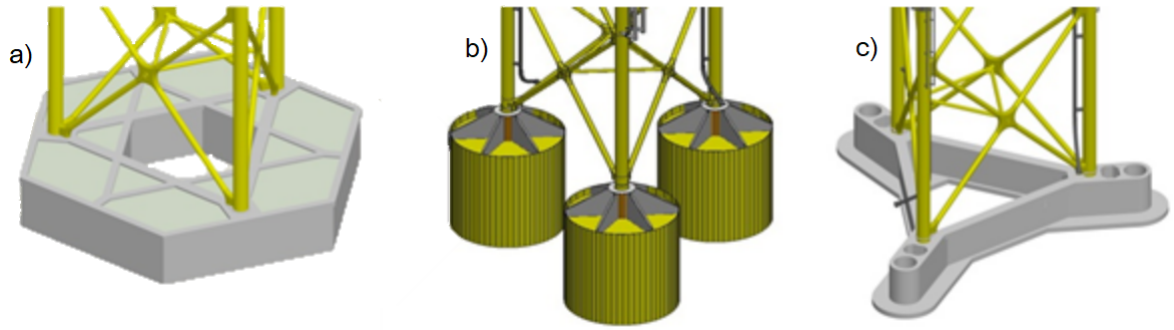

Figure 2.4: Solutions offered by the company Vici Ventus (a) gravity foundations (b) suction buckets (c) piling frame [15].

In gravity-based foundations, the overturning moment in the OWT is balanced by the in-place weight of the structure. The self-weight inherits from the high-density materials utilized and can be supplemented with additional ballast if needed. The lateral forces are balanced by friction between the foundation structure and the seabed, and the capacity can be increased further by adding skirts that penetrate the soil. This foundation type is particularly suited for areas where the soil conditions are harder [16].

In piled foundations, the structure is secured by driving piles into the seabed. This can be done by installing the jacket on preset piles, piling through the main legs of the jacket, or by piling through a pile frame [15]. This foundation type is suited for harder and sandy

soil conditions.

Suction buckets, or suction anchors, are fixed to the seabed by suction forces that arise from pressure differences between the water and the soil around the bucket [17]. The buckets, made from steel or concrete, are driven into the soil. According to eSubsea, they are both cost-effective and quick to install [16]. Suction buckets are suited for soft soil conditions.

2.2.4 Floating Substructures

The structural properties of floating turbine systems differ extensively from their bottom-fixed counterparts. Apart from the economic aspects, an essential consideration for floating substructures is that the design provides sufficient stability, buoyancy, and fatigue strength to support the wind turbine. In general, floating systems experience larger amplitude motions and natural periods far above the peak spectral wave period. This must be considered in the design [18]. Fatigue and installation of the mooring system are also of great importance. The three solutions shown in Figure 2.2 are all anchored by a mooring system, but their stabilization mechanism and to what degree they are influenced by wave actions are different for each design.

Tension-leg-platforms (TLPs) consist of a buoyant hull from columns and pontoons, stabilized by vertical pre-tensioned tendons anchored to the seabed. Compared to spar-buoys and semi-submersibles, the TLP exhibits a much stiffer dynamic behavior with natural periods typically below the peak spectral wave period, similar to bottom-fixed systems [18]. This stability advantage makes it possible for TLPs to have a smaller structure size with lower material costs. This extra stiffness will, however, make the substructure more susceptible to fatigue damage, especially in the mooring system, which itself also has a more expensive anchoring system compared to the other substructures [19].

Spar-buoy substructures consist of a slender hollow cylinder structure filled with ballast at the bottom end. The purpose of the ballast is to achieve a center of gravity below the center of buoyancy. This produces a stabilizing countermoment to the overturning moment from the turbine thrust. Spar substructures have small waterplane areas and are therefore typically less affected by hydrodynamic loads compared to other types of substructures [18]. The structure is kept in position by catenary mooring lines and provides a relatively stable system with a more straightforward configuration than, for instance, semi-submersibles. One drawback to this solution is that the tall hull structure makes it applicable only for great water depths, whereas the other solutions are more versatile in terms of depth. The transportation to the site is also challenging for the spar structure, and the turbine and substructure must be assembled offshore [19].

Semi-submersibles consist of multiple columns and pontoons and are partially stabilized by

ballast and partly stabilized by a restoring moment in the columns due to buoyancy. The dynamic properties are mainly governed by the column diameter and their distance from each other which leaves much room for customization. The natural periods of the system are typically above the peak spectral wave period [18]. The wind turbine can be placed either at the center of the substructure or above one of the columns. Mainly due to their versatility, semi-submersibles are the most popular support concept for floating offshore wind turbines, despite providing less stability than other alternatives. Semi-submersibles are applicable in a vast range of water depths. They have a more straightforward transportation process, and the installation of the turbine can be executed on the dockside [19].

3 | Structural Analysis

3.1 Design Principles

3.1.1 Partial Safety Method

A design approach called the partial safety method (PSM) is often used to verify the capacity of structures, and is the method that was applied in this thesis. In this method, it is verified that a design load effect S_d such as a deformation, a force, or a stress does not exceed the design resistance R_d of the structure, such as a capacity, a yield stress, or a critical deformation. Equation (3.1) is the design criterion in the PSM [8].

$$S_d \leq R_d \tag{3.1}$$

PSM is a probabilistic approach, and the design values used in the verification are based on characteristic values obtained from a probability analysis. According to the DNV standard *ST-0126*, a suitable choice for a characteristic load in ULS for offshore structures is the 98% quantile in the distribution of the annual maximum load effect. This yields a load effect with a return period of 50 years. The characteristic resistance should be taken as the 5% quantile in the distribution of the resistance to account for imperfections in the materials [8]. To account for uncertainties in the characteristic values, partial safety factors are used. The design load effect is obtained by multiplying the characteristic load effect S_{ki} with a load factor γ_{fi}. This factor is used to counteract exceedance due to unfavorable loading, inaccurate load models, the correlation between load effects, and inaccuracies in calculating the load effect. This factor is unrelated to material properties but varies with the limit state [20].

$$S_d = S_{ki}\gamma_{fi} \tag{3.2}$$

Similarly, the design resistance is obtained by dividing the characteristic resistance R_{ki} by the material factor γ_{mi}. This factor accounts for inaccurate material values and geometrical imperfections.

$$R_d = \frac{R_{ki}}{\gamma_{mi}} \tag{3.3}$$

3.1.2 Limit States

The verification of the design criterion in Equation (3.1) is done for different critical conditions called limit states. *ST-0126* states that a limit state is a condition beyond which a structure or structural component will no longer satisfy the design requirement [8]. The four most common limit states are the ultimate limit state (ULS), serviceability limit state (SLS), accidental limit state (ALS), and fatigue limit state (FLS).

In the ULS, structure integrity and safety are verified. In addition, the strength and stability of the structure are checked against a critical design load effect corresponding to the maximum load-carrying resistance. This includes verification of cross-sectional resistance, buckling, and control of the overturning moment or loss of equilibrium for the structure [8]. The characteristic load effects involved in ULS for offshore structures shall be taken as the 98% quantile of the annual distribution, i.e., the load magnitude whose return period is 50 years [8].

In the SLS, the functionality of the structure is verified. This limit state sets requirements for deflections and vibrations under normal operating load effects. This is done to secure a functional structure under everyday conditions [8].

In the ALS, the load-carrying capacity for accidental loads is verified. Accidental load effects are due to low-probability events, such as explosions, incorrect use of structure, impacts, and fire. Mutual for these effects is that they are often caused by human error and will, in many cases, cause local damage. Therefore, the objective of the ALS is to ensure capacity for accidental loads and secure integrity for the damaged structure [8].

In the FLS, capacity is verified for the effect of dynamic loads under normal conditions. Repeated changes in stress magnitude over a considerable timeframe lead to crack propagation in joints and other structural weak points. The consequence can be fracture for stress values much smaller than the ULS-stresses. The fractures due to fatigue are often brittle, leading to sudden failures, often without any notable signs. This is a significant security concern. The objective of FLS is to ensure the safety and longevity of the structure for a significant timeframe. For offshore structures, the aim of fatigue life is often in the region of 20-25 years [8].

3.2 Dynamic Analysis

A structure excited by any time-varying force exerts a dynamic response. Dynamic responses are in the majority oscillatory in nature, where the structure vibrates about its configuration of static equilibrium [21]. In the absence of varying loads, such as wind and waves, the structure will be in static equilibrium with the permanent loads. The vibrating motion induces displacements and thus stresses in the structure, and analyzing these effects is the primary objective of dynamic analyses.

The increasing scale of wind turbines, leads to increased slenderness of the structure due to its high mass compared to its stiffness against deflections. This makes the modern wind turbines more susceptible to critical vibrations induced by wind and waves [21]. Furthermore, such slender and flexible structures are made of higher-capacity materials that provide less energy dissipation. This may result in a more severe oscillatory response, which amplifies the importance of dynamic analysis of wind turbines. This section will discuss the major principles of dynamic analysis of multi degree of freedom (MDOF) systems, with regards to resonance amplification.

3.2.1 Response to Dynamic Loads

All dynamic vibrations can be analyzed by one governing equation, the equation of motion. The equation of motion is derived from *Newton's Second Law of Motion* and is often expressed in the general format shown in Equation (3.4) for a single degree of freedom system.

$$m\ddot{y}(t) + c\dot{y}(t) + ky(t) = f(t) \tag{3.4}$$

Equation (3.4) is a linear second-degree differential equation, where $\ddot{y}$, $\dot{y}$ and y are the DOF's acceleration, velocity, and displacement from the equilibrium state, and are all time-variant variables. $f(t)$ is the time-dependent load acting on the system. m, c, and k are the system's mass, damping, and stiffness and are in most cases taken as constants. Variability of these in time would yield a non-linear differential equation [21].

For systems of DOFs, often referred to as a multi-degree of freedom system, the Equation (3.4) becomes a matrix equation where the number of rows equals the number of DOFs:

$$\mathbf{M}\ddot{\mathbf{y}}(t) + \mathbf{C}\dot{\mathbf{y}}(t) + \mathbf{K}\mathbf{y}(t) = \mathbf{f}(t) \tag{3.5}$$

The procedure for obtaining the mass- and stiffness-matrix usually involves a finite element analysis. The first step is to determine mass and stiffness of the elements in the structure. The system mass and stiffness can then be obtained by applying a connectivity

matrix. The definitions of generalized stiffness, mass and load vector for a beam element through the finite element method are presented in Equation (3.6), Equation (3.7) and Equation (3.8), respectively:

$$k_{q,ij} = \int_0^L EI(x)\psi_i''(x)\psi_j''(x)\,dx \tag{3.6}$$

$$m_{q,ij} = \int_0^L m(x)\psi_i(x)\psi_j(x)\,dx \tag{3.7}$$

$$S^0_{q,ij} = \int_0^L p(x)\psi_i(x)\,dx \tag{3.8}$$

Where

$EI(x)$	is the bending stiffness of the element
$m(x)$	is the mass per element length
$p(x)$	is the distributed loads between end nodes
ψ_i	is the mode shape of element i in the discretized beam
ψ_j	is the mode shape of element j in the discretized beam ($i \neq j$)

The mass- and stiffness-matrix are essential in calculating the eigenfrequency of the structure. The eigenfrequency is the natural oscillation frequency of the system and is of high importance in dynamic analysis. It is calculated through *the Eigenvalue Problem*:

$$(\mathbf{K} - \lambda\mathbf{M})\mathbf{v} = \mathbf{0} \tag{3.9}$$

Equation (3.9) has a non-trivial solution when at least one of the eigenvectors $\boldsymbol{v}$ is nonzero. This is the case when the determinant of the coefficient matrix $(\boldsymbol{K} - \lambda\boldsymbol{M})$ is equal to zero [21], where $\omega = \sqrt{\lambda}$ is the eigenfrequency with unit rad/s. The eigenvectors, often called eigenmodes, represent the vibration pattern of the system when oscillating with a frequency close to the eigenfrequency corresponding to a given eigenmode.

3.2.2 Resonance

Resonance is a phenomenon that occurs when the exciting frequency is equal to or close to one of the natural frequencies of the system [21]. This result inherits from the general solution of the equation of motion. Equation (3.10) gives the general solution derived from a sine-load, where the first term is referred to as the transient solution and the second as the steady-state solution. The transient solution will diminish over time due to damping, and the total solution will thus be approaching the steady-state solution. One can observe that the steady-state solution amplifies due to the two terms in the denominator when

the frequency ratio $\beta = \frac{\omega_{load}}{\omega}$ approaches 1. This state of oscillation is called resonance. The design code *ST-0126* states that vibrations induced by resonance shall be avoided [8], as it leads to excessive deformations and stresses that might exceed the capacity and result in total failure of the structure.

Figure 3.1 illustrates the amplification of vibrations for different values of the damping coefficient ξ. Low damping results in higher amplification, which can be observed from the denominator in the steady-term, where the total solution is asymptotic in $\beta = 1$ for zero damping. Structures have small damping values, usually in the range $0.01 - 0.05$ for flexible members [6], making the phenomenon of resonance even more significant.

$$y_i(t) = (A_i cos(\omega_{di} t) + B_i sin(\omega_{di} t))e^{-\xi_i \omega_{ni} t} + \frac{p_{0i}}{k_i} \frac{(1-\beta_i^2)sin(\omega t) - 2\xi_i \beta_i cos(\omega t)}{(1-\beta_i^2)^2 + (2\xi_i \beta_i)^2} \tag{3.10}$$

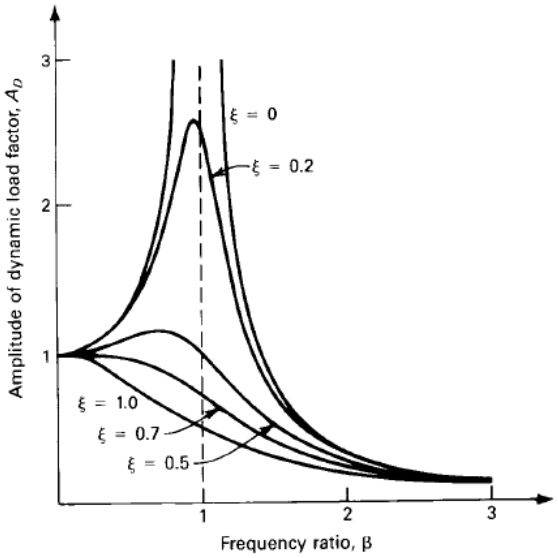

Figure 3.1: Dynamic amplification as a function of the frequency ratio β and the damping coefficient ξ [21].

3.2.3 Aerodynamic Damping

When a structure is subjected to wind buffeting loading, two additional terms are introduced into the equation of motion:

$$\mathbf{M}\ddot{\mathbf{y}}(t) + (\mathbf{C} - \mathbf{C}_{ae})\dot{\mathbf{y}}(t) + (\mathbf{K} - \mathbf{K}_{ae})\mathbf{y}(t) = \mathbf{f}(t) \tag{3.11}$$

Where $\mathbf{C}_{ae}$ and $\mathbf{K}_{ae}$ are the aerodynamic damping and aerodynamic stiffness respectively. In most cases, the former term is negative, which leads to an increase in the total damping of the structure when subjected to loads aligned with the wind direction [22].

3.3 Fatigue

3.3.1 General

Fatigue is a phenomenon that occurs in components and structures subjected to cyclic loading. Along with corrosion and wear, fatigue is one of the leading causes of damage in metallic members and can result in economic losses and dangerous situations. The damage mechanism is characterized by a stable and progressive crack growth which over time will lead to failure in the structural members. Failure can occur at stresses that are much smaller than the designed ULS-stresses. Moreover, the material failure is often brittle, giving no warning in advance. Depending on certain factors, the failure can, however, also be characterized by yielding of the effective cross-section [23].

It is common to distinguish between low cycle fatigue and high cycle fatigue with a separation set at $N = 10^4$ load cycles. During low cycle fatigue, the material experiences large cyclic plastic deformations. In contrast, the stress range is smaller during high cycle fatigue, with deformations primarily in the elastic domain. Accumulation of plastic deformations can, however, still occur at the crack zone due to stress concentrations [23]. According to *DNV-RP-C203*, strength assessment regarding high cycle fatigue is most relevant when designing offshore structures. These structures are subjected to environmental and service load effects of dynamic nature, which induces far more than 10^4 load cycles during the structure's lifetime. Low cycle fatigue can be relevant during transportation [7].

Four factors primarily influence the fatigue strength of a component. The first factor is the stress range, the difference between the maximum and minimum stress in a load cycle. The stress range has been shown to be the main factor influencing the fatigue life of welded details [23].

$$\Delta\sigma = \sigma_{max} - \sigma_{min} \tag{3.12}$$

The second factor is the geometry of the detail. Sharp geometrical changes, holes, and discontinuities will affect the stress flow in the detail and lead to stress concentrations. Locations where stress concentrations occur, are prone to fatigue cracks with a higher propagation rate. The third factor is material characteristics. A material with high tensile strength will have a longer fatigue life for the same stress range as cracks do not form as quickly. However, this will not affect the fatigue life of welded details as these are mainly governed by the crack propagation phase. The reason is that there are a large number of defects already present in the welds due to residual tensile stresses resulting from the cooling phase. The last factor affecting fatigue life is the influence

from corrosive and humid environments. Corrosion pits are prone to crack initiation, and these environments will significantly increase the crack propagation rate in metals, thus reducing the fatigue life. For offshore structures, in particular, the fatigue life expectancy can be increased by applying measures such as cathodic protection, paint, and coating of the members [23].

As mentioned in Section 3.1.2, fatigue design is covered in the FLS. Similar to the other limit states, the design check compares the load effects to the structural capacity. The most common design process is shown in Figure 3.2 where the use of S-N curves is applied. For marine structures, the design process is covered by *DNV-RP-C203* standard.

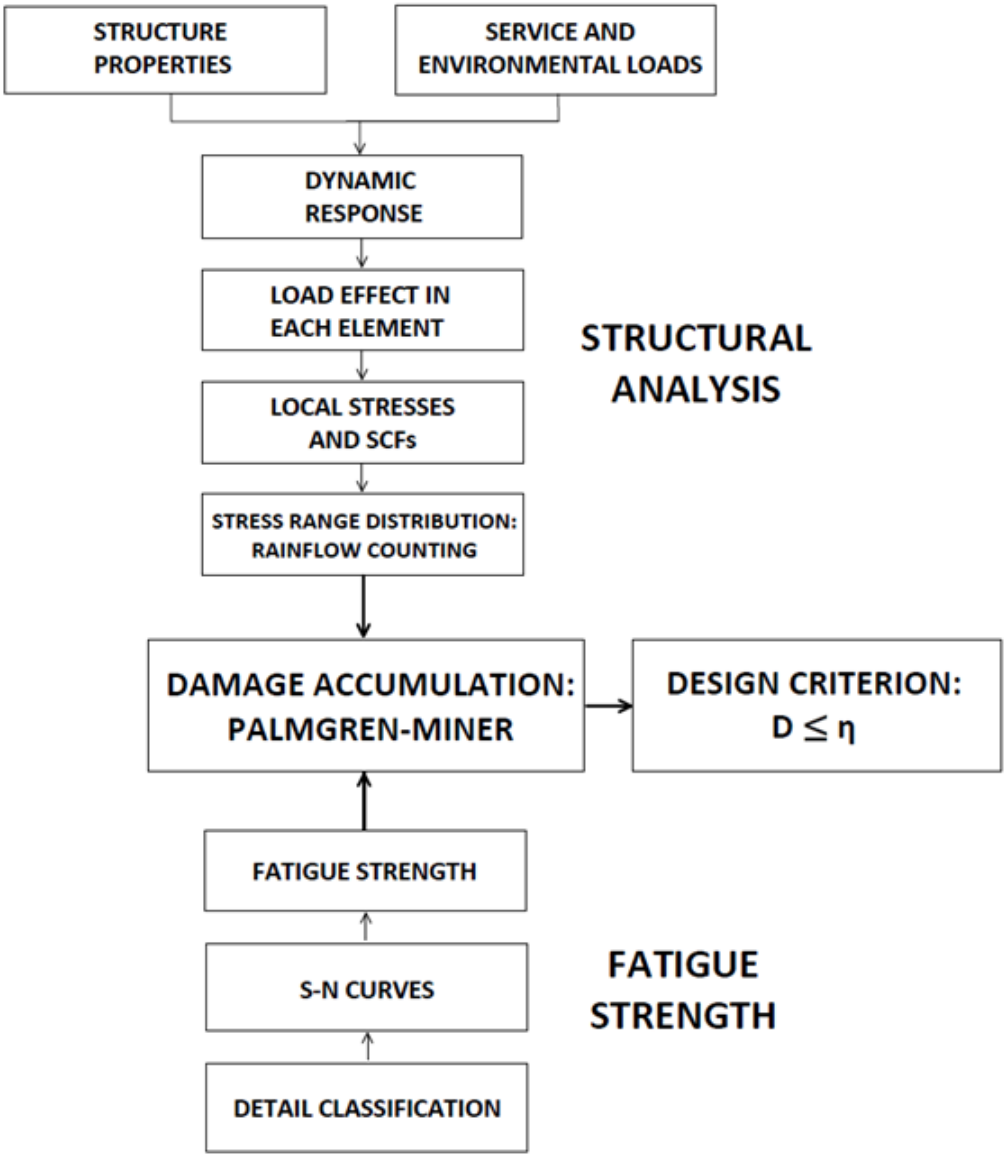

Figure 3.2: Design process for fatigue.

3.3.2 Structural Analysis and Cycle Counting

The goal of the structural analysis is to determine the long-term stress range distribution in the critical components. As illustrated in Figure 3.2, the first step is to assess the structural response to cyclic loads, i.e., determining a response time series from a load time series. Environmental loads from waves and wind are the most relevant for offshore structures. These loads are non-deterministic with a highly irregular nature. Therefore they need to be described stochastically by the use of spectra in the frequency domain [20]. Frequency spectra will be discussed in further detail in Chapter 4.

After assessing the total response of the structure, the next step is to determine the load effects in the members that are prone to fatigue damage. This can then be used to find the local stress ranges at critical locations in the component, where a fatigue crack is expected to initiate due to stress concentrations or so-called hot spots.

DNV-RP-C203 specifies three approaches for stress calculations when assessing fatigue life; Nominal, Hot spot, and Notch stress method. The three methods are illustrated in Figure 3.3, and each has different associated S-N curves. The notch stress method is the most extensive and is mainly used for details where it is difficult to apply the former two methods. This method will therefore not be discussed any further.

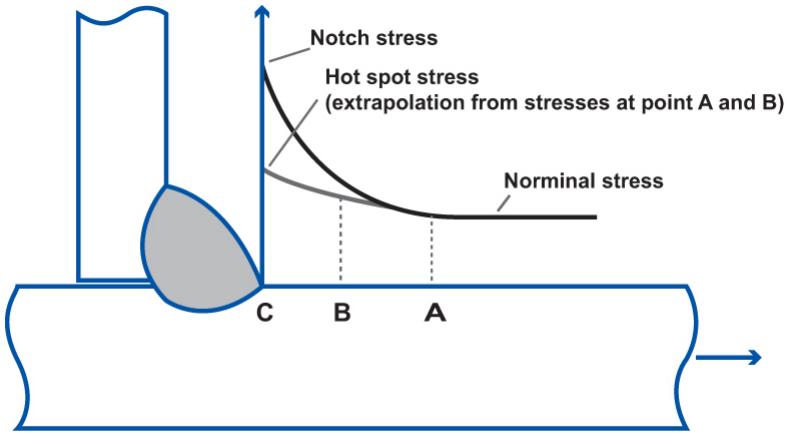

Figure 3.3: Nominal, hot spot and notch stresses in a welded detail [24].

The nominal stresses are uniform and are derived from classical beam theory. Stress concentrations due to the geometry of the detail or the weld profile are not included in this calculation. These effects are, however, accounted for in the detail classification with the corresponding S-N curves [7]. A modified nominal stress value for local effects must be applied for other stress-inducing effects, such as holes and eccentricities that are not characteristic for the detail and therefore not included in the S-N curves. This is done by the use of a stress concentration factor (SCF), as shown in Equation (3.13). The SCFs expresses the ratio between the nominal stress value and the stress value at

the location where the fatigue crack is expected to occur. SCFs can often be found in literature [23].

$$\sigma_{local} = SCF \cdot \sigma_{nom} \tag{3.13}$$

Unlike nominal stresses, hot spot stresses include all geometrical stress-raising effects in the detail, excluding the notch effects from the weld. This effect is accounted for in the corresponding hot spot S-N curve. The hot spot stress $\sigma_{hotspot}$ is determined by extrapolating the maximum principal stress distribution adjacent to the weld toe where the crack is expected to initiate [7]. This is illustrated in Figure 3.3. The hot spot stress for different details can be found from the nominal stress by using SCFs based on empirical values. This is not the same SCF as used in Equation (3.13).

$$\sigma_{hotspot} = SCF_{hotspot} \cdot \sigma_{nom} \tag{3.14}$$

After assessing the local stresses, the stress range distribution over time is determined by using a counting scheme. The most commonly applied scheme is the Rainflow counting algorithm. The result is a stress spectrum or a stress histogram as illustrated in Figure 3.4. The long-term stress range distribution is then evaluated with regard to the fatigue strength [23].

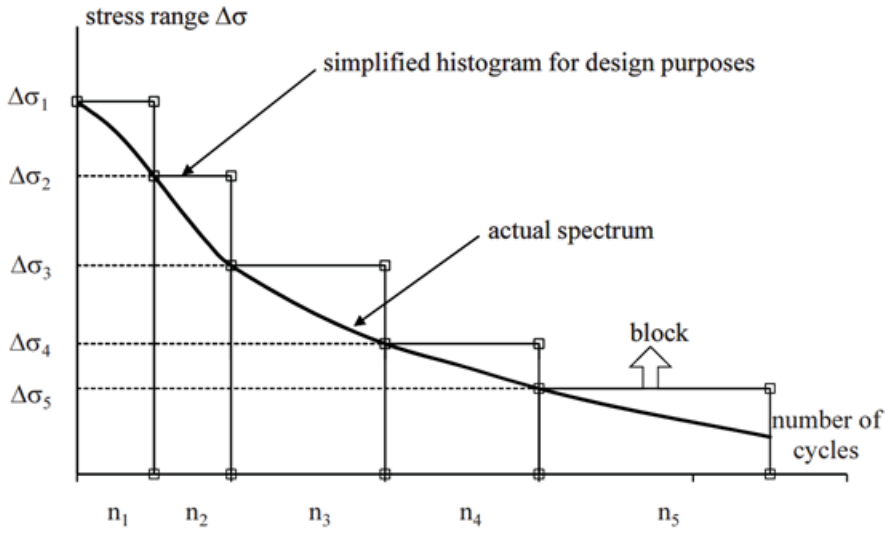

Figure 3.4: Stress spectrum and histogram from rainflow counting [23].

3.3.3 Fatigue Strength and S-N Curves

On the capacity side of the design check, the first step is to classify the detail and choose an appropriate S-N curve. In short, S-N curves provide a relationship between the magnitude and the number of load cycles to failure for a particular stress range. The curve is generally defined in the high cycle fatigue range from $N = 10^4$ to 10^8 load cycles. A logarithmic plot of the $\Delta\sigma$-N relationship is approximated by a linear slope in a large part of this range [23]. The general expression for the S-N curve is:

$$log(N) = log(a) - m \cdot log(\Delta\sigma) = log\frac{a}{\Delta\sigma^m} \tag{3.15}$$

Where

$\Delta\sigma$	is the constant amplitude stress range
N	is the predicted number of cycles to failure for stress range $\Delta\sigma$
m	is the slope coefficient
a	is a constant representing the influence of the structural detail

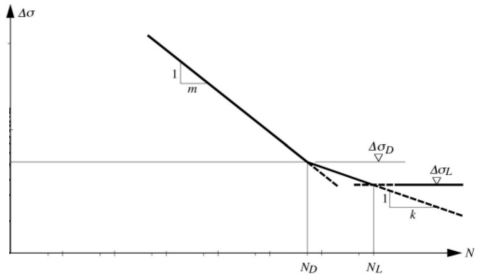

Figure 3.5: Typical S-N curve with defined fatigue limit $\Delta\sigma_D$, and cut-off limit $\Delta\sigma_L$ [23].

The upper limit of the S-N curve (in the low cycle fatigue range) will be close to twice the ultimate static strength of the component. As illustrated in figure Figure 3.5, the slope of the S-N curve will typically transfer to a flatter slope for large numbers of load cycles. The lower limit $\Delta\sigma_D$ is the fatigue limit. Stress ranges under this limit will not result in fatigue failure for all practical purposes, even for many load cycles. This, however, is only true if all stress ranges are below this limit. For cases where the stress ranges are both above and below the fatigue limit, the curve has to be applied to the cut-off limit $\Delta\sigma_L$ [23]. *DNV-RP-C203* operates with a fatigue limit at $N = 10^7$ cycles as opposed to the Eurocode, which uses $N = 5 \cdot 10^6$ [7]. The cut-off limit is usually fixed at $N = 10^8$.

The S-N curves are based on experimental data from tests performed in a lab. The experimental data have a high scatter, and the fatigue strength in the curves is set to be the mean-minus-two-standard-deviation. The curves thus provide a 97.7% probability of survival [7].

The choice of the S-N curve depends on several factors. First of all, the curves vary from one detail classification to another. Secondly, as discussed in Section 3.3.2, the different stress assessment methods each have different associated S-N curves. Thirdly, the environmental conditions must also be taken into account. *DNV-RP-C203* provides different S-N curves for air and seawater environments with or without cathodic protection.

3.3.4 Damage Accumulation

The S-N curves give the fatigue strength based on constant amplitude stress ranges. However, through their service life, most structures will be subject to a number of stress ranges that each cause fatigue damage. Therefore, these partial damage contributions must all be considered simultaneously to assess the total fatigue damage in the component. The most common way to do this is by the use of Palmgren-Miner's damage accumulation rule [7][23]:

$$Discrete: \quad D = \frac{n_1}{N_1} + \frac{n_2}{N_2} + \frac{n_3}{N_3} + ... = \sum_{i=1}^{k} \frac{n_i}{N_i} \tag{3.16a}$$

$$Continuous: \quad D = \int_0^{n_0} \frac{dn(\Delta\sigma)}{N(\Delta\sigma)} \tag{3.16b}$$

Where

D	is the total fatigue damage
n_i	is the number of stress cycles in stress block i
N_i	is the number of cycles to failure at constant stress range $\Delta\sigma_i$
$\frac{n_i}{N_i}$	is the partial damage from stress range i

This rule assumes that the partial damage contributions can be added linearly. The equation uses the long-term stress range distribution determined by rainflow counting, along with the fatigue strength values for each stress range in the S-N curve. The equation can be used both in summation and integral form. The summation expression in Equation (3.16a) is used when a discrete histogram is known. The integral form in Equation (3.16b) is used for a continuous stress range distribution. Damage accumulation for both a discrete and continuous stress range is illustrated in Figure 3.6.

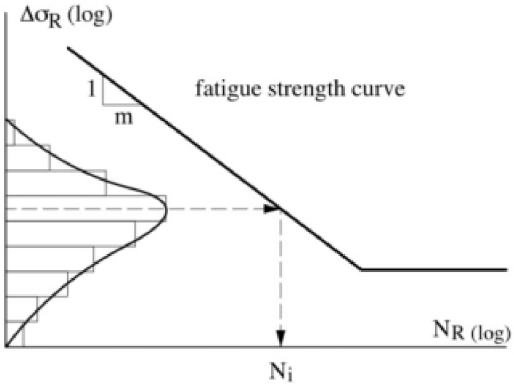

Figure 3.6: Damage accumulation of a discrete and continuous stress range distribution compared to the S-N curve [23].

Failure occurs when the accumulated damage exceeds a usage factor. The design criterion is therefore:

$$D \leq \eta \tag{3.17}$$

DNV-RP-C203 proposes a usage factor η as a function of design life (DL) and the design fatigue factor (DFF). The usage factor for example for $DL = 20$, and $DFF = 1$ is $\eta = 1$ [7].

3.3.5 Tubular Joints

Offshore jackets often consist of tubular members, where the members are welded together at interconnections. These interconnections are denoted tubular joints. Such interconnections represent structural discontinuities that give rise to high stress concentrations in the intersection planes [25]. Therefore, decreased fatigue strength due to stress concentrations is significant for the jacket design. Proper design of tubular joints requires detailed knowledge of stress concentration factors and the principal stresses in the welds, including the heat-affected zones surrounding the weld [25].

Tubular joints are a conjunction of a primary and one or more secondary members, often denoted chord and braces, respectively. The in-plane intersection between the chord and the braces are referred to as the crown. While the out-of-plane intersection is referred to as the saddle, see Figure 3.7 for the geometrical definitions of a tubular joint.

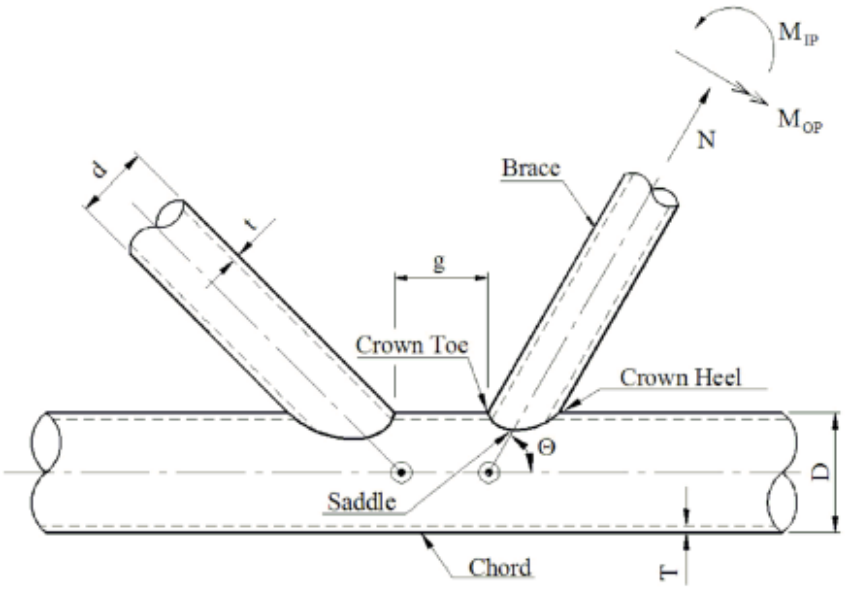

Figure 3.7: Geometrical definitions for tubular joints, retrieved from [7].

Fatigue assessment of tubular joints is commonly analyzed through the hot spot stress method. As discussed in Section 3.3.2, hot spot stresses can be obtained by a linear extrapolation of the nominal stresses at a given distance from the weld toe [7]. The distance to be utilized in the extrapolation depends on the geometrical properties of the chord and braces, and whether the goal is to analyze the chord side of the weld or the brace side. This method obtains the nominal stresses to be utilized in Equation (3.14). An illustration of the stress distribution surrounding the joint is provided in Figure 3.3, where the distance between points A and C is the extrapolation distance.

The hot spot stresses due to brace loads are calculated at the crown and saddle points by a summation of the nominal stress components induced by axial, in-plane, and out-of-plane bending action, multiplied by an SCF [7]. The SCFs are derived from FEAs of tubular joints based on the geometrical properties of the chord and braces. Another alternative is by the use of Efthymiou's equations for simple tubular joints, which can be found in the *DNV-RP-C203* appendix. The SCF should, at minimum, be equal to 1.5 for tubular joints if there is no available documentation [8].

The hot spot stresses might be higher for intermediate points between the crown and saddle points, the points 1, 3, 5, and 7 in Figure 3.8. These hot spot stresses can be calculated by linear interpolation of the axial stress and a sinusoidal variation of the bending stresses at the crown and saddle points [7]. Thus the design code recommends evaluating at least eight spots on the intersection between the chord and a brace.

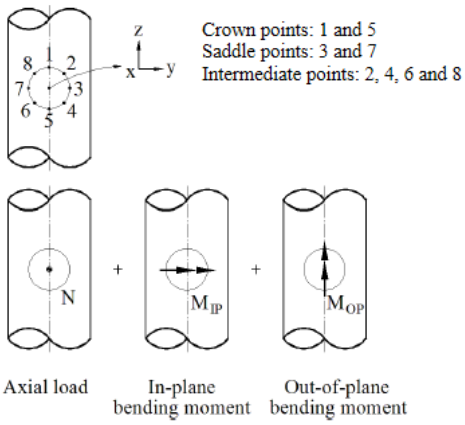

Figure 3.8: Hot spot calculation points and the brace axial- and bending actions, retrieved from [7].

DNV gives the following recommended practice for calculation of hot spot stresses in the intersection points addressed in Figure 3.8:

$$\sigma_1 = SCF_{AC}\sigma_x + SCF_{MIP}\sigma_{my} \tag{3.18a}$$

$$\sigma_2 = \frac{1}{2}(SCF_{AC} + SCF_{AS})\sigma_x + \frac{1}{2}\sqrt{2}SCF_{MIP}\sigma_{my} - \frac{1}{2}\sqrt{2}SCF_{MOP}\sigma_{mz} \tag{3.18b}$$

$$\sigma_3 = SCF_{AS}\sigma_x - SCF_{MOP}\sigma_{mz} \tag{3.18c}$$

$$\sigma_4 = \frac{1}{2}(SCF_{AC} + SCF_{AS})\sigma_x - \frac{1}{2}\sqrt{2}SCF_{MIP}\sigma_{my} - \frac{1}{2}\sqrt{2}SCF_{MOP}\sigma_{mz} \tag{3.18d}$$

$$\sigma_5 = SCF_{AC}\sigma_x - SCF_{MIP}\sigma_{my} \tag{3.18e}$$

$$\sigma_6 = \frac{1}{2}(SCF_{AC} + SCF_{AS})\sigma_x - \frac{1}{2}\sqrt{2}SCF_{MIP}\sigma_{my} + \frac{1}{2}\sqrt{2}SCF_{MOP}\sigma_{mz} \tag{3.18f}$$

$$\sigma_7 = SCF_{AS}\sigma_x + SCF_{MOP}\sigma_{mz} \tag{3.18g}$$

$$\sigma_8 = \frac{1}{2}(SCF_{AC} + SCF_{AS})\sigma_x + \frac{1}{2}\sqrt{2}SCF_{MIP}\sigma_{my} + \frac{1}{2}\sqrt{2}SCF_{MOP}\sigma_{mz} \tag{3.18h}$$

Where

$\sigma_x, \sigma_{my}, \sigma_{mz}$	are the nominal stresses a distance away from the weld toe
SCF_{AC}	is the stress concentration factor at the crown for axial loading
SCF_{AS}	is the stress concentration factor at the saddle for axial loading
SCF_{MIP}	is the stress concentration factor for in plane bending moment
SCF_{MOP}	is the stress concentration factor for out of plane bending moment

The fatigue strength of a tubular joint can be assessed through the S-N curves in *DNV-RP-C203*, categorized as T-curves. This category consists of three different S-N curves depending on the environmental conditions, one curve for air conditions, one for seawater conditions with cathodic protection, and one for joints in seawater with free corrosion.

The T-curves are utilized for hot spots on the exterior of the joint when it is welded from both the inside and outside [7]. However, the assessment of tubular joints only welded from the outside differs in the choice of S-N curve due to the probability of lacking penetration in combination with other effects such as lack of fusion [7]. This may result in a fatigue crack at the inside weld root propagating normal to the main fluctuating stress in the brace. In short, the assessment of fatigue cracks occurring at the inside weld root requires a different choice of S-N curve than fatigue cracks occurring at the outside weld toe.

The generic formula for S-N curves provided in Equation (3.15) is slightly modified due to the thickness dependency of welded joints, which arises from the relation between the local geometry of the weld toe and the thickness of the conjoined plates. This dependency is accounted for by a modification of the stress range. The S-N curve for tubular joints then reads:

$$log(N) = log(\bar{a}) - m \cdot log(\Delta\sigma(\frac{t}{t_{ref}})^k) \tag{3.19}$$

Where the reference thickness , t_{ref}, is 16 mm for tubular joints and the effective thickness, denoted as t, should be taken from Equation (3.20). Table 3.1 provides the adapted S-N curve parameters for the three T-curves, see Section 3.3.3 for the definition and explanation of the various parameters defining a S-N curve.

$$t_{eff} = min(14 + 0.66 \cdot L_t; t) \tag{3.20}$$

Where L_t is the attachment length for the weld.

Environment	m_1	log $\bar{a}_1$	m_2	log $\bar{a}_2$	Fatigue limit	Thickness exponent k
Air	$N \leq 10^7$ cycles		$N > 10^7$ cycles			
	3.0	12.48	5.0	16.13	67.09	0.25
Seawater with catodic protection	$N \leq 1.8 \cdot 10^6$ cycles		$N \geq 1.8 \cdot 10^6$ cycles			
	3.0	12.18	5.0	16.13	67.09	0.25
Seawater free corrosion	3.0	12.03	3.0	12.03	0	0.25

Table 3.1: T-curve parameters according to *DNV-RP-C203* [7]

4 Load Actions

4.1 Statistical Background

Section 3.1 described a design procedure, where the stochastic nature of the load actions are taken into account to ensure an appropriate level of safety and reliability of the design [9]. This section will introduce the terms probabilistic distribution and return period related to environmental loads, and provide procedures to obtain these.

A long-term distribution for the significant wave height can be found from a Weibull distribution:

$$F_{H_S}(h) = 1 - e^{-(\frac{h-\gamma}{\alpha})^{\beta}} \tag{4.1}$$

Where h denotes the significant wave height and γ, α, β are distribution parameters, which makes Equation (4.1) a 3-parameter distribution [9]. When performing a ULS-design, the annual maximum distribution is often of more interest. This can be expressed with Equation (4.2) where N is the number of t-hour sea states in one year [9].

$$F_{H_{S,max,1year}}(h) = (F_{H_S}(h))^N \tag{4.2}$$

To obtain characteristic parameters for the design, a return period T_R is often specified. This gives the probability of exceedance in one year equal to $1/T_R$. See Equation (4.3) for the characteristic significant wave height with return period T_R.

$$H_{S,T_R} = F_{H_{S,max,1year}}(h)^{-1}(1 - \frac{1}{T_R}) \tag{4.3}$$

The same procedure described above is often used for distributions of wind speeds, with different parameters in the Weibull distribution. In areas where hurricanes do not occur, the distribution of the annual 10-minutes mean wind speed can be approximated by Equation (4.2) with measurements of wind speeds instead of wave height [6]. The distribution for wind speeds is most commonly fitted by a 2-parameter Weibull, with one

scale parameter and one shape parameter, which are site- and height-dependent.

It is found from [26], that the wave periods and the wind-wave misalignment angles governing the North Sea, fit reasonably well to a lognormal distribution:

$$f(x) = \frac{1}{\sqrt{2\pi}\sigma x} \exp\left(-\frac{1}{2}\frac{(\ln x - \mu)^2}{\sigma^2}\right) \tag{4.4}$$

Where μ is the mean of the logarithmic values of the stochastic variable, and σ is the standard deviation.

Fatigue calculations require a statistical description of the sea states in the in-situ location of the structure in question. A statistical description of a sea state involves several dependent stochastic variables. The joint probability distribution function for n dependent variables in $\mathbf{Z} = [Z_1, Z_2, ..., Z_N]$ can be written as [26]:

$$f_{\mathbf{Z}} = f_{Z_1} \cdot f_{Z_2|Z_1} \cdots f_{Z_n|Z_1,...,Z_{n-1}} \tag{4.5}$$

4.2 Wind

Wind is an environmentally generated phenomenon due to temperature, and pressure differences between two points of equal elevation in the atmospheric boundary layer [27]. Air particles get drawn towards low-pressure areas to cancel out the inequality. The effect of wind-induced phenomena and the accompanying sea conditions is said to cause 70-80 % of the economic losses related to natural disasters. Wind speeds are generally stochastic and can thus be said to vary randomly in time [27]. This probabilistic nature causes difficulties in accounting for wind-related events in the design of structures.

The average size of wind turbines is increasing, as mentioned in Section 1.1, to yield a higher capacity factor. An increased rotor diameter requires taller and more slender structural components, making them significantly more vulnerable to wind-induced phenomena such as vortex shedding and flutter. To address these changing circumstances, wind engineering is more relevant than ever.

4.2.1 Wind Conditions

The wind conditions offshore vary significantly from the conditions found onshore. The mean wind velocity offshore can be assumed to flow parallel to the sea surface [28]. In contrast, topological and urban differences onshore disturb the flow pattern, invoke interference, and thus a high directional dependency. This often leads to increased mean wind speeds at sea. However, the turbulence fluctuations tend to vary more on land.

A wind field can be evaluated as a quasi-static effect [29], where it is decomposed into two parts, the mean wind speed, $\bar{U}(z,t)$, and a superimposed fluctuating wind gust, $u(x,y,z,t)$. The fluctuating component has zero mean in addition to a mean direction [10].

$$U(x,y,z,t) = \bar{U}(z,t) + u(x,y,z,t) \tag{4.6}$$

To establish statistical values of reasonable accuracy for these wind properties, the design codes require site-specific measurements with a sufficient sampling rate over a period of 10 years [10]. If such measurements are unavailable for the given construction site, hindcast wind data and theoretical models must be utilized [10]. Hindcasts are models run without data assimilation but constrained by a reanalysis on the boundaries and initial conditions [30]. The method approximates statistical data for locations without available measurements from measurements sampled at adjacent locations and is often utilized for wind- and wave data analysis. The wind speeds used for the research in this thesis are based on the *NORA10* hindcast. Due to some concerns regarding the reliability of *NORA10*'s predictions for high wind speeds [10], the wind speed above 15 m/s is slightly increased according to Equation (4.7) where U is the original value from *NORA10*. This adaptation is made to preserve a conservative design.

$$U_{cor} = U + 0.02 \cdot (U - 15) \tag{4.7}$$

As mentioned, the wind velocity varies with time and height above sea level. *NORSOK N-003* [10] provides the following Equation (4.8) for calculation of the characteristic wind.

$$u(z,t) = U(z)(1 - 0.41 \cdot I_u(z) \cdot ln\frac{t}{t_o}) \tag{4.8}$$

Where the 1-hour mean wind speed U(z) is given by:

$$U(z) = U_0[1 + C \cdot ln\frac{z}{z_0}] \tag{4.9}$$

The turbulence intensity, I_u, is an indicator of the intensity of the wind field turbulence. It is defined as the division between the standard deviation of the wind fluctuations and the mean wind velocity:

$$I_u(z) = 0.06[1 + 0.043U_0](\frac{z}{z_0})^{-0.22} = \frac{\sigma_u}{U} \tag{4.10}$$

Where

z_0 is the reference height 10 m
U_0 is the 1-hour mean wind speed at 10 m above sea level [m/s]
C is $5.73 \cdot 10^{-2}(1 + 0.15U_0)^{0.5}$
t_0 is 3600 s
t is the averaging period less or equal to t_0
σ_u is the standard deviation of the turbulence component

The given description of a wind field yields high validity for strong winds. However, it may deviate significantly for moderate wind conditions ($U_0 <$ 15-20 m/s) [10].

4.2.2 Wind Model

The stochastic behavior of a wind field makes it necessary to establish a wind model based on its spectral density, referred to as a frequency domain analysis [10]. The wind spectrum illustrates the range of wind frequencies that transmits the most energy to the structure. *NORSOK N-003* states that moderate to strong winds shall in general be described by the Frøya Wind Spectrum [10], see Equation (4.11) for the spectral density, S_u, at frequency f, where $n = 0.468$.

$$S_u(f) = 320\frac{(\frac{U_0}{10})^2(\frac{z}{z_0})^{0.45}}{(1+\hat{f})^{\frac{5}{3n}}} \tag{4.11}$$

$\hat{f}$ can be calculated from Equation (4.12).

$$\hat{f} = 172f(\frac{z}{z_0})^{\frac{2}{3}}(\frac{U_0}{10})^{-0.75} \tag{4.12}$$

The Frøya Spectrum was developed for neutral conditions over water in the Norwegian sea, hence is deemed considerably better than spectra based on studies over land, e.g., Davenport and Kaimal, for estimation of the energy content in low wind frequencies (high wind speeds) offshore [6]. However, if excitations over higher wind frequencies are important, the Kaimal spectrum could be utilized.

4.2.3 Design Wind

The design wind criteria depend on which limit state is up for assessment. As stated in Section 3.1.2, the capacity check is often based on wind speeds with a return period of 50 years. The wind load is thus derived from the results of the wind condition analysis described in Section 4.2.1. The wind force on a structure, with structural response velocities which are negligible compared to the wind velocity, can be found from Equation (4.13), as stated in N-003 [10].

$$F = \frac{1}{2}\rho C_D A[U_m + u(t)]^2 \approx \frac{1}{2}\rho C_D A[U_m^2 + 2U_m u(t)] \tag{4.13}$$

Where

ρ	is the air density $[kg/m^3]$
C_D	is the shape coefficient of the structural member $[-]$
A	is the projected area of the structural member normal to the wind direction $[m^2]$
U_m	is the mean wind speed [m/s]
$u(t)$	is the turbulence component

This approximation can often be found sufficient and can be evaluated by comparing the eigenfrequencies of the structure. This was described in Section 3.2. Low eigenfrequencies give slow vibrations and, thereof, low velocities.

In Equation (4.13) the higher-order term of the fluctuating component, $u(t)$, has been assumed negligible due to its normally small magnitude compared to the mean wind speed U_m. The fluctuation component in Equation (4.13) remains unknown. An article from University of Surrey [29] has utilized the estimation in Equation (4.14) for the assessment of the turbulent component, $\sigma_{u,NTM}$ of the normal turbulence model.

$$\sigma_{u,NTM} = \sqrt{\int_{f_{1P,max}}^{\infty} S_{uu}(f)df}, \quad u_{NTM} = 1.28\sigma_{u,NTM} \tag{4.14}$$

Where S_{uu} can be found from Equation (4.11) and $f_{1P,max}$ is the maximum rotating frequency of one of the wind turbines rotor blades. The period 1P is a property provided by the wind turbine manufacturer.

4.3 Marine Conditions

Marine conditions include waves, current, sea level, and marine growth. All these conditions impose external loads on marine structures, but the load action, magnitude, and frequency differ. Other notable marine conditions that will not be discussed are ice and temperature.

4.3.1 Current

As shown in Equation (4.15) the total current velocity consists of contributions from both tidal and wind-generated current. These contributions must be added as a vector sum [9].

$$U(z) = U_{tide}(z) + U_{wind}(z) \tag{4.15}$$

The current velocity varies with the distance z from the sea surface. For tidal currents, this velocity profile can be modeled with the power-law expression in Equation (4.16),

where d is the water depth, and U_{tide0} is the current velocity at surface level.

$$U_{tide}(z) = U_{tide0}(\frac{d+z}{d})^{1/7} \qquad for \quad z \leq 0 \tag{4.16}$$

For wind-generated currents, the variation can be modeled as linear to a reference depth d_0 of 50 m where the current is considered to be zero. This expression is shown in Equation (4.17), where U_{wind0} is wind-generated current velocity at surface level.

$$U_{wind}(z) = U_{wind0}(\frac{d_0+z}{d_0}) \qquad for \quad -d_0 \leq z \leq 0 \tag{4.17}$$

Tidal current at still water U_{tide0} must come from measurements, whereas the wind-generated current at surface level U_{wind0} can be estimated from the wind speed by using Equation (4.18). $V_{m,10m}$ is the 10-minute mean wind speed at 10 m height, and parameter k is in the range 0.016 - 0.033.

$$U_{wind0}(z) = kV_{m,10m} \tag{4.18}$$

Approximate data based on the *NORA10* hindcast model for the North Sea can be found in the appendix of the *NORSOK N-003* design standard. This appendix offers data on both $V_{m,10m}$ and U_{tide0}, which can be used in the preliminary analysis of the total current profile.

4.3.2 Waves

4.3.2.1 Wave Theories

The simplest wave is described by Airy theory, often referred to as linear wave theory. In linear theory, the wave profile is represented by the sine wave expression seen in Equation (4.19). In this formulation, η is the wave profile, A is the wave amplitude, ω is the angular frequency, and k is the wavenumber.

$$\eta(x,t) = A \cdot sin(\omega t - kx) \tag{4.19}$$

It is common to distinguish between wind-generated waves and swell waves. Wind-generated waves are caused by local wind. In contrast, swell waves have traveled over great distances and thus have a negligible correlation with local wind conditions [31]. In addition, swell waves are generally longer and flatter with a small amplitude compared to their wavelengths.

The linear wave formulation discussed above is generally only an accurate approximation

for particular sea state conditions dominated by swell waves. Wind-generated waves are steeper and are better described by non-linear wave models. Some frequently used non-linear models are cnoidal-, Stokes- or Dean's stream function wave theory [6]. One way to quantify the non-linearity of a wave is by the use of Ursell's number, shown in Equation (4.20). This number serves as an indicator of the applicability of the different non-linear wave theories.

$$U_R = \frac{S}{\mu^3} = \frac{H\lambda^2}{d^3} \tag{4.20}$$

Where

S is the wave steepness [-]
μ is the relative water depth / shallow water parameter [−]
λ is the wavelength [m]
d is the water depth [m]
H is the wave height [m]

Stokes wave theory is applicable in intermediate and deep water where $U_R < 30$. Cnoidal theory is applicable in shallow water where $U_R > 30$. Stream function theory is valid in a broader range of conditions and will be a good choice in the borderline $U_R \sim 30$ between cnoidal and Stokes [6].

4.3.2.2 Wave Spectrum

The wave theories discussed in Section 4.3.2.1 describe a regularity one seldom finds in a natural sea state. In reality, a sea state is an ever-changing combination of swell and wind-generated waves that can appear random in shape, height, phase velocity, and direction of propagation [6]. This irregularity can be modeled by the use of a wave spectrum. The wave spectrum gives the distribution of wave energy over the different frequencies present in the sea state [32]. Spectra such as Pierson-Moskowitz (PM) and JONSWAP are frequently used to describe wind-generated sea states. The PM-spectrum shown in Equation (4.21) describes a fully developed sea state [33].

$$S_{PM}(\omega) = \frac{5}{16} \cdot H_s^2 \omega_p^4 \cdot \omega^{-5} exp\Big(-\frac{5}{4}\Big(\frac{\omega}{\omega_p}\Big)^{-4}\Big) \tag{4.21}$$

Where

H_s is the significant wave height [m]
ω_p is the peak angular frequency [rad/s]
ω is the angular wave frequency [rad/s]

The JONSWAP-spectrum shown in Equation (4.22) is the PM-spectrum modified by three new parameters to better fit measurements made in the North Sea [33]: the peak enhancement factor γ, the normalizing factor A_γ, and the spectral width parameter σ. This spectrum more accurately describes a sea state that is not fully developed. Generally, for the JONSWAP-spectrum, the wave energy will be distributed over a narrower band of frequencies, and the peak will be taller than that of the PM-spectrum.

$$S_J(\omega) = A_\gamma S_{PM}(\omega)\gamma^{exp(-0.5(\frac{\omega-\omega_p}{\sigma\omega_p}))^2} \tag{4.22}$$

A sea state is often assumed to be constant for a duration of 3-6 hours. The most important parameters in the description of a sea state are the significant wave height H_S and the spectral peak period T_P. The significant wave height is usually defined as the mean wave height of the largest third of the waves in a sea state. It can also be determined from the wave spectrum by the definition of the zeroth spectral moment m_0 (the variance of the wave profile η) [9]:

$$H_S = H_{m0} = 4\sqrt{m_0} \tag{4.23}$$

The peak spectral period T_P is the inverse of the peak frequency in the wave spectrum, which is the most energy-dense frequency in the sea state.

4.3.2.3 Wave Loads

Hydrodynamic loads on slender structures like piles and steel jackets can be calculated by using Morison's load formula given in Equation (4.24). This formula has two contributions. The first contribution is the inertia force. The second contribution is the drag force [6].

$$f(t) = \rho V C_M \dot{v}(t) + \frac{1}{2}\rho C_D S v(t)|v(t)| \tag{4.24}$$

Where

v	is the fluid particle (waves and/or current) velocity $[m/s]$
$\dot{v}$	is the fluid particle (waves and/or current) acceleration $[m/s^2]$
ρ	is the mass density of the fluid $[kg/m^3]$
V	is the volume of the member $[m^3]$
S	is the projected area normal to force direction $[m^2]$
C_M	is the mass coefficient $[m/s^2]$
C_D	is the drag coefficient $[m/s^2]$

4.3.3 Sea Level

Different sea levels impose different loads and must therefore be accounted for in the design of marine structures. The variations in sea level are mainly due to two unrelated contributing factors. The first contribution is the tidal effects due to gravitational forces from the sun and the moon. This effect has a regular and predictable nature. The second contribution is storm surges induced by strong winds pushing water onshore, changes in atmospheric pressure, or both. Depending on location and conditions, the effect can be either increased or decreased sea level. However, for offshore locations, the impact of storm surges is expected to be small compared to coastal areas and regions with shallow water. A third long-term contribution that is worth mentioning is a global increase as a result of climate change [6].

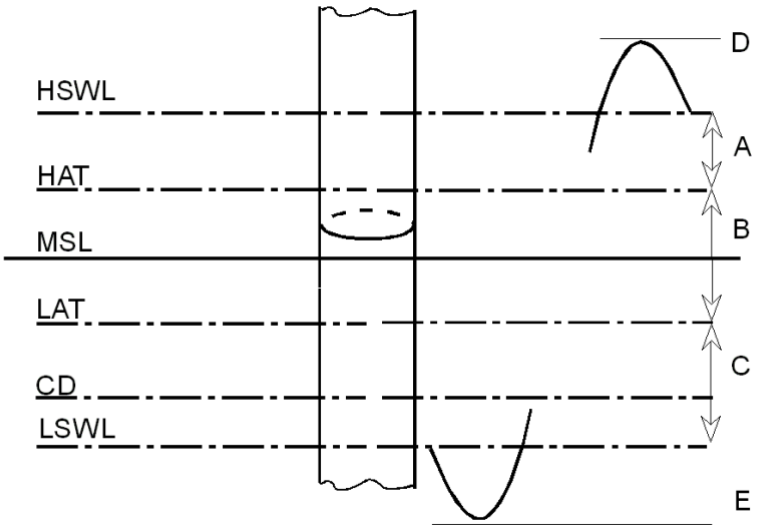

Figure 4.1: Sea level definitions [9].

Figure 4.1 illustrates some different sea level definitions. HAT is the highest expected astronomical tide. Similarly, LAT is the lowest astronomical tide. Together they define the tidal range. MSL is the mean surface level and is defined as the average sea level in the tidal range [9]. SWL is the still water level. In design, this is the level at which wave actions are applied [6]. The design water level can either be the highest still water level (HSWL) or the lowest still water level (LSWL) for a specific return period. HSWL is the combination of HAT and a positive storm surge, whereas LSWL is the combination of LAT and a negative storm surge. Both HSWL and LSWL can be critical depending on the location and structure, so in principle, both have to be checked. For locations where the contribution from storm surge is small and can be neglected, HSWL and LSWL can be set equal to HAT and LAT, respectively.

4.3.4 Marine Growth

Marine structures will be subject to marine growth. This inflicts various load effects, both direct and indirect. The marine growth will increase the members' total self-weight, roughness, and diameter. The increased self-weight will influence the static and dynamic behavior of the structure. The increase in roughness affects the coefficients in Morison's equation for drag C_D and inertia C_N, which, along with the increased diameter, will lead to larger hydrodynamic forces. Cleaning may be necessary to secure structural integrity [9].

The magnitude and importance of marine growth depend on temperature, salinity, water depth, and several other site conditions. Density and thickness values for calculation of marine growth on the Norwegian continental shelf can be found in *NORSOK N-003* [10]. According to this standard, the thickness of marine growth can be assumed to increase linearly over two years after the structure has been placed in the sea [10].

5 | Modeling: Ultimate Limit State

As a basis for the concept study, Olav Olsen provided two substructure models for the 15-MW RWT, one for the straight-legged jacket and one for the skew-legged. The two models are similar in many aspects and differ primarily in geometry. These models served as a foundation for further work and provided a first draft for geometry and section choice.

Traditionally steel jackets have been designed with skew legs. One advantage of a skew-legged design is that it keeps the transition piece small while at the same time giving the structure a large moment arm at the seabed. This simplifies the process of making an economical and efficient substructure. However, as new markets in the offshore wind industry are emerging and the demand for cheaper solutions increases, there is a need for innovation. According to Olav Olsen, the competitive advantage of the straight-legged jacket, as opposed to the traditional skew-legged jacket, lies in its potential for standardization. Standardization might turn out to be one of the most beneficial factors when it comes to making more cost-effective solutions for large wind farms, such as in Southern North Sea II. In this chapter, the FEM modeling, design of the jackets in Sesam, and modeling choices regarding environmental conditions applied in the ultimate limit state are discussed in detail.

5.1 Assumptions

The basis for the jacket design is the 15-MW RWT, and thus the turbine and tower weight are based on the NREL report [5]. No site-specific data measurements were available. Other environmental load effects are primarily based on data for preliminary use from the *NORA10* hindcast, found in the *NORSOK N-003* standard. Data from a nearby located site called Dogger Bank is used in the fatigue analysis. Soil conditions are not included in the model.

The depth in Southern North Sea II ranges from 53-72 m. In the model, the water depth is set to 60 m, which is assumed to correspond to LAT. By using the average depth, the concept will be easier to scale up for deeper regions and scale down for shallower

regions. The four legs of the jacket are constrained for all translations and rotations at the seabed. This assumption is based on the relatively stiff anchoring solutions discussed in Section 2.2.3. This simplification deals with the lack of soil data from the construction site. It is worth noting that this will affect the global stiffness properties of the structure and thus the dynamic properties.

Many of the design choices regarding hydro properties were based on a parametric study conducted early in the project, with the intention of providing a conservative design. In the calculation of Morison's coefficients, linear wave theory for intermediate water depths was applied to calculate wavelengths and particle velocity. This is not entirely accurate, as Stokes' 5th order theory was used to model the waves in Sesam, but the simplification was expected to yield adequate results. In addition, parameters such as the roughness of members have been assumed based on the *DNV-RP-C-205* standard.

The transition piece was not modeled in detail, but the material properties and cross-sections in this location was nevertheless chosen to resemble the stiffness and mass of an actual transition piece. This is discussed further in Section 5.4.

The turbine tower was modeled in Sesam as the tower properties significantly affects the dynamic properties of the jacket-tower system. Diameters and thickness were modeled as proposed in the NREL report [5] spanning from the transition piece at 28 m to the RNA at 144.582 m above the sea surface. A detailed description of the tower geometry can be found in Appendix A.1.

All the elements in the jacket frame were modeled as beam elements, and the whole jacket was assumed to be covered in coating protecting it against corrosion.

5.2 Geometry

5.2.1 Straight-Legged Jacket

The jacket is symmetrical about the two horizontal axes'. The geometry is shown in Figure 5.1. As can be seen from the figure, the distance between the area centers of the legs is 22 m. The total height of the legs is 80 m resulting in a position for the transition piece at 20 m above calm sea surface level. There are five rows of X-bracings on each side with varying spacing. The first row starts at 6.4 m above the seabed. This irregular interval is partly governed by an attempt to avoid placing joints in the splash zone as these will be significantly more susceptible to corrosion and fatigue. The reason is that they will be subject to full exposure to saline water but will have no protection from galvanic anodes as they are located above the surface. There are no bracings in the horizontal plane.

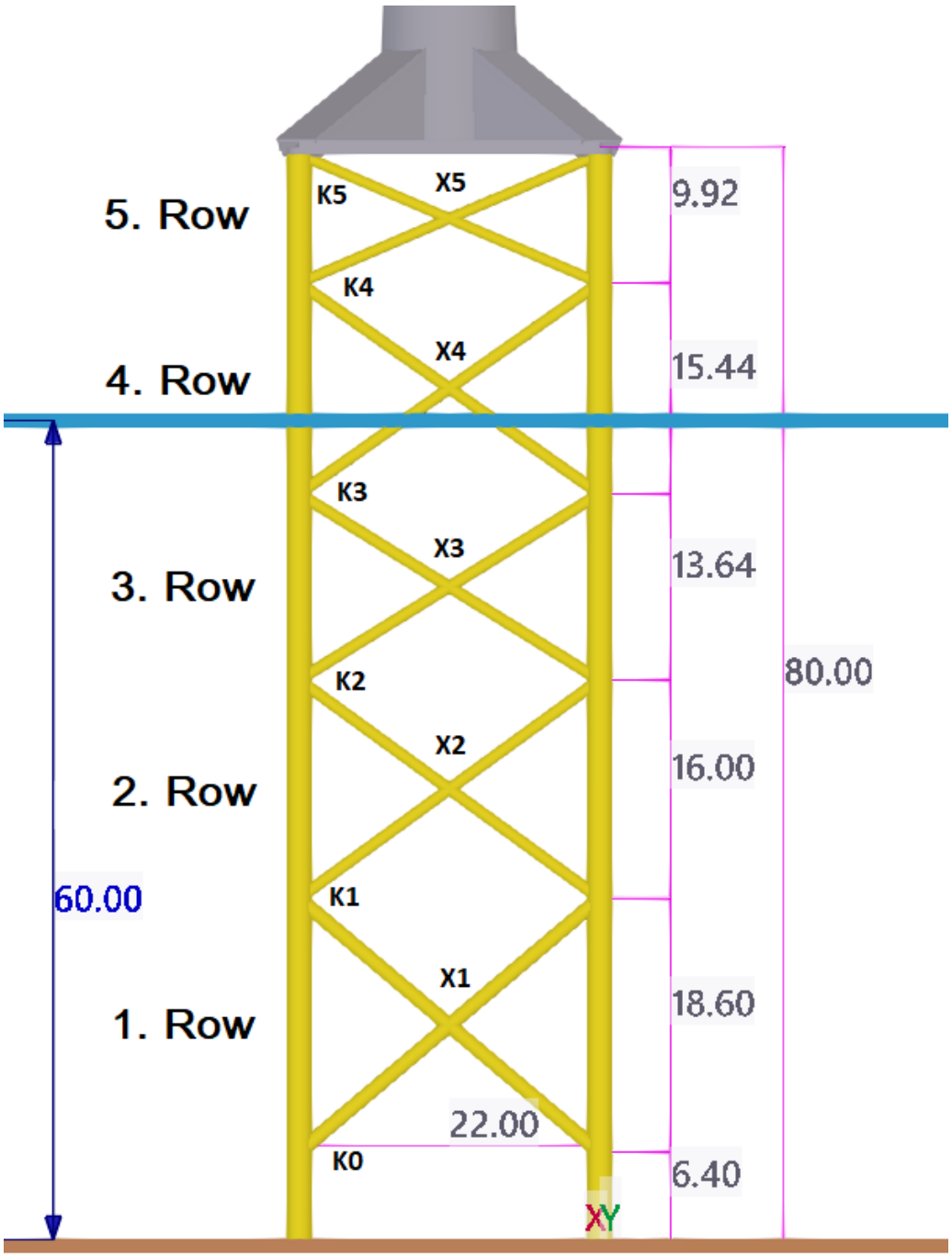

Figure 5.1: Dimensions of the straight-legged jacket in meters.

5.2.2 Skew-Legged Jacket

The geometry of the skew-legged jacket is in many ways similar to the straight-legged one. It is symmetrical about the two horizontal axes, the total height is 80 m, and rows of bracings are equally spaced as for the straight-legged. In contrast, the distance between legs is greater at the seabed, measuring 25 m, and smaller at the transition piece measuring 14 m. As a consequence, the size of the X-bracings increases with increasing depth. The geometry of this jacket is shown in Figure 5.2.

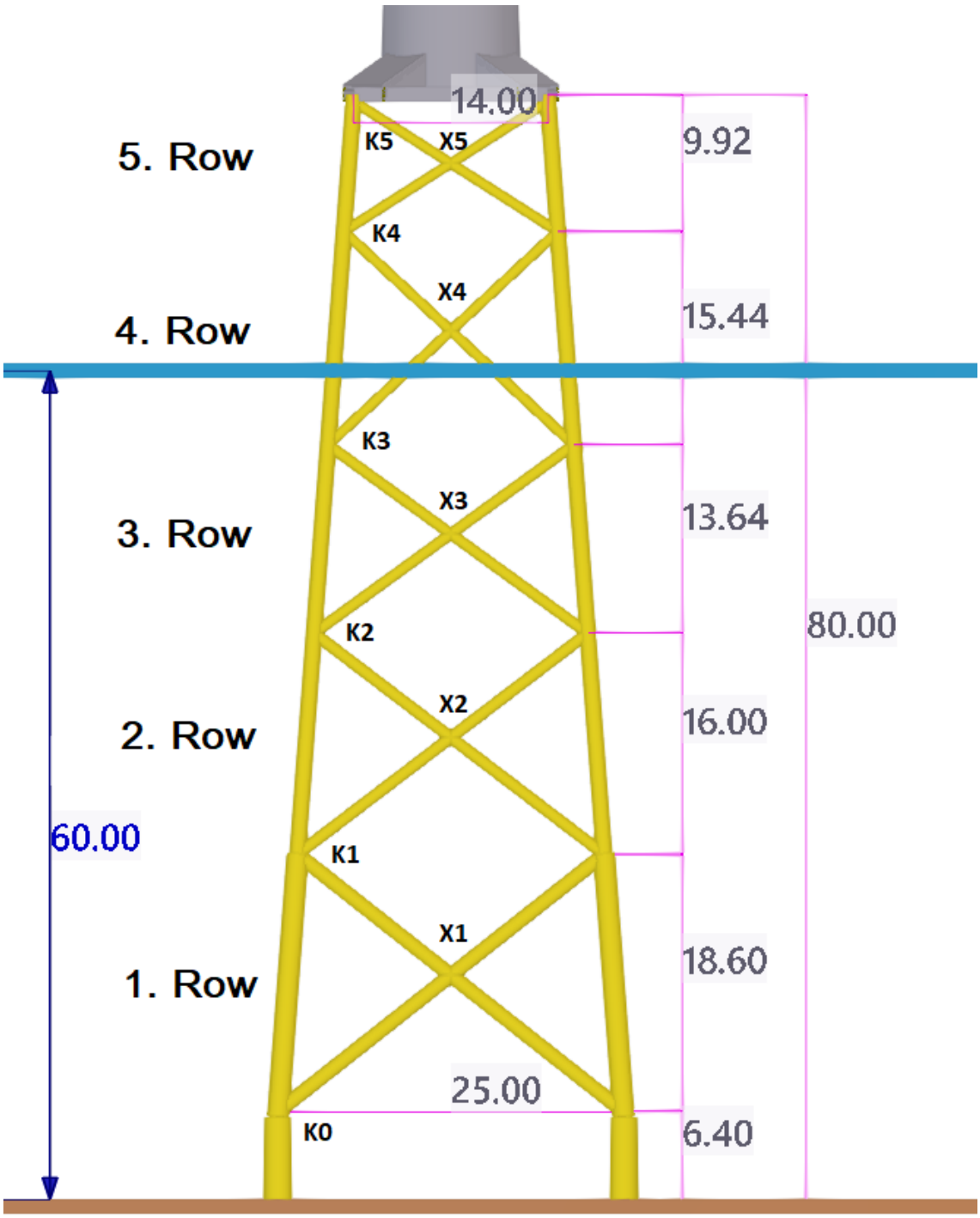

Figure 5.2: Dimensions of the skew-legged jacket in meters.

5.3 Member Properties

The geometry, section, and material choice are also similar for the two jackets. This provides a basis for comparison between the two concepts.

5.3.1 Straight-Legged Jacket

The choice of cross-sections and steel grades are illustrated in Figure 5.3 and summed up in Table 5.2. All members are circular hollow sections (CHS). The jacket is standardized with CHS 1400x40 cross-section for the legs and CHS 900x30 for the bracings. Stubs and cans are included in all joints with 10-20 mm greater thickness than the base element. The diameter of the legs is verified to be large enough to design joints without having overlapping bracings. All members in the jacket consist of S355 steel. The lowermost elements in the jacket are 4.4 m tall members with CHS 1800x80 sections. These members are modeled with increased stiffness to resemble anchoring to the foundation solution, and are not included in the code check.

5.3.2 Skew-Legged Jacket

The choice of cross-sections and steel grades are illustrated in Figure 5.4 and summed up in Table 5.3. The skew-legged jacket also consists only of circular hollow sections (CHS), with sections and material similar to the straight-legged counterpart.

5.3.3 Jacket Masses

The total masses of the jackets are listed in Table 5.1. The mass of the tower, RNA, and transition piece are not included. As can be seen from the table, the two jackets are comparable in weight but differ slightly due to different geometry.

Jacket	**Mass [tonnes]**
Straight-legged	1120
Skew-legged	1055

Table 5.1: Mass of the jackets.

Member	Position [m]	Section (CHS)	Section (Can/Stub)	Steel grade
Legs	0. row	1400x60	-	S355
	1. row	1400x40	1400x60	S355
	2. row	1400x40	1400x60	S355
	3. row	1400x40	1400x60	S355
	4. row	1400x40	1400x60	S355
	5. row	1400x40	1400x60	S355
Bracings	1. row	900x30	940x40 930x40	S355
	2. row	900x30	940x40 930x40	S355
	3. row	900x30	940x40 930x40	S355
	4. row	900x30	940x40 930x40	S355
	5. row	900x30	940x40 930x40	S355

Table 5.2: Member properties for the straight-legged jacket.

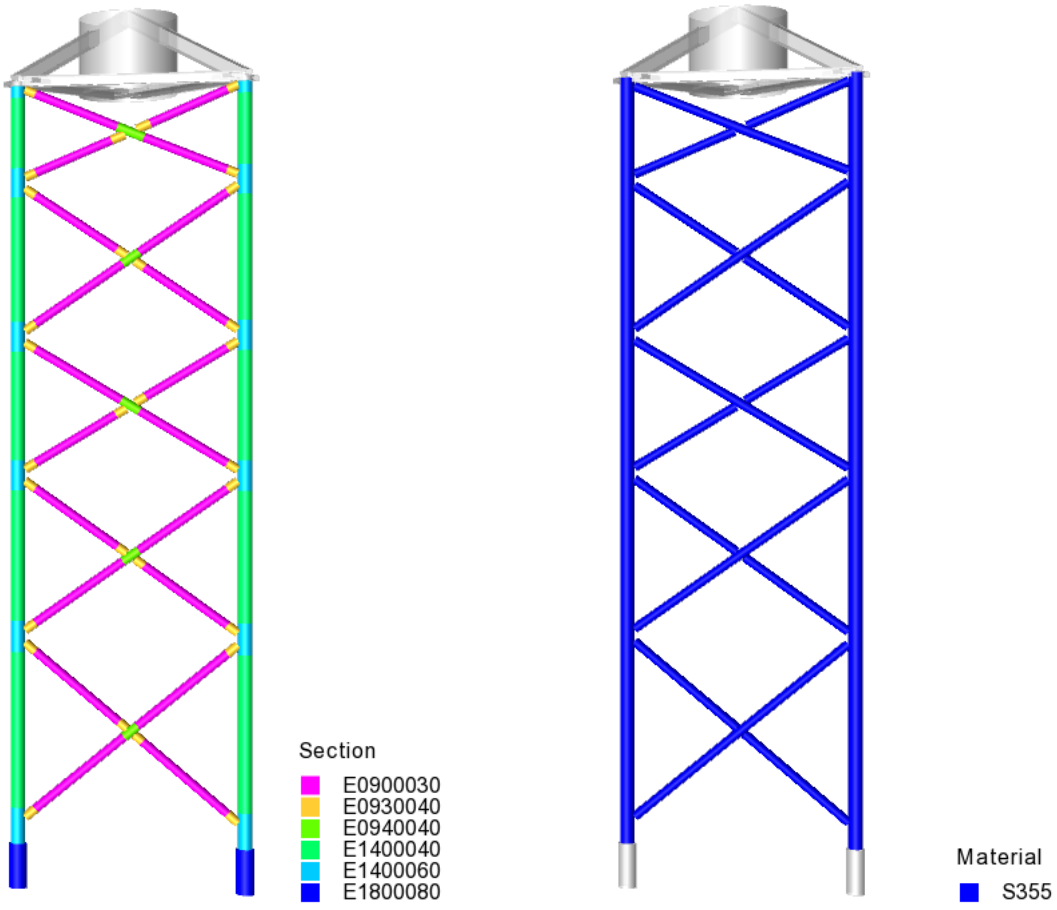

(a) Sections (b) Steel grades

Figure 5.3: Member properties for the straight-legged jacket.

Member	Position [m]	Section (CHS)	Section (Cone/Stub)	Steel grade
Legs	0. row	1400x60	-	S355
	1. row	1400x40	1400x60	S355
	2. row	1400x40	1400x60	S355
	3. row	1400x40	1400x60	S355
	4. row	1400x40	1400x60	S355
	5. row	1400x40	1400x60	S355
Bracings	1. row	900x30	940x40 930x40	S355
	2. row	900x30	940x40 930x40	S355
	3. row	900x30	940x40 930x40	S355
	4. row	900x30	940x40 930x40	S355
	5. row	900x30	940x40 930x40	S355

Table 5.3: Member properties for the skew-legged jacket.

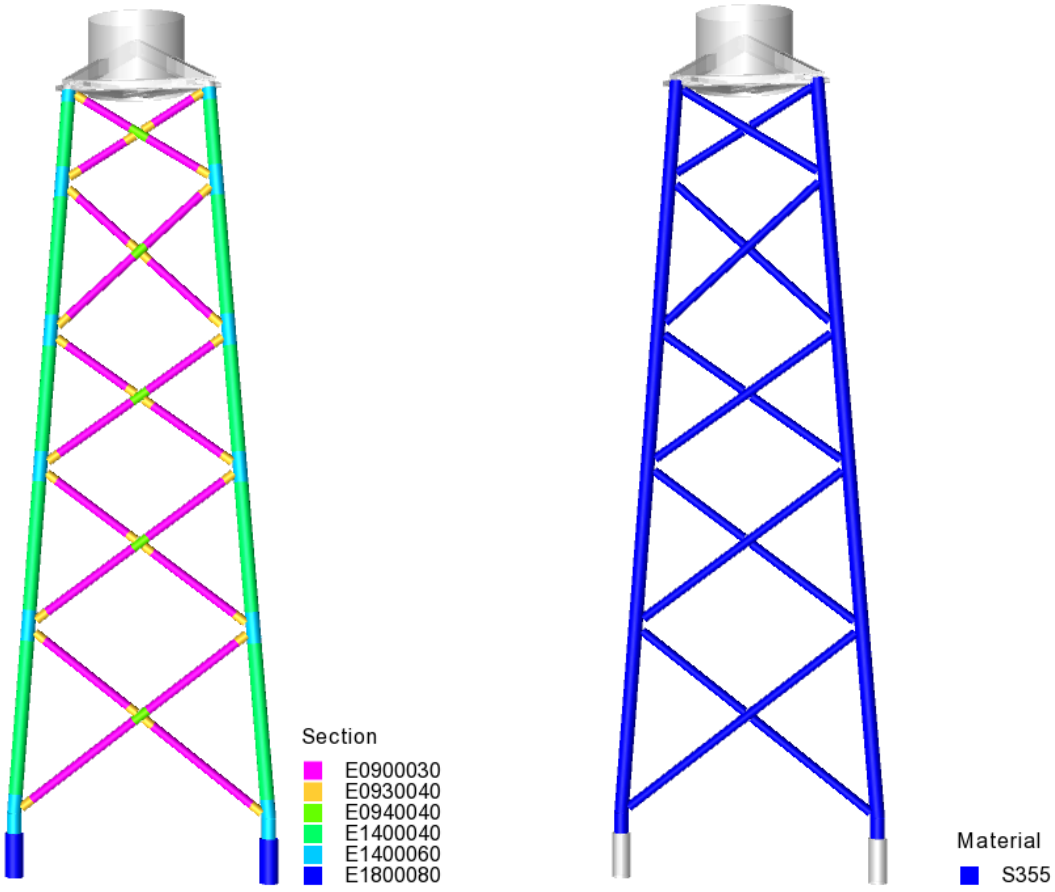

(a) Sections (b) Steel grades

Figure 5.4: Member properties for the skew-legged jacket.

5.4 Transition Piece

The transition piece (TP) used in combination with the jackets is a solution made by the company Vici Ventus. The concept is shown in Figure 5.5a for a three-legged jacket. The design of the TP was not in the scope, and the utilizations were not considered in the code check. However, both mass and stiffness of the TP were of great importance when considering the dynamic properties of the tower-jacket system and how the loads were transferred from the tower to the jacket. The TP was therefore simplified but modeled to resemble the real behavior. The model of the TP for the straight-legged jacket with four legs is shown in Figure 5.5b. It consists of the bottom part of the tower structure, four struts with an approximate angle of 35°, four supporting beams below the tower, and four smaller beams spanning between the legs of the jacket. The design is similar for the skew-legged jacket, but as the distance between the legs is smaller, the TP is naturally smaller. Approximate TP-masses are listed in Table 5.4. One of the assumptions made was that the TP provided a completely stiff connection between the tower and the jacket. This was achieved in the model by increasing the elastic modulus of the material in the TP until the natural frequency of the first lateral mode converged.

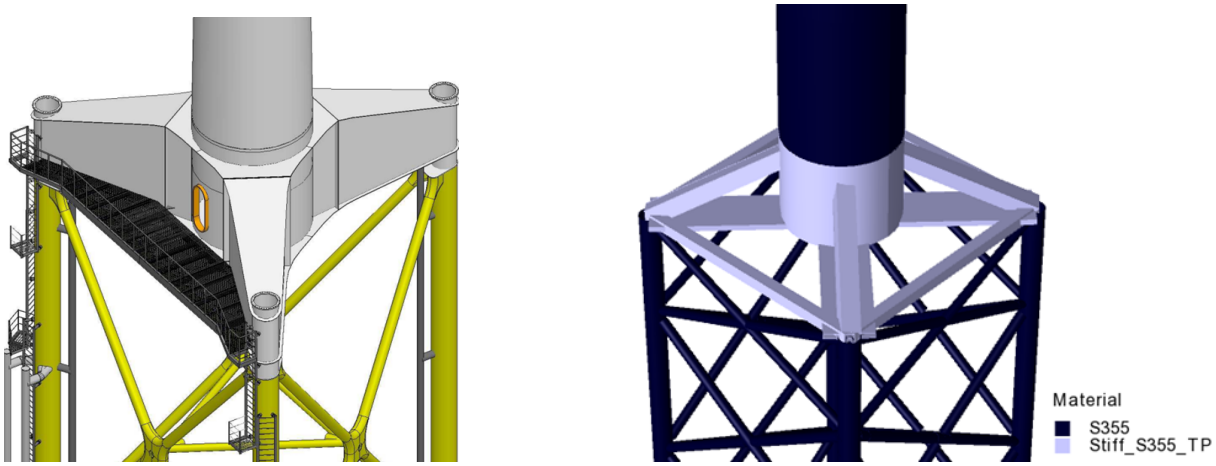

(a) TP concept by Vici Ventus [15]. (b) TP modelled in Sesam.

Figure 5.5: Transition piece: Concept and model.

Jacket	TP Mass [tonnes]
Straight-legged	405
Skew-legged	285

Table 5.4: Mass of the transition pieces.

5.5 Joints

The legs and bracings are connected in a K-shaped joint where the bracings are welded directly onto the legs. The X-shaped joints between bracings are achieved in a similar manner. The welded connections will be relatively stiff and are modeled as rigid connections in Sesam.

In proximity to the joints, the tubular members have been given an additional thickness, often referred to as a stub of heavy wall or a can. This is done in reference to the *NORSOK N-004* standard [11]. The stubs are visible in Figure 5.3 and Figure 5.4.

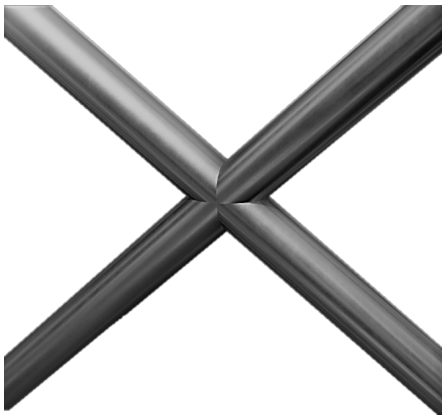

Figure 5.6: X-joint

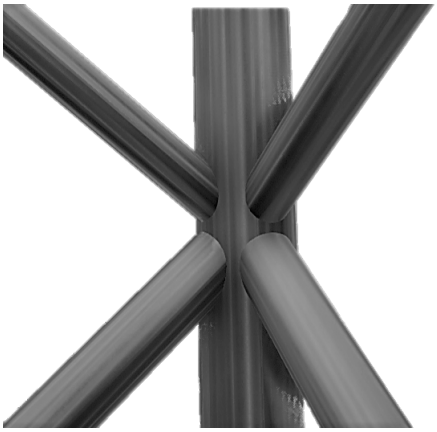

Figure 5.7: K-joint

5.6 Applied Loads - ULS

5.6.1 Turbine Loads

Wind loads from the turbine were imposed as point loads and moments at the tower top according to global coordinates. The loads are based on curves from the performance simulations presented by the NREL report [5] along with aeroelastic simulations performed in Bladed. The plots from these simulations can be found in Appendix A.2.

The curves in the NREL report illustrate that both thrust and generator torque increases with increasing wind speeds up to a rated value of 10.59 m/s. For above-rated wind speeds, the rotor speed is regulated by pitching the blades out of the wind flow, and the generator thrust decreases up to the cut-out wind speed of 25 m/. The torque, however, stays constant in the above-rated domain. An above cut-out wind case of 34 m/s was chosen for extreme conditions and corresponds to a condition with 50-year return period [10]. In this case, the turbine is assumed to be idle and was modeled as such in Bladed.

The model operates with six turbine load cases: Two for the rated wind speed, two for cut-out wind speed, and two for the above cut-out wind condition. Each of these were applied both at 0° (perpendicular) and at 45° to the jacket, illustrated in Figure 5.8. The wind loads utilized in the load cases for the ULS analysis are summarized in Table 5.5. The loads are equal for both jackets.

Load case	F_x [kN]	F_y [kN]	F_z [kN]	M_x [kNm]	M_y [kNm]	M_z [kNm]
Rated wind 0°	2500.00	0	0	20000.00	-54000.00	5000.00
Rated wind 45°	1767.77	1767.77	0	52300.00	-24000.00	5000.00
Wind above cut-out 0°	400.00	0	0	0	-65000.00	600.00
Wind above cut-out 45°	282.84	282.84	0	45962.00	-45962.00	600.00
Wind cut-out 0°	1200.00	0	0	21000.00	-50000.00	6250.00
Wind cut-out 45°	848.00	848.00	0	50200.00	-20500.00	6250.00

Table 5.5: Point loads and moments from the turbine in global coordinates.

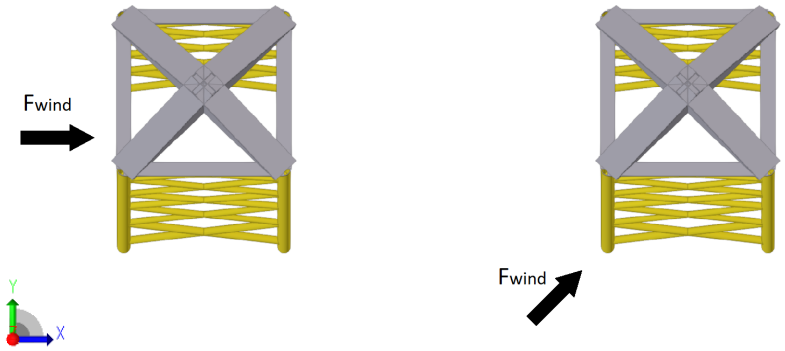

(a) Loads at 0°. (b) Loads at 45°.

Figure 5.8: Turbine load directions.

5.6.2 Tower and Jacket Loads

Hydrodynamic loads, self-weight, and wind loads on the turbine tower and jacket were calculated in Sesam based on the governing parameters listed in Table 5.6. The wind profile acting on the tower structure was modeled following *NORSOK N-003* [10]. It is equivalent to the profile and turbulence intensity described in Section 4.2.1.

Wave loads are calculated in Sesam by the use of Morison's equation as described in Section 4.3.2. Three main sea states were included in the model. One was an extreme sea state with a 50-year design wave with a height of 22 m and periods ranging from 13-16 s. This sea state was used in combination with the loads from the idle turbine at above cut-out wind speeds. The second sea state was for normal operating conditions with rated wind speeds. This sea state had a wave height of 7 m with a period of 8.5 s. This was the sea state with the largest turbine loads. The last sea state was for cut-out wind conditions and had a wave height of 9 m and a period of 9.5 s. All these wave heights and periods were chosen in accordance with *NORSOK N-003* and Olav Olsen, based on experience from similar projects. The waves were modeled by the use of Stokes' 5th order wave theory, and they were applied in the same directions as the wind loads, at 0° and 45° to the jacket. The drag and inertia coefficients were calculated according to *DNV-RP-C205* standard [6] with linear wave theory and based on the legs of the jacket. The calculation of these coefficients can be found in Appendix B. The legs were assumed to be fully covered by marine growth, increasing the total diameter, mass, and roughness of the members. In addition, complete flooding of the jacket legs was assumed.

The current velocity profile was calculated as described in Section 4.3.1 with preliminary values for tidal current velocity and mean wind speed taken from the appendix in the *NORSOK N-003* standard [10]. As a simplification, the total current was assumed to decrease linearly from 1.25 m/s at the surface to 0 m/s at the seabed. A power law expression better models the tidal current profile. However, the tidal current is small compared to the wind-generated current, so this simplification was not expected to invoke notable inaccuracies.

Values for density and thickness of marine growth were determined based on the *NORSOK N-003* standard. The total weight of the rotor-nacelle-assembly was modeled as a point mass in the center of the tower top based on values from the NREL report [5]. The center of gravity of the RNA does not coincide with the tower axis. This eccentricity induces a moment about the global y-axis, which was extracted from the aeroelastic simulations in Bladed and imposed at the tower top. This was included in the M_y component seen in Table 5.5.

Load parameters	Source	Value
Wind profile	NORSOK N-003 - 6.4.3	$C_D = 0.65$ (smooth cylinder) $z_0 = 10$ m $t_0 = 3600$ s (1-hour average)
Morison's coefficients (Full marine growth)	DNV - RP - C205 - 6	$C_D = 1.05$ $C_M = 1.20$
Sea state (Extreme conditions)	Dr. Techn. Olav Olsen AS NORSOK N-003	$U_0 = 34$ m/s $H = 22$ m $T = 13$-16 s
Sea state (Rated conditions)	Dr. Techn. Olav Olsen AS NORSOK N-003	$U_0 = 10.59$ m/s $H = 7$ m $T = 8.5$ s
Sea state (Cut-out conditions)	Dr. Techn. Olav Olsen AS NORSOK N-003	$U_0 = 25$ m/s $H = 9$ m $T = 9.5$ s
Current velocity at surface	DNV - ST - 0437 - 2.4.8 NORSOK N-003 - Appendix A	$V_m = 1.25$ m/s
Marine growth	NORSOK N-003 - 6.11.1	$t = 100$ mm (0 m - 40 m) $t = 50$ mm (41 m - 60 m) $\rho = 1300\ kg/m^3$
Nacelle/rotor assembly mass	NREL 15-MW RWT report	$m = 1212$ t

Table 5.6: Parameters used in Sesam to calculate loads from hydrodynamic conditions, gravity and wind.

5.7 Load Combinations - ULS

All six wind load cases were tested with simultaneous loads from waves, current, self-weight, and buoyancy. Wave and wind load actions were applied in the same global direction, which was expected to be critical. The loads were combined such that the chosen wave height and period corresponded with a correlating magnitude of the wind speeds. It can be seen from Table 5.8 and Table 5.5 that the maximum thrust on the turbine does not act simultaneously with the largest waves. The load factors used in the combinations are listed in Table 5.7. For environmental loads, the factor is normally 1.35. An extra safety factor of 1.1 was included in the wind load to account for gusts and uncertain wind conditions. The structure was then checked for maximum base shear and maximum overturning moment as the design load effect, resulting in 20 load combinations. The load combinations are summed up in Table 5.8.

Load effect	Factor
Dead load	1.1
Environmental loads excl. wind	1.35
Wind load	1.485
Buoyancy	1.0

Table 5.7: Load factors used in the model.

Load comb.	Waves			Wind		Buoyancy	Self-weight	Water level
	Dir	Height	Period	Dir	Speed			
LC1 (Shear)	0	22 m	13 s	0	34 m/s	Included	Included	LAT
LC2 (Moment)	0	22 m	13 s	0	34 m/s			
LC3 (Shear)	0	22 m	14.5 s	0	34 m/s			
LC4 (Moment)	0	22 m	14.5 s	0	34 m/s			
LC5 (Shear)	0	22 m	16 s	0	34 m/s			
LC6 (Moment)	0	22 m	16 s	0	34 m/s			
LC7 (Shear)	45	22 m	13 s	45	34 m/s			
LC8 (Moment)	45	22 m	13 s	45	34 m/s			
LC9 (Shear)	45	22 m	14.5 s	45	34 m/s			
LC10 (Moment	45	22 m	14.5 s	45	34 m/s			
LC11 (Shear)	45	22 m	16 s	45	34 m/s			
LC12 (Moment)	45	22 m	16 s	45	34 m/s			
LC13 (Shear)	0	7 m	7.5 s	0	10.59 m/s	Included	Included	LAT
LC14 (Moment)	0	7 m	7.5 s	0	10.59 m/s			
LC15 (Shear)	45	7 m	7.5 s	45	10.59 m/s			
LC16 (Moment)	45	7 m	7.5 s	45	10.59 m/s			
LC17 (Shear)	0	9 m	9.5 s	0	25 m/s	Included	Included	LAT
LC18 (Moment)	0	9 m	9.5 s	0	25 m/s			
LC19 (Shear)	45	9 m	9.5 s	45	25 m/s			
LC20 (Moment)	45	9 m	9.5 s	45	25 m/s			

Table 5.8: The load combinations included in the ULS code check of the jackets.

6 | Results: Dynamic Analysis

Dynamic analysis of structures was described in detail in Section 3.2, where the importance of resonance amplification was highlighted. *DNV-ST-0126* states that a dynamic investigation of a structure should be performed to avoid concurrence between the structural eigenmodes and energy-rich frequency ranges of dynamic loads being excited [8]. The turbine structure is mainly subjected to three dynamic loads, the rotor rotation, waves, and wind, which will all be assessed in this section. In order to evaluate the dynamic effects due to variable loads, the eigenvalue analysis was simulated according to the models described in Chapter 5. The reader should note that 1P and 3P in this section refer to the passing frequency of one of the rotor blades and the frequency of each blade-passing, respectively. 1P and 3P vary with the wind conditions the turbine is subjected to.

The first five eigenmodes of the straight- and skew-legged jacket are illustrated in Figure 6.1 and Figure 6.4, where red coloring implies high excitations and blue coloring suggests little movement from the state of equilibrium. Since the jackets are symmetrical, the lateral modes have an identical oscillation mode about its perpendicular axis, which was excluded from the illustration. The eigenfrequencies and eigenperiods were extracted on tabular form in Table 6.2 and Table 6.3, where the modes' oscillation patterns are indicated in the last column.

The wave and wind spectra along with the first eigenfrequency of each mode was plotted in Figure 6.2 and Figure 6.3. The spectra parameters along with the frequency ranges for 1P and 3P are listed in Table 6.1.

Plot	**Parameters**
Frøya Spectrum	$U_0 = 25$ m/s $z_0 = 10$ m
JONSWAP	$H_S = 1$ $T_P = 4.5$ $\gamma = 3.3$
1P	$f_{1P} = [\ 0.08\ ,\ 0.12\ ]$ Hz
3P	$f_{3P} = [\ 0.25\ ,\ 0.38\ ]$ Hz

Table 6.1: The chosen values for the spectra plots along with the frequency ranges of 1P and 3P for the wind turbine.

6.1 Straight-Legged Jacket

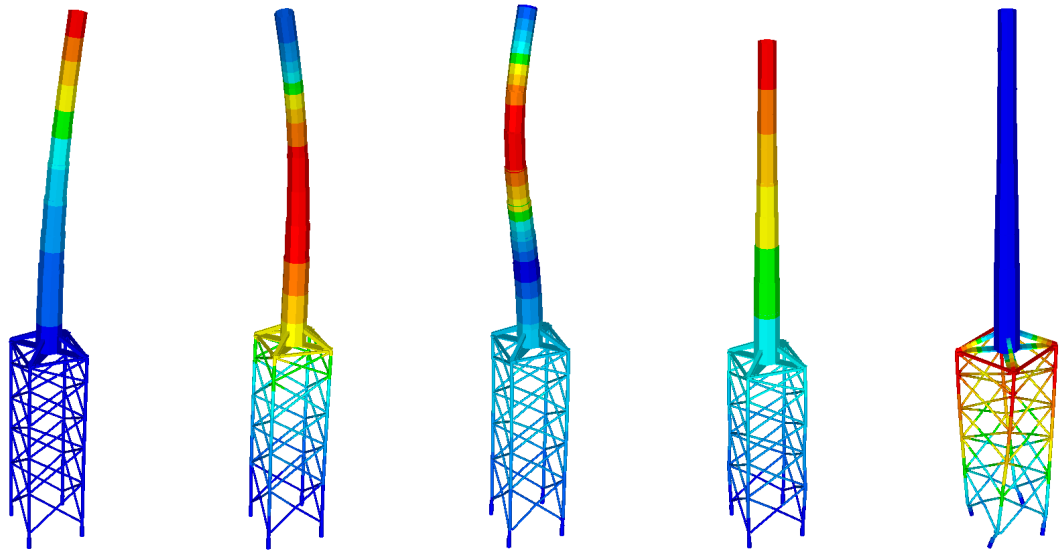

(a) 1. mode (b) 2. mode (c) 3. mode (d) 4. mode (e) 5. mode

Figure 6.1: The first five eigenmodes of the straight-legged jacket.

Mode	Frequency [Hz]	Period [s]	Shape
1.	0.2137	4.6785	1. Lateral
2.	1.2714	0.7865	2. Lateral
3.	3.1174	0.3208	3. Lateral
4.	3.4231	0.2921	Vertical
5.	3.5698	0.2801	Torsional

Table 6.2: The first five eigenfrequencies with corresponding eigenperiod for the straight-legged jacket.

To assess the risk of resonance of the structure due to the dynamic loads, their power spectral density (PSD) was plotted in Figure 6.2. One can observe that the first eigenfrequency of the straight-legged jacket deviates from the most energy-rich frequencies of the exciting loads, expect for the waves. *DNV-ST-0126* recommends the requirement given in Equation (6.1) to avoid rotor-induced vibrations [8]. The first eigenfrequency is located between the operating frequency ranges of 1P and 3P and satisfies the recommendation.

$$\frac{f_R}{f_{0,n}} \leq 0.95 \quad or \quad \frac{f_R}{f_{0,n}} \geq 1.05 \tag{6.1}$$

The first lateral eigenmode is expected to coincide with the peak of the JONSWAP-spectrum at some stages of the turbine's lifetime. The spectra plotted in Figure 6.2 were

normalized to simplify the interpretation of the frequency ranges, as the magnitude of the energy contents has no direct relation to the occurrence of resonance. It can be seen from Table 6.2 that the higher-order eigenmodes do not coincide with the critical frequency ranges of the dynamic loads.

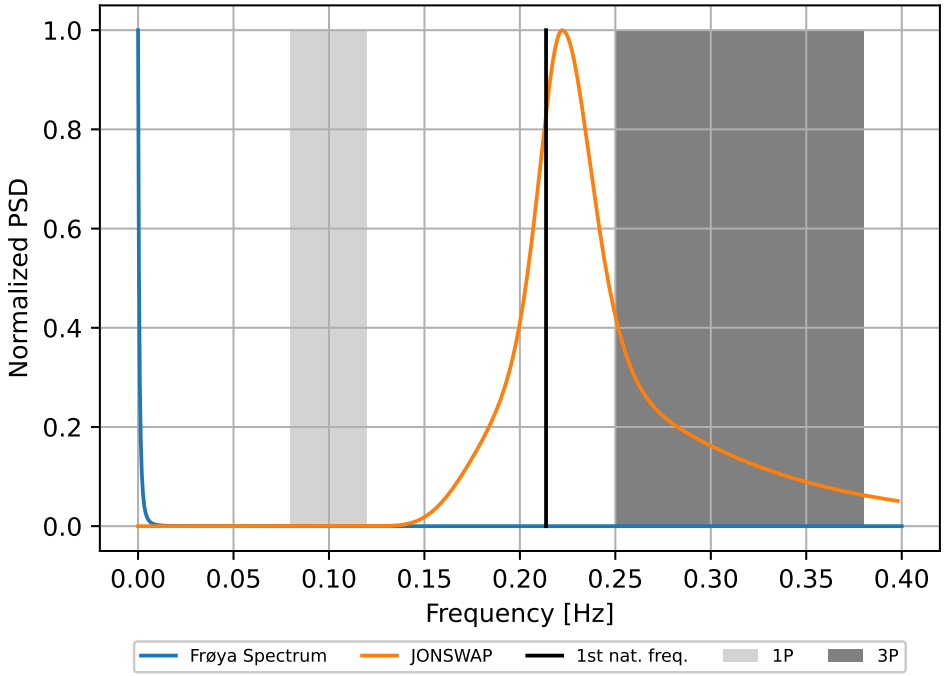

Figure 6.2: Straight-legged jacket-tower's natural frequency relative to the normalized power spectral density (PSD) of the dynamic loads.

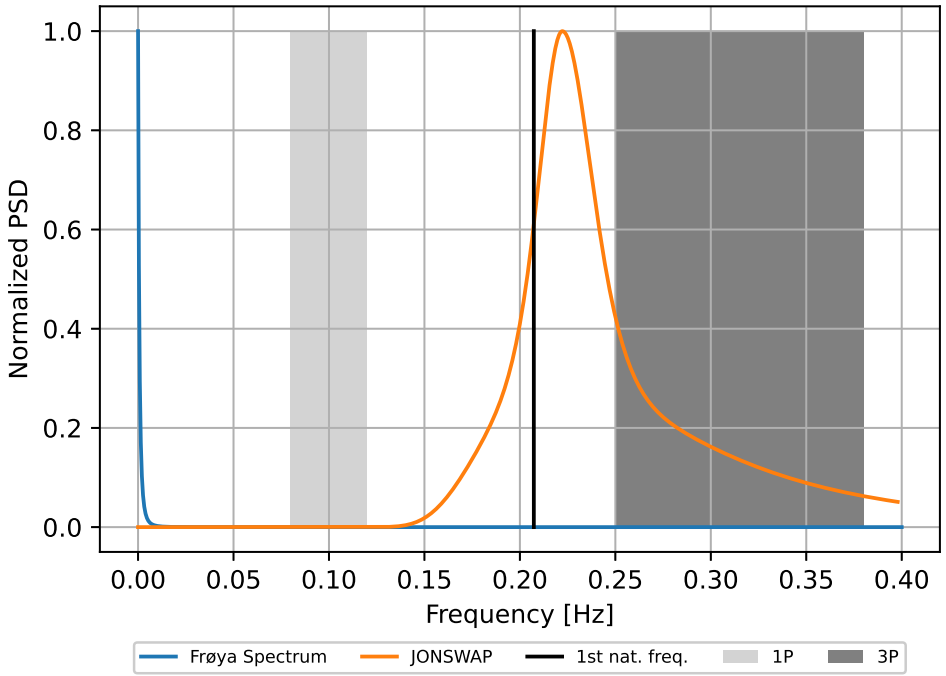

Figure 6.3: Skew-legged jacket-tower natural frequency relative to the normalized power spectral density (PSD) of the dynamic loads.

6.2 Skew-Legged Jacket

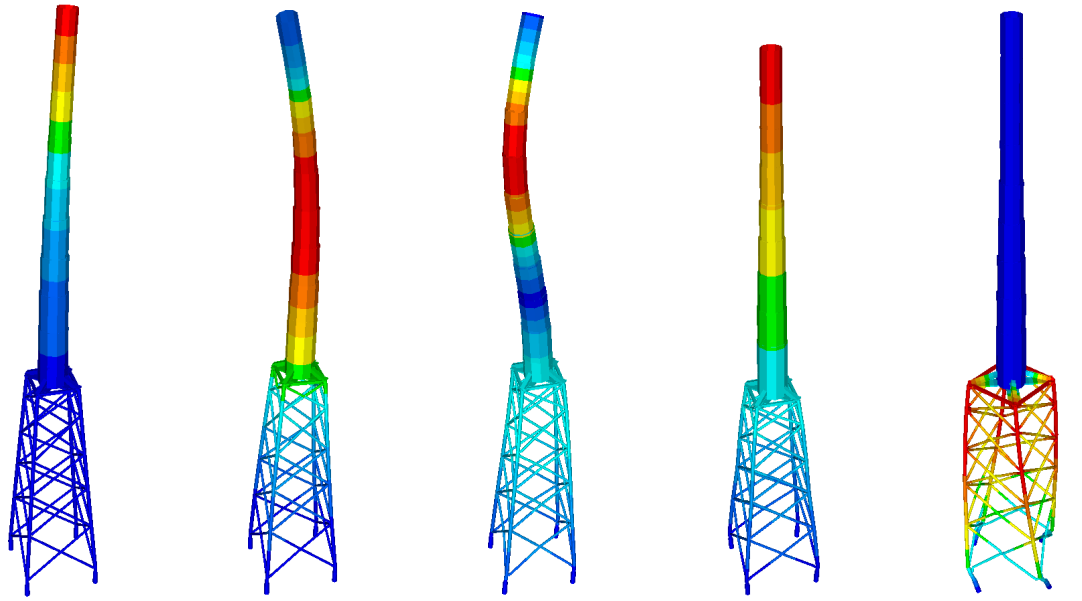

(a) 1. mode (b) 2. mode (c) 3. mode (d) 4. mode (e) 5. mode

Figure 6.4: The first five eigenmodes of the skew-legged jacket.

Mode	Frequency [Hz]	Period [s]	Shape
1.	0.2073	4.8239	1. Lateral
2.	1.3674	0.7313	2. Lateral
3.	3.1751	0.3150	3. Lateral
4.	3.4377	0.2909	Vertical
5.	4.6983	0.2128	Torsional

Table 6.3: The first five eigenfrequencies with corresponding eigenperiod for the skew-legged jacket.

As for the straight-legged jacket in Section 6.1, the PSDs for the exciting dynamic loads along with the first eigenfrequency of the skew-legged jacket are plotted in Figure 6.3. It can be observed that the first eigenfrequency deviates more than 5% from the operating turbine frequencies 1P and 3P and thus satisfies the requirement in Equation (6.1). The first eigenmode can be seen to be located relatively close to the peak of the wave spectrum, whereas the remaining modes are located at much higher frequencies.

6.3 Discussion

A comparison of the eigenfrequencies of the two analyzed jackets can be seen in Table 6.4. Positive differences indicate that the straight-legged jacket has a higher eigenfrequency for the given mode and visa versa. The first eigenfrequency for the jackets is in good agreement, which is a direct result of the transition piece modeling, where the material stiffness was increased due to the assumption of a completely stiff TP, see Section 5.4. Consequently, the two configurations are comparatively susceptible to resonance in the first eigenmode. However, resonance can be considered irrelevant for the higher-order modes for both jackets. Even though the first eigenmode is sensitive to the energy-rich wave frequencies, the analyses reports low excitations of the jacket members for the first eigenfrequency. The peak of the JONSWAP-spectra plotted in Figure 6.2 and Figure 6.3 shifts towards higher frequencies for a decreased spectral period T_P, see Section 4.3.2.2. Resonance in the tower is thus plausible, but this thesis was mainly focused on the jacket structures. Hence, excessive excitations due to resonance can be viewed as improbable to cause failure in the jacket structure but could be of importance for the propagation of fatigue cracks.

It should be noted that the torsional eigenmode yields the highest discrepancy between the two configurations. This result can also be observed from Figure 6.1 and Figure 6.4, where the straight-legged jacket is subjected to more excessive excitations than the skew-legged jacket. This signifies that the skew configuration has a higher torsional stiffness than the straight configuration. This could be a consequence of the skew jacket's larger moment arm at the foundation. A larger moment will make the skew jacket stiffer at the seabed where the structure is unbraced. This could explain the substantial difference in the 5. mode. This discrepancy inherits from the eigenvalue problem governing a dynamic analysis, described in Section 3.2, where a lower stiffness yields a lower eigenfrequency. In addition, the transition piece for the straight-legged jacket is significantly heavier than for the skew-legged jacket, where mass inertia is placed farther from the axis of rotation for the former.

Mode	**Frequency Straight[Hz]**	**Frequency Skew[Hz]**	**Δ[%]**
1.	0.2137	0.2073	3.0
2.	1.2714	1.3674	-7.5
3.	3.1174	3.1751	-1.9
4.	3.4231	3.4377	-0.4
5.	3.5698	4.6983	-32.8

Table 6.4: A comparison between the eigenfrequencies of the straight- and skew-legged jacket.

As discussed in Section 5.4, the elastic modulus was defined with a high value for the

members in the transition piece. This modeling assumption led to considerable differences in the dynamic properties of the OWTs, especially for the first lateral mode, second lateral mode, and the vertical mode, see Table 6.5. From a practical point of view, achieving a transition piece with stiffness equal to the one chosen in this thesis might prove difficult and expensive. Realistically, the stiffness of the transition piece will turn out to be somewhere between the chosen stiffness and the stiffness corresponding to an elastic modulus of 210 GPa. It will be especially challenging for the straight-legged jacket due to the required size of the TP. This inherits from the fact that axial stiffness decreases with an increased beam length. Though the eigenfrequencies of the OWT for a soft transition piece still deviate from the blade frequencies 1P and 3P, the eigenperiod might coincide with some wave periods depending on the site-specific wave statistics. By assuming an eigenfrequency between the two cases, one can expect eigenperiods in the range of $4.8 - 6.7$ s for the skew-legged jacket and $4.7 - 6.0$ s for the straight jacket in the first lateral mode. In addition, a less stiff transition piece would imply higher rotations in the TP, which would furthermore inflict high displacements in the top of the tower. A consequence of this result is an increased eccentricity for the RNA, which would induce a significant bending moment in the tower.

Mode	$f_{stiff,straight}$**[Hz]**	$f_{straight}$**[Hz]**	Δ**[%]**	$f_{stiff,skew}$**[Hz]**	f_{skew}**[Hz]**	Δ**[%]**
1. Lateral	0.2137	0.1666	-28.3	0.2073	0.1499	-38.3
2. Lateral	1.2714	1.2641	-0.6	1.3674	1.3439	-1.7
3. Lateral	3.1174	2.4300	-28.3	3.1751	2.5244	-25.8
4. Vertical	3.4231	2.1919	-56.2	3.4377	2.5437	-35.1
5. Torsional	3.5698	3.5448	-0.7	4.6983	4.6302	-1.5

Table 6.5: A comparison between the eigenfrequencies for the chosen stiff transition piece and a transition piece with the elastic modulus of 210 GPa.

7 | Results: Ultimate Limit State

This chapter will highlight the results from the analysis in the ULS. It will include code checking of the structural components for the two jacket configurations presented in Chapter 5. The code check was performed in Sesam based on *NORSOK N-004* [11], a design code developed with particular emphasis on cross-sections and joints frequently found in offshore conditions. The modeling choices that affect the code check were presented in Chapter 5 and will be further discussed in this section.

As mentioned in Section 3.1.2, the ULS-check aims to determine whether the components of the structure have sufficient strength and stability for the most critical load condition. The possibility for annual exceedance of the capacity should be equal to or less than 0.02%, i.e., a combined load effect whose return period is at least 50 years [8]. According to the design code *DNV-ST-0126*, all structural components in the jackets were checked for both excessive yielding and buckling.

For the straight-legged jacket, the utilization for the different members and joints are illustrated in Figure 7.1. In Table 7.1, the maximum element utilization in each row is listed along with component type, critical load combination, and critical *NORSOK N-004* code check equation. Similarly Figure 7.2 and Table 7.2 presents the utilizations in the skew-legged jacket design. Note that for K-joints and legs, there are six rows, where the 0. row equals the element/joint closest to the seabed. For reference, check Figure 5.1 and Figure 5.2. In the load combination column, the following notations describe the load properties:

RW	rated wind conditions with wind speed 10.59 m/s.
CW	cut-out wind conditions with wind speed 25 m/s.
EW	extreme wind conditions with wind speed 34 m/s.
Tx	refers to wave period x.
Hx	refers to wave height x.
Dx	refers to load direction x in degrees.
Sh	refers to wave loads resulting in maximum shear.
Mo	refers to wave loads resulting in maximum overturning moment.

7.1 Utilizations Straight-Legged Jacket

Member	Position	Component	Load Comb.	Equation	Utilization
Legs	0. row	1400x60 (S355)	EW: T16_H22_D45_Sh	Uf 6.27	0.78
	1. row	1400x40 (S355)	EW: T16_H22_D45_Sh	Uf 6.27	0.83
	2. row	1400x40 (S355)	RW: T7.5_H7_D45_Sh	Uf 6.27	0.61
	3. row	1400x40 (S355)	RW: T7.5_H7_D45_Sh	Uf 6.27	0.52
	4. row	1400x40 (S355)	RW: T7.5_H7_D45_Sh	Uf 6.27	0.44
	5. row	1400x40 (S355)	RW: T7.5_H7_D45_Sh	Uf 6.27	0.40
Bracings	1. row	900x30 (S355)	EW: T16_H22_D0_Sh	Uf 6.50	0.70
	2. row	900x30 (S355)	EW: T16_H22_D0_Sh	Uf 6.50	0.47
	3. row	900x30 (S355)	EW: T16_H22_D0_Sh	Uf 6.50	0.40
	4. row	900x30 (S355)	EW: T13_H22_D45_Sh	Uf 6.50	0.32
	5. row	900x30 (S355)	EW: T16_H22_D0_Sh	Uf 6.27	0.14
K-joints	0. row		EW: T16_H22_D0_Sh	Uf 6.57	0.54
	1. row		EW: T16_H22_D0_Sh	Uf 6.57	0.33
	2. row		EW: T16_H22_D0_Sh	Uf 6.57	0.34
	3. row		EW: T16_H22_D0_Sh	Uf 6.57	0.35
	4. row		EW: T13_H22_D0_Sh	Uf 6.57	0.32
	5. row		EW: T16_H22_D0_Sh	Uf 6.57	0.10
X-joints	1. row		EW: T16_H22_D0_Sh	Uf 6.57	0.62
	2. row		EW: T16_H22_D0_Sh	Uf 6.57	0.47
	3. row		EW: T13_H22_D0_Sh	Uf 6.57	0.30
	4. row		EW: T13_H22_D0_Sh	Uf 6.57	0.29
	5. row		EW: T16_H22_D45_Sh	Uf 6.57	0.09

Table 7.1: Utilizations of members and joints in the straight-legged jacket.

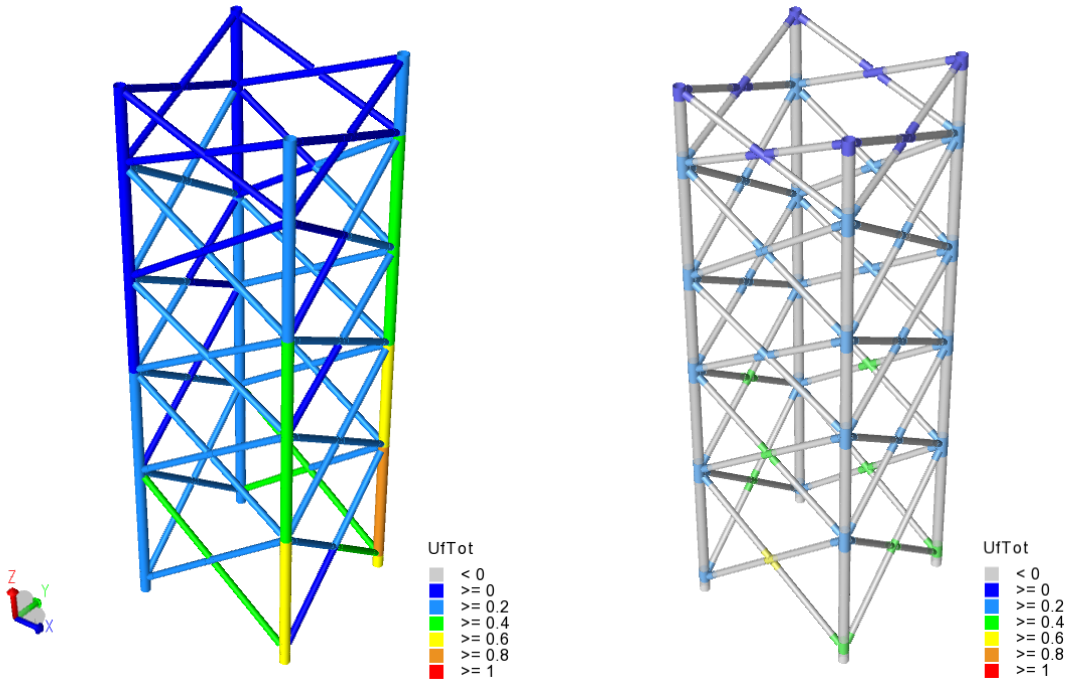

(a) Member utilizations.

(b) Joint utilizations.

Figure 7.1: Utilizations of members and joints in the straight-legged jacket.

7.2 Utilizations Skew-Legged Jacket

Member	Position	Component	Load Comb.	Equation	Utilization
Legs	0. row	1400x60 (S355)	EW: T16_H_22_D45_Mo	Uf 6.27	0.74
	1. row	1400x40 (S355)	EW: T16_H_22_D45_Mo	Uf 6.27	0.90
	2. row	1400x40 (S355)	RW: T7.5_H7_D45_Mo	Uf 6.27	0.59
	3. row	1400x40 (S355)	RW: T7.5_H7_D45_Mo	Uf 6.27	0.56
	4. row	1400x40 (S355)	RW: T7.5_H7_D45_Mo	Uf 6.27	0.52
	5. row	1400x40 (S355)	RW: T7.5_H7_D45_Mo	Uf 6.27	0.57
Bracings	1. row	900x30 (S355)	EW: T16_H22_D0_Sh	Uf 6.50	0.61
	2. row	900x30 (S355)	EW: T16_H22_D0_Sh	Uf 6.50	0.36
	3. row	900x30 (S355)	EW: T13_H22_D0_Sh	Uf 6.50	0.32
	4. row	900x30 (S355)	EW: T13_H22_D45_Mo	Uf 6.50	0.26
	5. row	900x30 (S355)	RW: T7.5_H7_D45_Sh	Uf 6.27	0.12
K-joints	0. row		EW: T16_H22_D0_Mo	Uf 6.57	0.34
	1. row		EW: T16_H22_D0_Sh	Uf 6.57	0.29
	2. row		EW: T16_H22_D0_Sh	Uf 6.57	0.30
	3. row		EW: T13_H22_D0_Sh	Uf 6.57	0.30
	4. row		EW: T13_H22_D45_Mo	Uf 6.57	0.25
	5. row		EW: T16_H22_D0_Mo	Uf 6.57	0.05
X-joints	1. row		EW: T16_H22_D0_Sh	Uf 6.57	0.47
	2. row		EW: T16_H22_D0_Mo	Uf 6.57	0.39
	3. row		EW: T13_H22_D0_Sh	Uf 6.57	0.31
	4. row		EW: T13_H22_D45_Mo	Uf 6.57	0.29
	5. row		EW: T16_H22_D0_Mo	Uf 6.57	0.07

Table 7.2: Utilizations of members and joints in the skew-legged jacket.

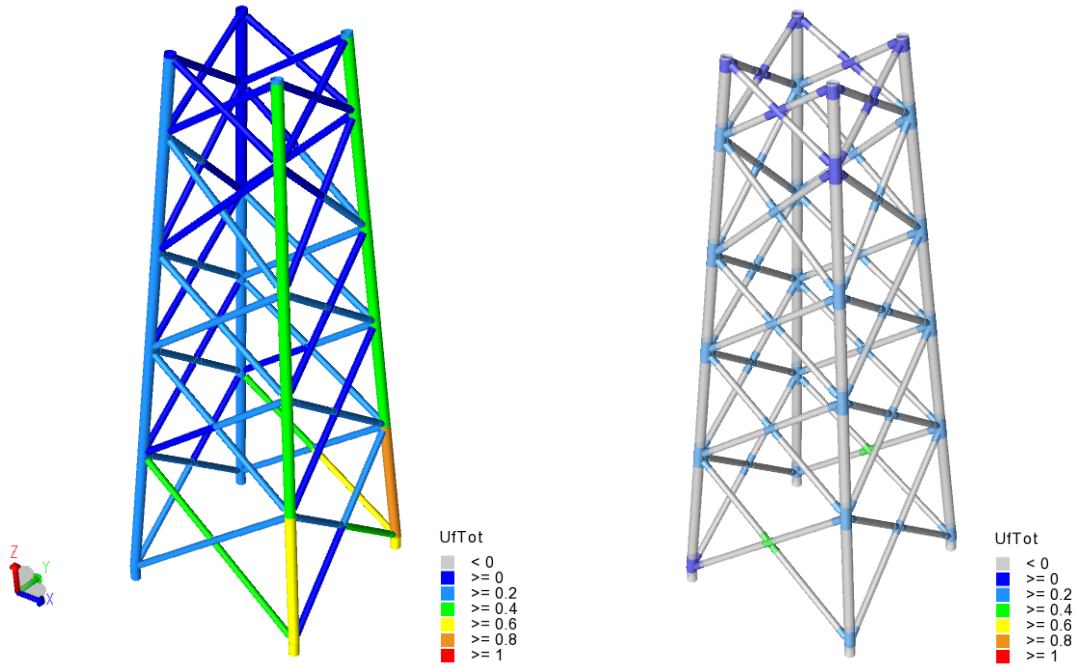

(a) Member utilizations.

(b) Joint utilizations.

Figure 7.2: Utilizations of members and joints in the skew-legged jacket.

7.3 Discussion

As can be seen from the presented tables, extreme conditions with a wind speed of 34 m/s are critical for most members and joints. Under these conditions, the turbine is idle, resulting in a smaller thrust than for the operating modes RW and CW. However, the design wave is significantly larger. For this structure configuration, it was observed that periods of 16 s impose greater loads for the same wave height compared to periods of 13 s and 14.5 s. One part of the structure that stands out in both jackets is the upper half of the legs. The utilization in these members is governed by load combinations with rated wind speeds. This implies that the upper parts of the legs are more affected by the forces and moments induced on the jacket from the turbine, whereas the rest of the jacket is more affected by wave loads.

The deformation and distribution of axial forces in the jackets for a few chosen loads and load combinations are shown in Appendix C. In short, the self-weight of the structure, tower, and RNA, leads to large compression forces in the legs of the jackets. Lateral loads from wind and waves are to a large degree taken up as tension/compression pairs in the bracings and the legs. In both designs, the critical wind and wave load direction for the legs is at 45° relative to the jacket. An explanation for this is: loads from this direction will mainly be taken up as axial moment pairs in two legs. For loads applied at 0°, all four legs are activated, leading to smaller forces in each leg. This is the opposite for the bracings, as only two planes of bracings are activated for loads imposed at 0°, whereas all four planes are activated when loaded at a 45° angle. Loads imposed at 0° are therefore critical for almost all rows of bracings.

The governing code check equations are similar for both jackets with eq. 6.27 for the legs, 6.50 for most bracings, and 6.57 for all joints. Eq. 6.27 checks for combined compression and bending and has reduction factors to account for buckling in the members. Eq. 6.50 is similar but also includes contributions for the hydrostatic pressure. Unlike the legs, the bracings are not flooded, and the effect of hydrostatic pressure was hence taken into account. However, the jackets were also tested with fully flooded bracings, and the contribution was observed to be insignificant. Finally, Eq. 6.57 is a resistance check for joints considering the interaction between axial force and bending moment in the braces. All critical equations are included in Appendix G.

Table 7.3 presents a comparison of the utilizations in the two jackets, where the straight jacket is used as reference. This table shows that the skew jacket has a lower utilization in all joints and bracings, whereas the straight jacket has a lower utilization in the legs. Loads, member sections, and material are similar for the two jackets. This implies that the two concepts distribute loads differently. The straight jacket distributes a more significant part of the loads to the bracings, whereas the skew jacket distributes a more significant

part to the legs.

The highest utilizations are all located in the lower half of the jackets, in the 1. row. The highest utilization in the legs is 0.83 in the straight jacket compared to 0.90 in the skew jacket. The highest utilization in the bracings is 0.70 in the straight compared to 0.61 in the skew. The highest utilization in the K-joints is 0.54 in the straight compared to 0.34 in the skew. Finally, the highest utilization in the X-joints is 0.62 in the straight compared to 0.47 in the skew.

The highest utilization difference in the jackets is located in the 5. row. The skew jacket has a 42.5% higher leg utilization but a 23.4% lower utilization in the bracings compared to the straight jacket. In addition, the skew jacket has lower utilization in both joint types, with 50.0% in the K-joints and 24.2% in the X-joints.

Member	**Position**	**Straight Jacket**	**Skew Jacket**	**Δ[%]**
Legs	0. row	0.78	0.74	5.1
	1. row	0.83	0.90	-8.4
	2. row	0.61	0.59	3.3
	3. row	0.52	0.56	-7.7
	4. row	0.44	0.52	-18.2
	5. row	0.40	0.57	-42.5
Bracings	1. row	0.70	0.61	12.9
	2. row	0.47	0.36	23.4
	3. row	0.40	0.32	20.0
	4. row	0.32	0.26	18.8
	5. row	0.14	0.12	14.3
K-joints	0. row	0.54	0.34	37.0
	1. row	0.33	0.29	12.1
	2. row	0.34	0.30	11.8
	3. row	0.35	0.30	14.3
	4. row	0.32	0.25	21.9
	5. row	0.10	0.05	50.0
X-joints	1. row	0.62	0.47	24.2
	2. row	0.47	0.39	17.0
	3. row	0.30	0.31	-3.3
	4. row	0.29	0.29	0.0
	5. row	0.09	0.07	22.2

Table 7.3: Comparison of the utilizations.

The utilization difference of the joints can be particularly important for FLS design. All joints were modeled with FLS capacity in mind, which was expected to be critical. This is the reason why most joints are below 50% utilization. The bracings and the legs could have been optimized further. This could be done by differentiating sections or by using S420 steel in components with high utilization. However, as there are significant uncertainties in environmental loads, turbine loads, soil conditions, water depth, etc., many assumptions had to be made. Some extra conservativeness in the design was considered beneficial to account for this.

8 | Modeling: Fatigue Limit State

The finite element models taken as input in the fatigue analysis was the same models that were designed and optimized in ULS. There are, however, some extra assumptions, and different loads, which will be described in this chapter. As opposed to the ULS, the FLS analysis was simulated in the time-domain.

Sesam offers two analysis methods for detailed design of offshore wind turbines. A sequentially performed method called the superelement method, and the integrated method. In the FLS analysis, *the superelement method* was chosen, see Figure 8.1 for an illustration of the workflow. The method exports a FE-mesh of the jacket and the transition piece containing stiffness-, mass-, and damping matrix along with the generalized hydrodynamic loads associated with each of the structure's eigenmodes. The next step of the superelement procedure was to export the six degrees of freedom at the interface node, the node connecting the substructure and tower, along with the matrices to an aeroelastic tool called Bladed. In Bladed, the superelement was simulated along with the wind turbine concept model, after which the wind turbine loads were extracted at the interface node. By utilizing such an approach, the simulation ensures kinematic compatibility between the dynamic properties of the substructure and the wind turbine at the interface node. Finally, the wind load simulations were exported to the software utilized for the fatigue calculations in this thesis, Sesam Wind Manager. Sesam Wind Manager combines the resulting time series from the aeroelastic simulation in Bladed and the hydrodynamic simulation in Wajac to assess the dynamic stresses' influence on fatigue damage in the jacket structure.

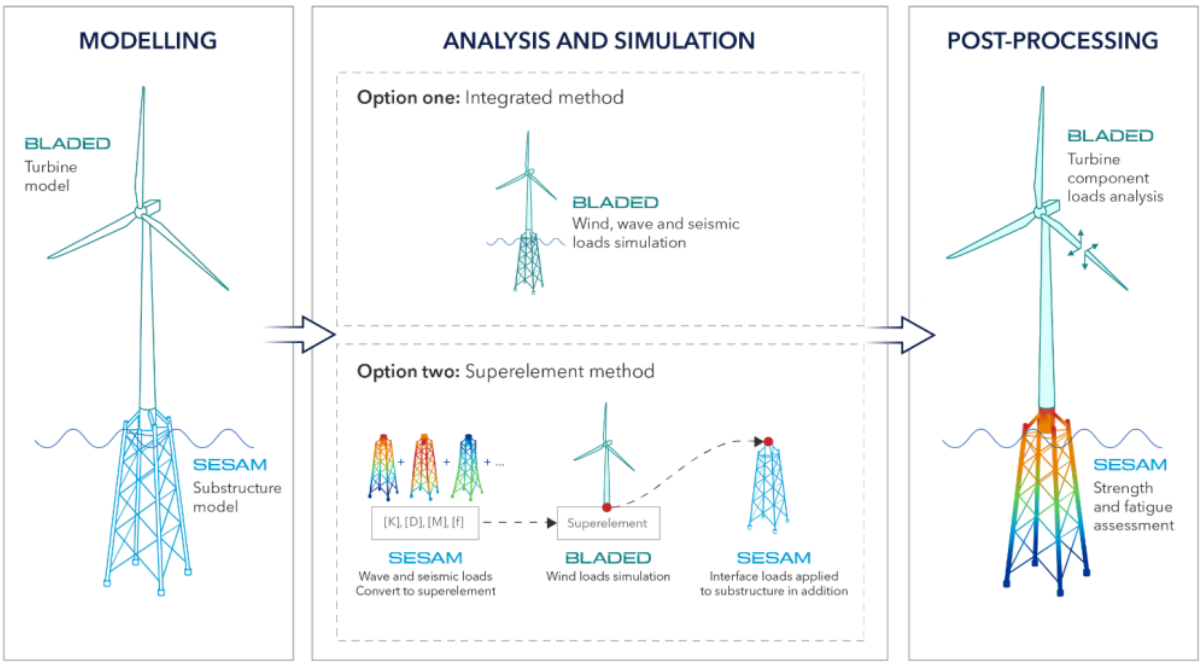

Figure 8.1: Sesams's two approaches for a detailed design of offshore wind turbines [34].

The modeling approach described above characterizes a coupled model simulation, where sufficient interaction between the structural responses and the dynamic aeroelastic- and hydrodynamic forces is ensured. Papers on decoupled and coupled models from 2014 [35], and from 2017 [36] describes a coupled model where the displacements, velocities, and accelerations of the substructure were passed onto an aeroelastic simulation tool. In this thesis, the eigenmodes and their corresponding structural properties were utilized for the interaction at the interface node. Sesam confirms this approach to be a coupled model though not equivalent to the former [34]. However, hydroelastic feedback is not accounted for in the aeroelastic model, as the wave loads are known from the start through the superelement.

The superelement was calibrated by performing a spectral- and spatial convergence analysis. Spectral convergence reveals how well the free vibration modes of the superelement correspond to those of the original model in GeniE, whereas a spatial convergence compares the responses for a specific loading [37]. A sufficient convergence was obtained by including 50 structural modes in the superelement, see Appendix E for an overview of the relative error for each mode.

8.1 Fatigue Properties

8.1.1 SCFs

The stress concentration factors for the different weld details and hot spots around the circumference of the tubular elements were modeled based on the parametric Efthymiou equations, where the geometric parameters were extracted from the finite element model. The Efthymiou equations utilized in the analysis for this report can be found in the appendix of *DNV-RP-C203* [7].

8.1.2 S-N Curves

The S-N curves applied in the calculations depend on whether the detail is welded from both sides or not, see Section 3.3.5. Therefore, it was found necessary to determine the common practice for welding in jackets to make a proper choice of S-N curve assignment. According to Olav Olsen, common practice is that the stubs and cans in a joint are welded with a double-sided weld. The leg and brace are then attached to the can/stub with a single-sided weld. By pursuing this approach, the single-sided weld, which is more susceptible to fatigue degradation, is placed a distance away from the joint, increasing the fatigue life of the detail. The double-sided welded joints were therefore utilized for all tubular joints by the assignation of T-curves.

B1-curve: assigned to the middle of the beam elements in the model, where there are no welded details.

D-curve: assigned to the end of the cans closest to the joint. For fatigue assessment of a double-sided circumferential butt weld.

F3-curve: assigned to the end of cans and stubs farthest from the joint. In other words, between the can/stub and the element. For fatigue assessment of a single-sided circumferential butt weld.

T-curve: assigned to all the joints, as all interconnections are tubular joints welded from both sides.

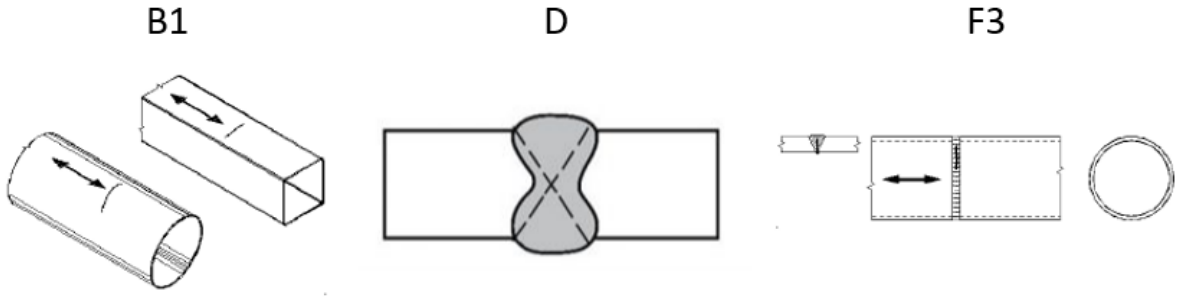

Figure 8.2: The welding details and their corresponding S-N curves [7].

8.2 Aeroelastic Model

The aeroelastic model of the 15-MW reference turbine was provided by DNV and simulated in the aeroelastic tool Bladed. Turbulence effects were excluded from the simulations due to no available site-specific measurements. All wake effects were also neglected as the thesis investigated fatigue damage on isolated wind turbines. The wind was simulated with an idled turbine for wind speeds below cut-in and above cut-out. The turbine was set to operational mode for simulations with wind speeds in the region of 3 - 25 m/s.

8.3 Load Assessment

The long-term environmental conditions were found statistically based on data from the report *Joint Probability Distribution of Environmental Conditions for Design of Offshore Wind Turbines* [26]. The report provided the long-term probability distributions for the significant wave height H_S, wave period T_Z, mean wind speed U and the wind-wave misalignment θ at Dogger Bank. The marginal probability distributions for these parameters can be found in Appendix D. The data is valid for sea states with a duration of three hours. Dogger Bank is a site located southwest of Southern North Sea 2, and was assumed to provide similar conditions. The distributions are based on 60 years of hindcast data released by the Norwegian Meteorological Institute.

The report also provided the correlation and all needed parameters and simplifications to produce a four-parameter joint distribution, as seen in Equation (8.1). This joint distribution can predict the most probable sea states at the location.

$$f_{\theta,U,H_S,T_Z} \approx f_\theta \cdot f_{U|\theta} \cdot f_{H_S|U} \cdot f_{T_Z|H_S} \tag{8.1}$$

For the FLS analysis, sea state probabilities were initially calculated from the four-parameter distribution. The problem with this approach was that even relatively large bin sizes in the parameters H_S, T_Z, U, and θ resulted in a vast amount of sea states. As the work in this thesis was conducted with limited computing power, further simplifications had to be made. Firstly, the wind-wave misalignment was neglected entirely. The wind-wave misalignment may excite low-damped vibrational modes for cross-wind excitations that changes the accumulated fatigue damage, see Section 3.2. Still, the importance in terms of fatigue is smaller than for the other parameters [26]. In addition, a jacket substructure is found to be less sensitive to wind-wave misalignment compared to, e.g., monopile substructures [38], which in turn decreases the importance of wind-wave misalignment in FLS analysis of jackets. Instead, the sea state probabilities were based on the joint probability distribution of the wave height and the mean wind speed. A

contour plot of this distribution is shown in Figure 8.3. This distribution was determined from the marginal distribution of the wind speed U and the conditional distribution of H_S given U. The joint probability:

$$f_{U,H_S} = f_U \cdot f_{H_S|U} \tag{8.2}$$

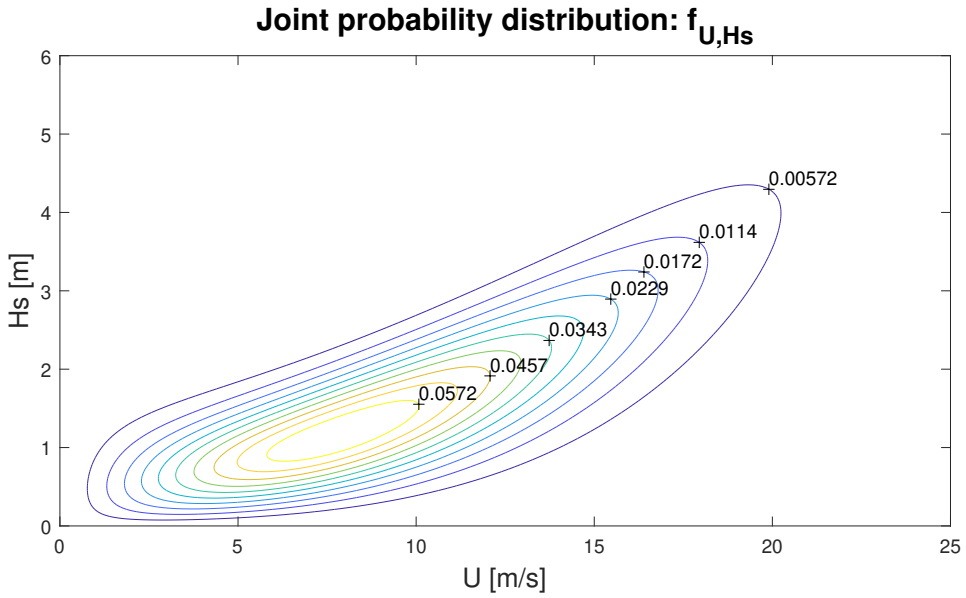

Figure 8.3: Contour plot of the joint distribution $f_{U,Hs}$.

For wave heights, the bin sizes were chosen to be 1m for all bins except the first bin, which had a size of 0.5 m. The probabilities in each bin were then integrated and assigned to the intermediate wave height value in the bin, giving probabilities for wave heights of 0.25 m, 1 m, 2 m, 3 m, 4 m, ... 20 m. Similarly, for the mean wind speeds, the bin sizes were chosen to be 2 m/s for all bins, resulting in probabilities for 1 m/s, 3 m/s, 5 m/s, ... 39 m/s. One remark is that this might be a non-conservative approach for some sea states, as the probabilities of the upper values in a range are assigned to the middle value. However, the goal of the thesis was not to provide a complete FLS design for the jackets but rather to catch the significant trends. For this purpose, the simplification was considered to be acceptable.

The period T_Z was included in the sea states as a function of the significant wave height H_S, which was interpolated from the conditional probability of T_Z given H_S. The period was rounded to the closest 0.5 s. This assumption is justified by the relatively high correlation of 0.79 between T_Z and H_S stated in the report [26]. The process is illustrated in Figure 8.4 and resulted in a linear function:

$$T_Z(H_S) = 0.8365 \cdot H_S + 3.4255 \tag{8.3}$$

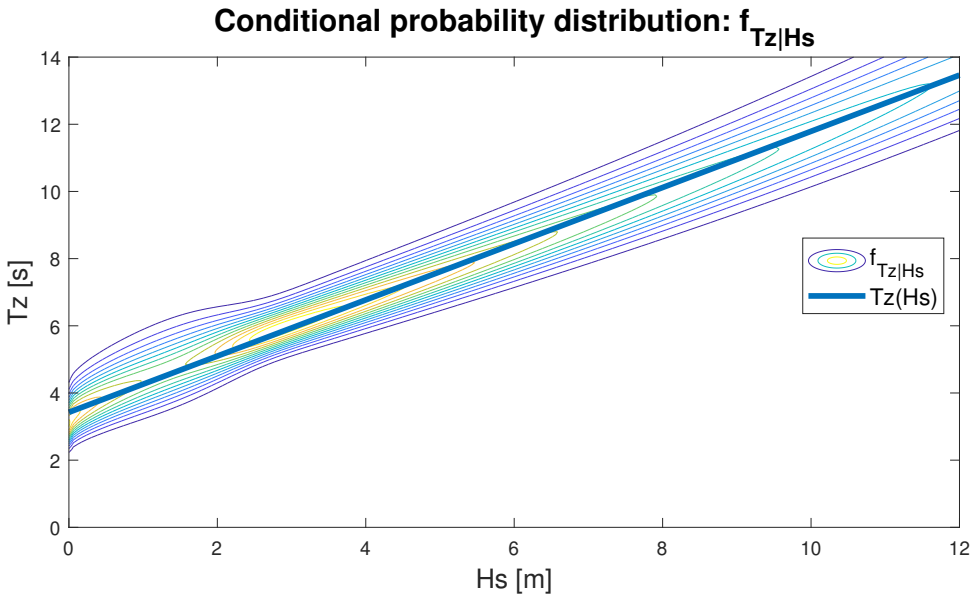

Figure 8.4: Contour plot of the conditional distribution $f_{Tz|Hs}$ and the linear function $Tz(Hs)$.

Appendix D includes the scripts used to calculate these sea state. Sea state prediction by this approach resulted in 420 sea states with varying probabilities. Only the 80 most probable sea states of the 420 were included to speed the calculations up further. At this point, the probability of occurrence decreased drastically. This captured sea states with significant wave heights up to 9 m and speeds up 31 m/s. Tall waves were in Chapter 7 found to be critical in ULS for most parts of the jackets. Therefore, it was desirable to investigate how they influence fatigue damage even though these sea states have a relatively low probability of occurrence. The ten most common sea states are listed in Table 8.1. These ten accounted for approximately 66.5% of the sea states.

Sea state	U **[m/s]**	H_S **[m]**	T_Z **[s]**	**Prob. [-]**
1.	7	1	4.5	0.1029
2.	9	1	4.5	0.0897
3.	11	2	5	0.0822
4.	5	1	4.5	0.0815
5.	13	2	5	0.0706
6.	9	2	5	0.0611
7.	11	1	4.5	0.0547
8.	3	1	4.5	0.0428
9.	15	3	6	0.0398
10.	15	2	5	0.0395

Table 8.1: The 10 most probable sea states at Dogger Bank.

8.4 Fatigue Analysis

The fatigue analysis was conducted with the superelement approach presented above. A simulation time length of 10 minutes for each of the 80 sea states is proposed by *ST-0437* to be adequate [9]. The Rayleigh coefficients for mass and stiffness proportional damping were chosen to be 0.001897 and 0.011745, respectively, which was utilized in a concept study for a similar jacket conducted by DNV [39]. The sea states determined in Section 8.3 contain no directional data for wind and sea, and the directions had to be chosen independently. Some generic directions relative to the jacket were selected to assess this parameter's importance, rather than actual meteorological directions. Two separate analyses were conducted on each jacket, with load directions similar to in the ULS analysis, at 0° and 45° relative to the jacket, see Figure 8.5. The directions were set constant throughout the whole simulation, meaning that no multi-directionality in the wind and waves was accounted for. Current was also not included in the sea states.

The code check was conducted with a DFF set to 3.0. In the software, the fatigue damage was then accumulated for 20 years which is proposed by *ST-0126* to be an appropriate lifetime. All S-N curves were applied according to Section 8.1.2. The S-N curve variations due to the environment (air, seawater, free corrosion) are chosen automatically by the software based on the limits set for the splash zone. The splash zone was assumed to span from 3.36 m below to 9.08 m above the surface level. The FLS code checking input file is included in Appendix F.

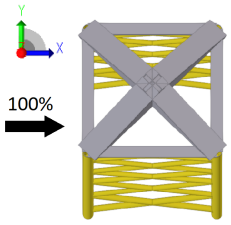

(a) Straight 0°

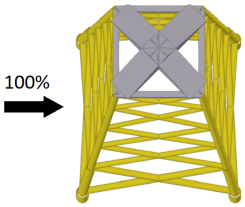

(b) Skew 0°

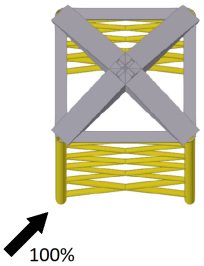

(c) Straight 45°.

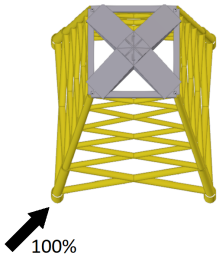

(d) Skew 45°.

Figure 8.5: Wind and wave directions for the fatigue analysis.

9 | Results: Fatigue Limit State

In this chapter, the results from the fatigue analysis are presented. Sesam Wind Manager scales damage values according to the chosen DFF of 3.0 and the target lifetime of 20 years. This means that all damage given above 1.0 exceeds the fatigue capacity of the structure.

In Section 9.1, the utilization of the top 10 hot spots in the two jackets is tabulated for sea states applied at 0° and 45° degrees relative to the jackets. The damage is listed in four tables, two for each jacket. The tables also provide information about what sea state contributed the most to the damage and what probability this sea state has. The critical joints are shown in Figure 9.1.

In Section 9.2 the maximum damage is shown in each row of joints, as opposed to the maximum hot spots. This section gives a side-by-side comparison of the performances of the two jackets in terms of fatigue.

In Section 9.3 the fatigue damage in the jackets is assessed for a variety of sea states, where either the wind speed or the wave height was held constant while the other was varied. This section is different from the former two in that it is a pure parametric study, where the goal was to determine whether wind or waves drove the fatigue damage in different parts of the jackets. In contrast to earlier the probability of each sea state was set equal and was not based on statistics from Dogger Bank. The presented damage is normalized.

A similar, but slightly different naming convention as the one used in Chapter 7 for the sea states is applied here:

Ux	refers to the mean wind speed x.
Hx	refers to wave height x.
Tx	refers to wave period x.

9.1 Maximum Fatigue Damage

9.1.1 Straight-Legged Jacket

Sea state	Prob.[%]	Joint	Side	Damage [-]
U7H1T4.5	10.3	37-X	Chord	2.623
U11H2T5	8.2	25-X	Chord	1.529
U11H2T5	8.2	30-X	Chord	1.424
U15H3T6	4.0	37-X	Chord	0.965
U7H1T4.5	10.3	37-X	Brace	0.501
U21H5T7.5	0.52	6-K	Chord	0.489
U21H5T7.5	0.52	8-K	Chord	0.470
U3H1T4.5	4.3	13-X	Chord	0.451
U3H1T4.5	4.3	13-X	Chord	0.445
U11H2T5	8.2	30-X	Brace	0.403

Table 9.1: Straight jacket loaded at 0°.

Sea state	Prob.[%]	Joint	Side	Damage [-]
U11H2T5	8.2	30-X	Chord	1.225
U3H1T4.5	4.3	37-X	Chord	0.529
U5H1T4.5	8.1	25-X	Chord	0.504
U5H1T4.5	8.1	13-X	Chord	0.503
U3H1T4.5	4.3	13-X	Chord	0.393
U11H2T5	8.2	30-X	Brace	0.354
U5H1T4.5	8.1	25-X	Chord	0.241
U3H1T4.5	4.3	37-X	Chord	0.209
U3H1T4.5	4.3	37-X	Brace	0.207
U5H1T4.5	8.1	25-X	Brace	0.181

Table 9.2: Straight jacket loaded at 45°.

The critical joints from Table 9.1 and Table 9.2 are shown in Figure 9.1a. It can be observed that the accumulated damage exceeds the utilization factor $\eta = 1.0$ in a few hot spots. For loads applied at 0° (x-direction in the figure), there is generally greater accumulated damage compared to the case with loads applied at 45°. For 0°-loads, both K- and X-joints are among the top 10 hot spots, whereas for loads applied at 45°, all are X-joints. The critical X-joints are located in the 4. row of bracings, which is in the splash zone. All critical K-joints are located in the 1. row.

The probability of occurrence has a significant influence on the fatigue damage, as some of the most frequent sea states are represented in the tables reported. Generally, for loads applied at 0°, most of the damage in the X-joints is due to sea states with variations around the rated wind speed, with moderate wave heights. On the other hand, the critical

sea state for the K-joints (joints 6 and 8) has a lower probability, with taller waves, higher wind speeds, and longer periods. Interestingly, when the loads are applied at 45°, the most damaging sea states are characterized by lower wind speed, small wave heights, and short periods.

9.1.2 Skew-Legged Jacket

Sea state	Prob.[%]	Joint	Side	Damage [-]
U11H2T5	8.2	39-X	Chord	1.119
U11H2T5	8.2	39-X	Chord	0.397
U11H2T5	8.2	35-X	Chord	0.363
U11H2T5	8.2	18-X	Chord	0.332
U11H2T5	8.2	25-X	Chord	0.320
U23H6T8.5	0.16	7-K	Chord	0.250
U23H6T8.5	0.16	8-K	Chord	0.248
U21H5T7.5	0.52	14-K	Chord	0.213
U11H2T5	8.2	39-X	Brace	0.187
U21H5T7.5	0.52	13-X	Chord	0.153

Table 9.3: Skew jacket loaded at 0°.

Sea state	Prob.[%]	Joint	Side	Damage [-]
U5H1T4.5	8.1	35-X	Chord	0.829
U11H2T5	8.2	25-X	Chord	0.414
U5H1T4.5	8.1	35-X	Chord	0.283
U11H2T5	8.2	39-X	Chord	0.214
U11H2T5	8.2	18-X	Chord	0.209
U5H1T4.5	8.1	35-X	Chord	0.150
U11H2T5	8.2	25-X	Brace	0.110
U23H6T8.5	0.16	14-K	Chord	0.093
U23H6T8.5	0.16	14-K	Chord	0.092
U21H5T7.5	0.52	17-K	Chord	0.090

Table 9.4: Skew jacket loaded at 45°.

As can be seen from Table 9.3 and Table 9.4, the skew jacket has less fatigue damage in the top 10 hot spots compared to the straight jacket, and the damage exceeds $\eta = 1.0$ for only one joint. Similar to the straight jacket, damages are generally more significant for loads applied at 0°. High probability sea states characterized by rated wind speed contributed most for all X-joints. The primary contributing sea states for the K-joints have a lower probability, taller waves, higher wind speeds, and longer periods.

For loads applied at 45°, all hot spots have utilization below 1. For the skew jacket, this direction has pretty similar critical sea states as when loads are applied at 0°, with only one joint governed by a below-rated sea state.

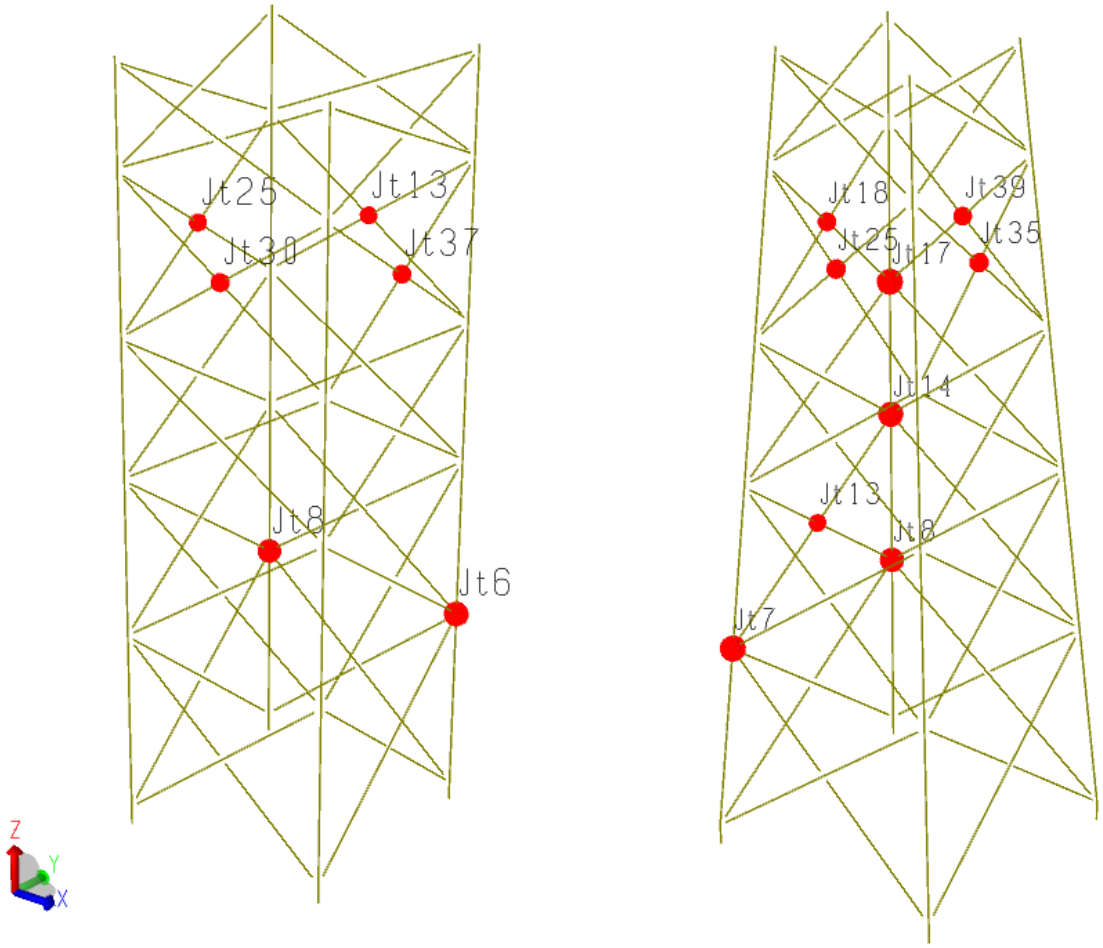

(a) Straight jacket.

(b) Skew jacket.

Figure 9.1: Joints with highest fatigue damage.

9.2 Fatigue Damage Comparison

The fatigue damage by row of joints in the two jacket configurations is shown in Figure 9.2 for the K-joints and in Figure 9.3 for the X-joints. The x-axis in the chart specifies the row of joints, where K0 and X1 are the joints closest to the seabed. The damage for each row, plotted on the y-axis, was retrieved from the highest damaged hot spot in the highest damaged joint in the row. In short, the skew jacket performs better, with less accumulated damage in almost all joints. Wind and waves applied at 0° (perpendicular to the jacket) result in more fatigue damage.

From Figure 9.2, it can be seen that the K-joints have the highest utilizations in the lower part of the jackets. One exception is row K0, which stands out with relatively low damage. All joints have accumulated damage below the utilization factor $\eta = 1.0$.

From Figure 9.3, it can be seen that the damage is insignificant in all joints, except for the X4 row. In this row, all analyses exceeds the utilization factor, except for the skew jacket

loaded at 45°. In particular, the straight jacket performed poorly, with a maximum hot spot damage of 2.63. Even for a chosen DFF of 2.0, which can be used in the splash zone only if inspection is performed regularly, the straight jacket still exceeded the utilization factor. The significant damage in this row is primarily due to the joints being located in the splash zone.

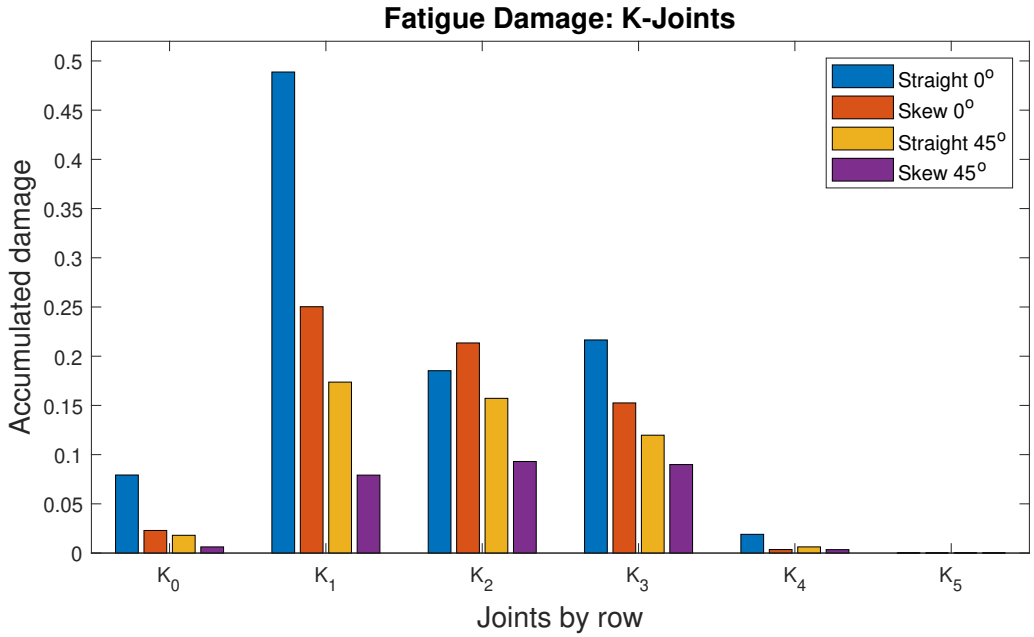

Figure 9.2: Maximum fatigue damage in the K-joints.

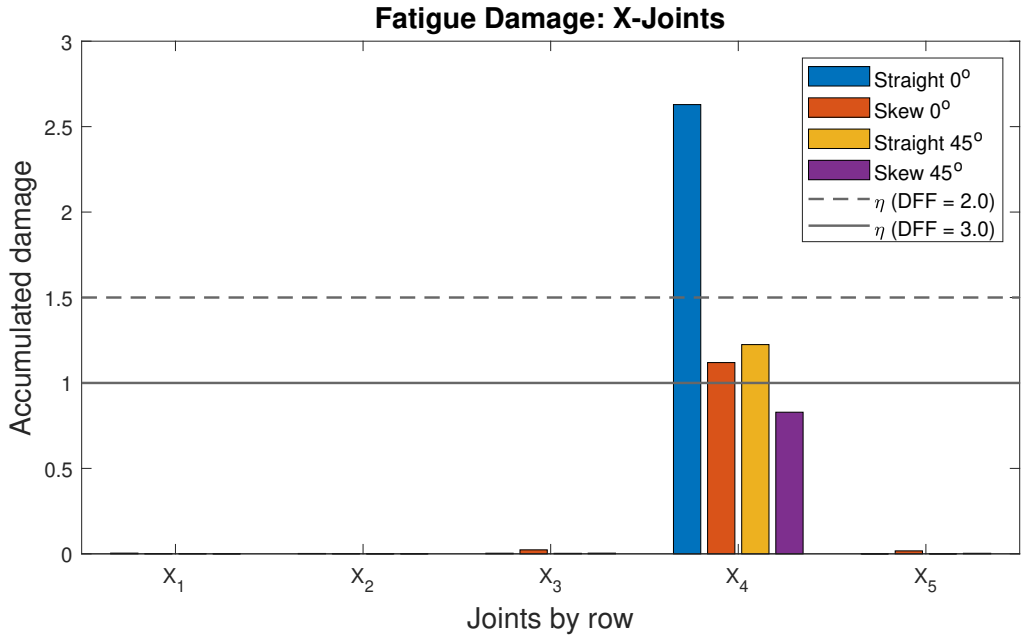

Figure 9.3: Maximum fatigue damage in the X-joints.

9.3 Fatigue Influence for Varying Wind and Waves

The following section will look into the effect of varying wind speed and wave height on the damage in the jacket structures. To investigate this, normalized damage was plotted against height above seabed for sea states for varying wind speeds and wave heights independently. The damage was extracted and plotted for K-joints for the same leg, the leg with most damage overall, and for X-joints on the jacket side facing negative x-direction, see Figure 9.1. All sea state simulations were performed with equal probability of occurrence to achieve a thorough assessment of how these parameters affected the damage. Normalization was accomplished by dividing the damage in the joints for all sea states by the highest utilized joint included in each plot. Directional effects were investigated by running the simulations with the environmental loads at 0° and 45° relative to the jackets. To establish a link between the plots for varying wind and waves, the sea state $U17H2T5$ was included in all the plots.

The normalized damage in the straight jacket with loads applied along the x-axis was plotted for the legs and braces in Figure 9.4 and Figure 9.5 respectively. Similarly for loads imposed at 45° to the straight jacket, see Figure 9.6 and Figure 9.7.

The corresponding plots for the skew jacket can be seen in Figure 9.8, Figure 9.9, Figure 9.10, and Figure 9.11.

9.3.1 Straight-Legged Jacket

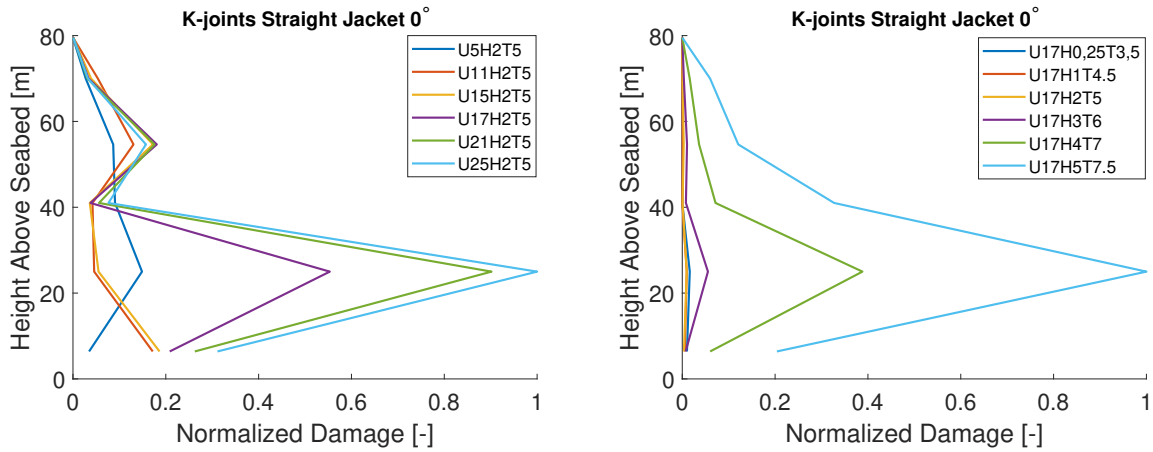

(a) Varying wind speed.

(b) Varying wave height.

Figure 9.4: Normalized damage in the legs plotted against height above seabed for the straight jacket.

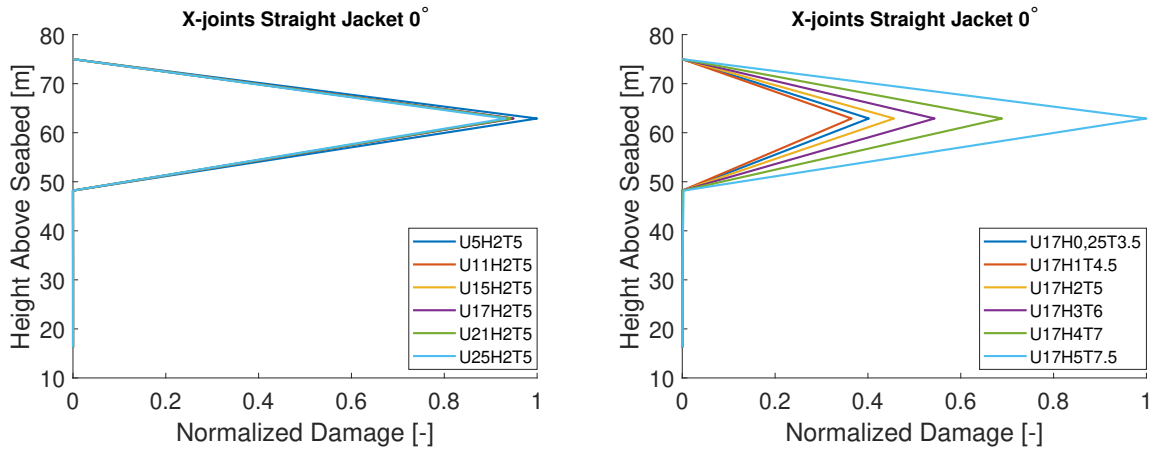

(a) Varying wind speed.

(b) Varying wave height.

Figure 9.5: Normalized damage in the braces plotted against height above seabed for the straight jacket.

From the plots with loads set 45°, the normalized damage can be seen to be less concentrated than for the case with loads 0° to the jacket. This reflects the maximum utilizations listed in Table 9.1 and Table 9.2, where the latter simulation yields considerably less fatigue damage, especially in the legs of the jacket. Additionally, it can be seen that rated wind conditions (10.59 m/s) tend to induce fatigue damage in the K-joints in the 4. row of the straight jacket when the loads are imposed 45° relative to the jacket, see Figure 9.6a.

The results for 45°, see Figure 9.5b and Figure 9.7b, show a higher discrepancy in the braces' normalized damage between high and low waves. For instance the sea state

$U17H1T4.5$ yielded substantially higher normalized damage when loads were applied 0° relative to the jacket than for loads set to 45°. For varying wind, it is worth noting that the load case $U5H2T5$ shows twice the normalized damage compared to the other wind speeds, see fig. 9.7a for 45°.

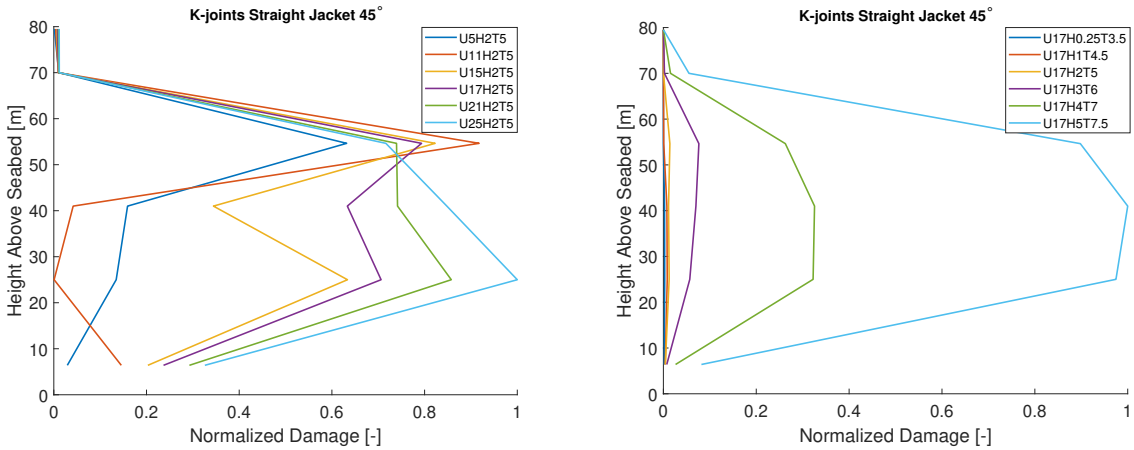

(a) Varying wind speed.

(b) Varying wave height.

Figure 9.6: Normalized damage in the legs plotted against height above seabed straight jacket, loaded at 45°.

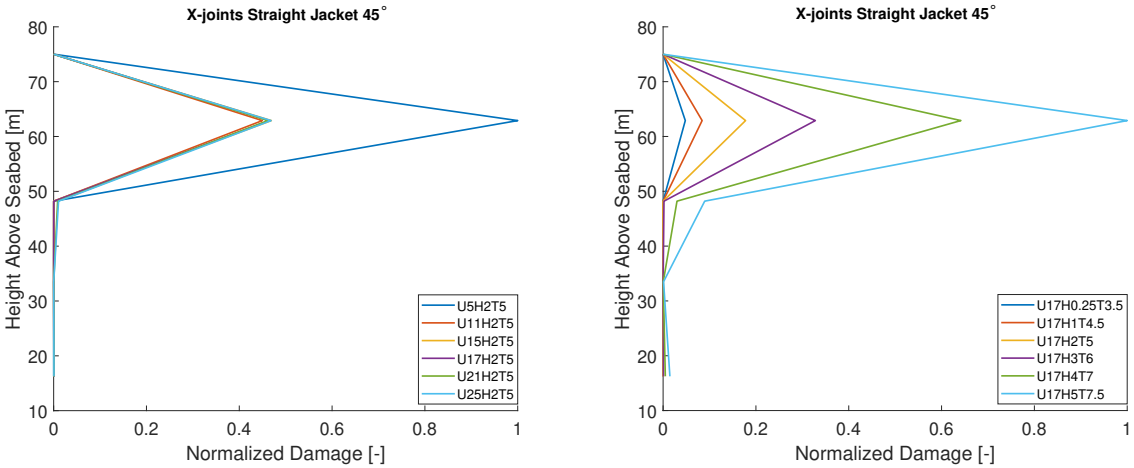

(a) Varying wind speed.

(b) Varying wave height.

Figure 9.7: Normalized damage in the braces plotted against height above seabed for the straight jacket, loaded at 45°.

9.3.2 Skew-Legged Jacket

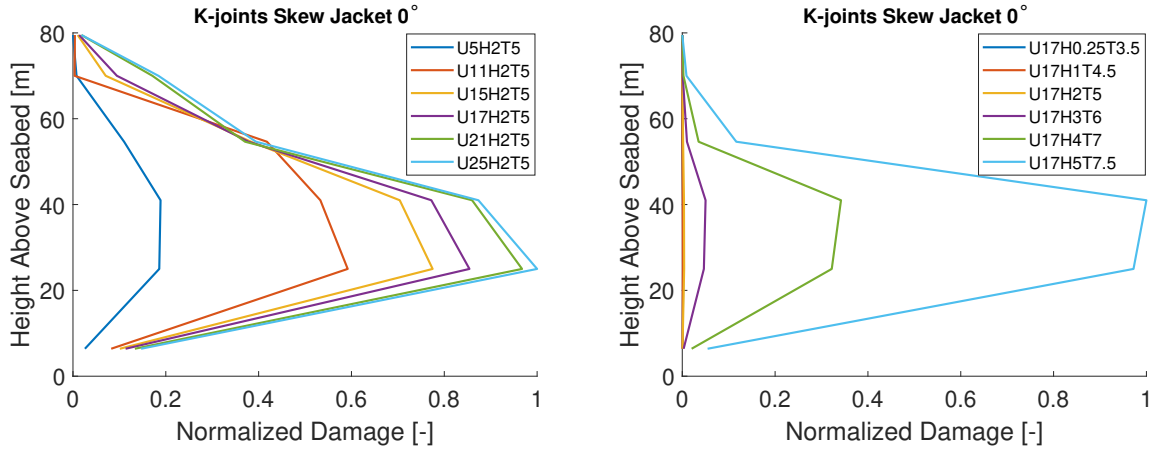

(a) Varying wind speed.

(b) Varying wave height.

Figure 9.8: Normalized damage in the legs plotted against height above seabed for the skew jacket.

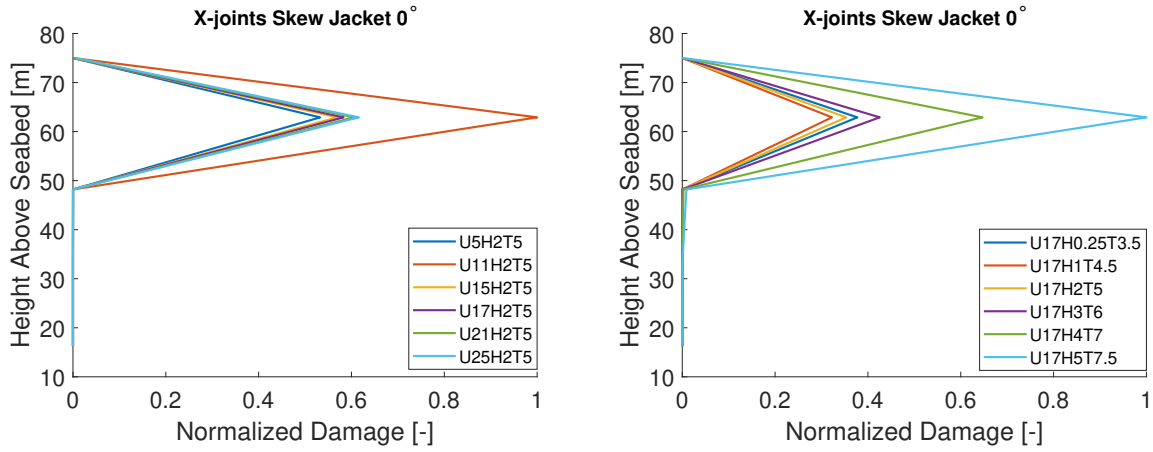

(a) Varying wind speed.

(b) Varying wave height.

Figure 9.9: Normalized damage in the braces plotted against height above seabed for the skew jacket.

The plots in Figure 9.8 show a relatively similar normalized damage in the legs for loads applied at 0°, compared to the straight jacket shown in Figure 9.4.

As for the straight-legged jacket, the normalized damage in the legs of the skew-legged jacket appear to be less concentrated for loads at 45°. However, the damage seems to be shifted towards the 4. row for the K-joints. The shift emerges most dominant for variation in the waves, see Figure 9.10b.

Rated wind appears to inflict higher normalized damage in the braces for loads propagating at 0° relative to the skew jacket than 45° relative to the other chosen wind speeds, see Figure 9.9a.

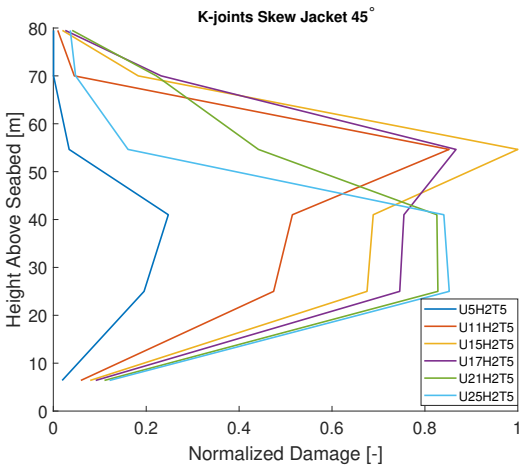

(a) Varying wind speed.

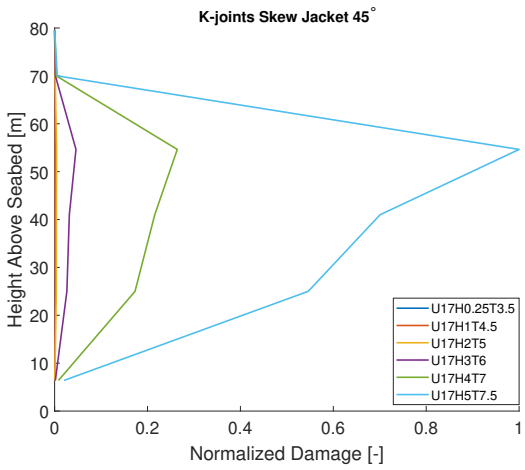

(b) Varying wave height.

Figure 9.10: Normalized damage in the legs plotted against height above seabed skew jacket, loaded at 45°.

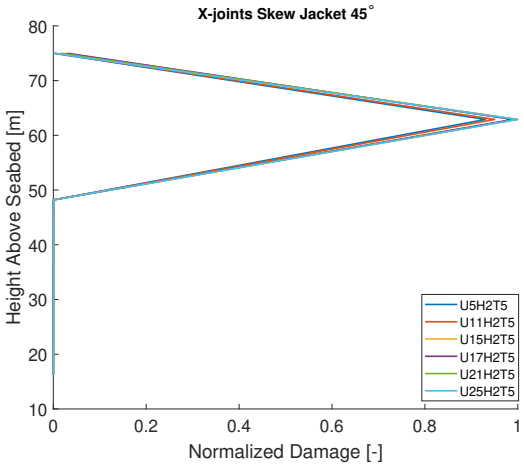

(a) Varying wind speed.

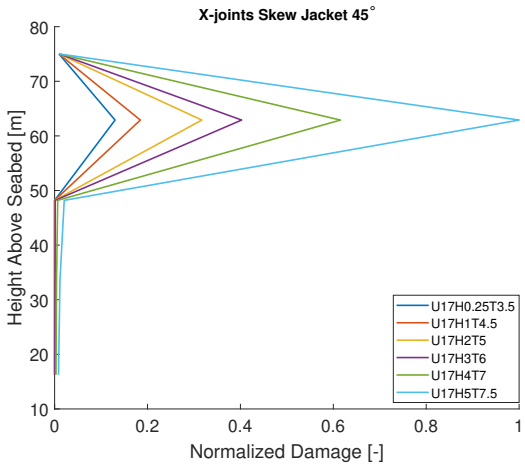

(b) Varying wave height.

Figure 9.11: Normalized damage in the braces plotted against height above seabed for the skew jacket, loaded at 45°.

9.4 Discussion

9.4.1 Maximum Fatigue Damage

The tables that were presented in Section 9.1 revealed some interesting trends. Firstly, all critical hot spots listed in the tables are in the joints assigned with the T-curve. Even though the joints were expected to be critical in terms of fatigue, the one-sided butt welds between the element and can/stub, assigned with the F3-curve, were also expected to show prominent damage. This was not the case, and none of these hot spots is among the top 10.

Secondly, for the hot spots in the X-bracings, the critical sea states are some of the most frequent sea states with wind conditions in proximity to or below the rated wind speed. Some examples are sea states such as *U11H2T5*, *U7H1T4.5*, *U5H1T4.5* and *U15H3T6*. Therefore, the X-bracings seem to be more susceptible to damage due to operating conditions, where turbine wind loads are the dominating contributor.

In contrast, some other hot spots are governed by sea states that appear less frequently. These hot spots are all located in K-joints, mainly in the lower parts of the jacket. The primary damage contributing sea states for these hot spots are sea states such as *U23H6T8.5* and *U21H5T7.5*, with higher wind speeds and taller waves. The turbine loads are drastically decreased for above-rated wind speeds as the blades are pitched out of the wind. This implies that the K-joints seem to be more susceptible to damage due to waves rather than turbine loads.

The sea states appearing in the top 10 hot spots in the straight jacket loaded at 45° stand out from the other analyses. This particular configuration has other damage-driving effects. As can be seen from Table 9.2, most of the top 10 hot spots in this configuration have small loads from wind and waves, with sea states such as *U3H1T4.5* and *U5H1T4.5*. This may seem strange, but there are two possible explanations. Firstly, the waves with heights 1-2 m in these sea states have periods of 4.5-5 s, which coincides well with the 1. eigenmode of the system. The 1. eigenperiod is 4.68 s for the straight jacket and 4.82 s for the skew jacket. However, this mode is mainly characterized by deflections in the tower and not the jacket itself. This was discussed in detail Chapter 6. All eigenmodes with large jacket deflections have frequencies far above any load frequency from normal environmental loads from wind and waves. Because of this, the effect from resonance is probably not critical in terms of damage contribution. If it had been, this would have also been reflected in the other configurations.

The main contribution is probably due to the wavelength in these sea states in relation to the jacket geometry. In linear theory [6], wavelength of deep water waves can be approximated by the equation:

$$\lambda = \frac{g \cdot T^2}{2\pi} = 1.56 \cdot T^2 = 1.56 \cdot 4.5^2 = 31.59m \tag{9.1}$$

The distance between the legs in the straight jacket is 22 m, resulting in a diagonal distance between legs of 31.11 m. The leg closest and farthest from the incoming waves will experience simultaneous wave crests, while the middle legs will experience wave troughs. For waves with a period of 4.5 s, the bracings will therefore be put in a state of alternating tension and compression, with a relatively large stress range, even for small waves, see Figure 9.12. In this illustration, the wave loads on the braces themselves are not considered, but the argument stays the same. One remark is that this will probably not result in actual alternation between tension and compression in the bracings, but rather relieving and increasing stresses without the load changing sign. This is because of the constant thrust load from the turbine, but as discussed in Section 3.3; it is the stress range due to cyclic loads and not the absolute magnitude of the stresses that induces crack propagation. It is also worth noting that the damages due to this effect might be inflated due to the assumptions used to derive the statistical model for the sea states. When the waves were discretized, wave height values from 0.5 - 1.5 m were lumped into the value of 1 m. For $H_S = 1$ m, the corresponding period $T = 4.5$ s was then found by applying the linear relationship established in Section 8.3. The consequence of this simplification is that some wave periods are over-represented, and some are left out entirely. In reality, the modeled $T = 4.5$ s, which coincidentally turned out to be a relatively damaging period for the configuration, would be a range of periods between 3.8 - 4.7 s, according to Equation (8.3).

Another factor that applies to all configurations, which may contribute to the overestimation of damage, is the simplification that all sea states are applied from only one direction during the jacket's 20-year lifetime. Though thought to be a conservative approach, this is not realistic.

9.4.2 Fatigue Damage Comparison

As all critical hot spots were located in the joints, this is what was focused on further. In Section 9.2, all rows of joints in the different configurations were compared. One important observation that can be made from the comparison of X-joints was that the damage in the 4. row overshadowed all others. The main reason for this is that this row is located in the splash zone, which has several consequences for the joints. First of all, this is a wet surface that is not covered by cathodic protection measures and is thus extra prone to corrosion. This results in an S-N curve with lower fatigue strength. Secondly, these joints are directly subjected to impact by the wavefront, leading to out-of-plane deformations in the bracings and thus significant stress ranges in the joints. One condition specific to the straight jacket is that the bracings in the splash zone are longer than the bracings in the

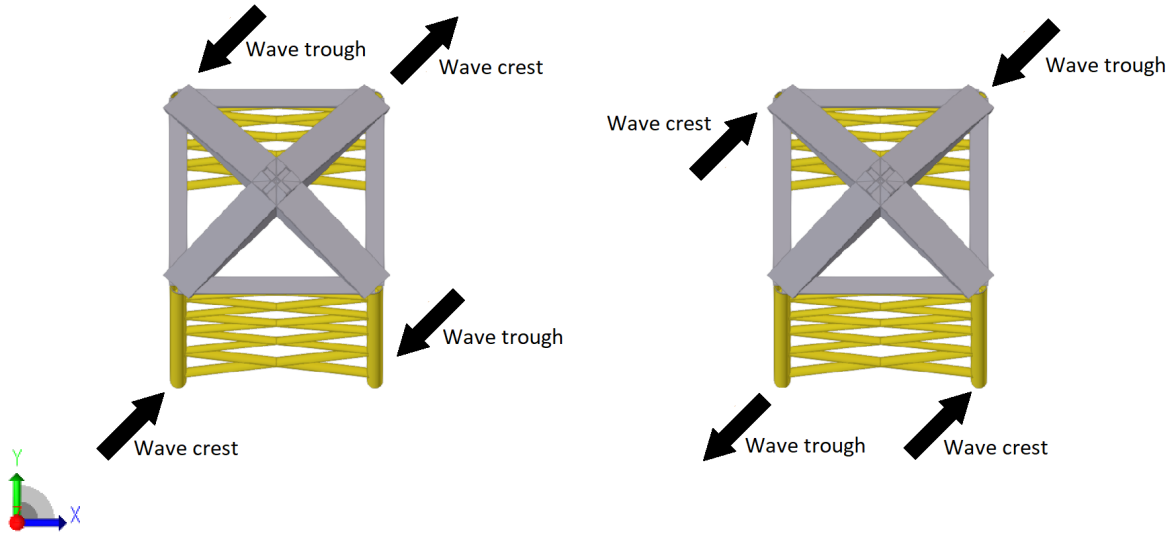

(a) Wave trough on middle legs.

(b) Wave crest on middle legs.

Figure 9.12: Simultaneous wave loads ($T = 4.5$ s) on the legs leading to alternating tension and compression in the braces.

skew jacket. This magnifies the damage in the upper bracings and is partly the reason why the straight jacket has more than twice the damage compared to the skew jacket, as seen in Figure 9.3. It is generally desirable to keep as many joints out of the splash zone as possible, as fatigue design in this location is costly.

Another takeaway is that both jackets performed better for sea states applied at 45°. This is expected for the same reasons as in the ULS-design; loads applied at 0° will activate only two planes of bracings and thus leads to more extensive stress ranges. This result implies that the jackets accumulate less fatigue damage for the former case and should be carefully considered in a complete wind turbine design with a jacket undercarriage, see Appendix C for illustrations of the load response.

In Figure 9.2, it can be observed that for the K-joints, there is a trend of decreasing damage when moving up the jacket. As a standardization measure to ease the design and installation process, all joints are designed to be similar. Therefore, the stress ranges are expected to be more significant close to the seabed, and the trend is as expected. However, this trend has one exception: the K0-row with relatively minor damage compared to other rows. This may partly be explained by the fact that there are only two braces connected to the leg in this joint, in contrast to four for the other rows, leading to lower stress ranges in the joint.

9.4.3 Fatigue Influence for Varying Wind and Waves

The plots show similar trends between the straight- and the skew jacket simulations. The K-joints in both configurations seem to accumulate the most damage in the 2. row from the seabed. However, the skew jacket can also be seen to accumulate more damage in the 3. row. This implies that the damage is more concentrated for the K-joints in the straight jacket, which is unfavorable concerning the total fatigue life of a structure. For damage in the braces, both simulations indicate that the X-joints in the 4. row, located in the splash zone, are most susceptible to fatigue damage.

An inspection of Figure 9.5a reveals that varying the wind speeds has close to zero effect on the normalized damage for the braces in the straight-legged jacket loaded at 0°. The effect is similar for the braces in the skew jacket for loads induced at 45°. One of the exceptions is for the skew jacket in rated wind speed conditions loaded at 0° relative to the jacket, see Figure 9.9a.

The variation of waves is observed to have similar effects on both jacket configurations yielding increased normalized damage for increased wave heights and wave periods, with a few exceptions. The most distinct being the sea state $U17H0.25T3.5$ accumulating more damage than $U17H1T4.5$ in the X-nodes. Another noticeable result from the simulations with varying waves was the leap in accumulated normalized damage from $H_s = 4$ to $H_s = 5$ in both joint types, especially the K-joints, see Figure 9.4b and Figure 9.8b. It was discovered in the statistical analysis that a sea state with $H_s = 5$ is approximately three times less probable than a sea state with $H_s = 4$, if the wind speed is equal. This indicates that this leap in damage will not occur often but significantly affects the structure's fatigue life.

10 | Complementary Discussion

The former discussion sections were used to discuss the results of the various analyses' independently. This chapter is reserved for a more general discussion, where observations are made across the different performed analyses. The influences of the various assumptions are discussed.

10.1 Ultimate Limit State

The focus of the ULS analysis in the thesis was to provide two viable jackets that could then be used to compare the ULS and FLS-properties. The jackets were designed with similar geometry, sections, and material to provide a basis for comparison. The jackets were also standardized with only two member types, not considering stubs and cans, and the K- and X-joints were similar in all parts of the jackets.

There are mainly two reasons why the jackets were standardized in this manner. Firstly, it simplified the design and analysis process by reducing the number of different member types to take into account. Secondly, standardization might prove to be an essential measure in establishing large-scale wind turbine farms, such as in Southern North Sea II. Rather than having numerous optimized designs specific to each turbine, it is desirable to have 2-3 applicable standardized designs for the whole region. Having similar joints in the entire jacket is emphasized by Dr. Techn. Olav Olsen AS to be particularly beneficial for simplifying the design and installation process in the jackets and reducing the risk of construction errors. This can significantly reduce the design and production costs in such projects.

There are, of course, some obvious drawbacks to this approach. When standardized, some parts of the jacket will be largely over-dimensioned, with low utilization. This is especially the case for elements located in the top of the jackets, as was seen in Chapter 7. Material usage is an important consideration in all projects as it is often one of the main cost-driving factors. In addition, the environmental and climatic footprint of projects is quickly on the rise as a more critical factor. The best balance between optimization and standardization can be hard to define and requires consideration on its own.

The analysis was performed as a quasi-static calculation. However, the load effects from wind and marine conditions have a dynamic nature, and some of the dynamic interaction effects between these have not been considered, damping being the most significant. To include these effects, it is desirable to perform a dynamic ULS analysis, much like the one carried out for the FLS.

The dynamic loads had to be included as static loads to carry out the analysis. The most straightforward way to do this was to include the loads and moments as their maximum values under the different conditions. This was not too challenging, as Sesam automatically calculates the wave actions that impose maximum moment and shear in the jacket. There are, however, some load effects that were conservatively assumed to act simultaneously. For instance, the maximum wave height, wind speed, and current speed were assumed to act simultaneously, which is unlikely.

The analyses were entirely linear. In a complete design, it is desirable to include non-linear effects, [8] to determine left-over plastic capacity to restrict expenses. Plastic capacity is often assessed in the accidental limit state, e.g., remaining capacity following an impact. Assessment of plastic capacity is usually determined through a push-over analysis, where it is determined whether a structural collapse or soil failure occurs first.

10.2 Omitted Load Effects

Many load effects had to be omitted to be able to run the analyses. First of all, no SLS or ALS considerations were made as this was considered out of the thesis's scope. However, seismic events, impacts from ships, and other accidental load effects are highly relevant. In a complete analysis of the jackets, these load effects would have to be considered. Vortex-induced vibrations (VIV) imposed on the structure from wind and waves are also something that was left out entirely. It is worth noting that VIVs can inflict significant fatigue damage on jackets and should therefore be considered in a complete design [6].

According to *ST-0437*[9], the multi-directionality of wind and waves can, in some cases, have an important influence on the loads acting on the jacket. Due to lacking statistical data on wind and wave directions in Southern North Sea II, this was not accounted for in the concept study, where generic directions of 0° and 45° relative to the jacket were applied. In addition, wake effects from nearby turbines were also neglected. The wake effect will lead to lower wind speeds for the downwind turbine, but at the same time, more turbulent airflow, which can increase the dynamic mechanical loading [40]. Both these effects might be interesting to look into in future work.

As briefly discussed in Section 3.3, low cycle fatigue is generally not of much relevance

when designing offshore structures. An exception to this is during the transportation of the structure to the site, where cyclic load effects in the low cycle fatigue range can occur. According to *ST-0126*[8], damage occurring during stages of transportation, installation and pre-operation shall be taken into account when assessing the fatigue capacity of the structure. This was not prioritized in this concept study.

Capacity reduction due to corrosion is of great importance when designing structures in marine conditions. For simplicity, this was not accounted for at all in the ULS-design. In the FLS, it was only accounted for in the choice of the S-N curve in the splash zone.

10.3 Transition Piece Stiffness

The dynamic effects inherited from the modeling choices of the transition piece were discussed in Section 6.3. This choice might have significant implications on fatigue damage, as dynamic excitations are closely linked to the occurrence of cyclic stress ranges in the structural details. The eigenperiods for the first lateral mode in both jackets were observed to be in the range of $4.7 - 6.7$ s depending on the TP's stiffness. One should note that this interval includes approximately all the most probable wave periods stemming from the statistical analysis conducted for the fatigue calculations. All the 80 sea states are listed in Appendix D. The transition piece modeling can hence be of great significance for the stress range distribution in the jackets induced by large excitations from sea states containing wave periods in this interval. Such waves can likewise imply high accumulated damage in the transition piece, which, however, is a subject out of the scope of this thesis.

10.4 Influence of Turbulence

Turbulence was excluded in the aeroelastic simulations utilized in the fatigue analysis. It is worth noting that turbulence can increase the accumulated fatigue damage from sea states with low wind speeds. This originates from the definition of turbulence intensity given in Section 4.2, where lower wind speeds imply an increased turbulence intensity. An increased turbulence intensity entails an elevated magnitude of the vertical and perpendicular wind components compared to the mean wind speed. This can cause the turbine RNA and tower to be imposed excitations at an angle from the direction of the mean wind speed, which in turn decreases the aerodynamic damping of the system, a consequence stemming from the theory presented in Section 3.2. Higher accumulated damage for low wind speeds where a turbulence model was included is supported by the findings from an article published by the University of Florence [41].

In the ULS-model, a wind profile taking turbulence into account was imposed on the

tower. However, the point loads and moments in the tower top were set static. To preserve a conservative design, the turbine loads were added an additional safety factor of 1.1, taking uncertainties of dynamic effects into account.

10.5 Influence of a Soil Model

The effects of pile-soil interaction on the dynamic properties of a jacket structure in the North Sea were investigated in [42]. It was reported that a jacket structure including a pile-soil model had a 1 % lower eigenfrequency than a bottom-fixed jacket. This deviation would result in a 1 % higher eigenperiod and was considered negligible. A consequence of including a pile-soil model in this paper would therefore have shifted the first eigenperiod closer to the third most probable wave period discovered in Section 8.3 and further from the most probable period. Based on the findings from the report, assuming a bottom-fixed jacket can be viewed as valid for an early design stage. However, the design code [8] states that interaction with the foundation shall be assessed in a complete design of an offshore wind turbine.

As discussed in Section 10.1, the ultimate limit state was assessed by purely linear approaches. A push-over analysis requires the implementation of a pile-soil model. However, when operating in linear stress ranges, a pile-soil model will not be expected to influence the ULS much [8] when performing quasi-static analyses.

10.6 Choice of Wave Theory and Sea Level

The choices of wave theory and sea level were based on a parametric study carried out early in the project.

Sesam provides several different options in terms of wave theory. The choice of wave theory is essential for representing the waves correctly and achieving precise wave loads. The site conditions in Southern North Sea II correspond to intermediate-deep water waves, where Sesam provides two appropriate options; Stokes 5th order theory and Stream function theory. Stream function theory is generally a more versatile theory, but the parametric study showed minimal differences between the two. However, as Stokes' 5th order theory resulted in slightly larger loads, this theory was chosen for the models.

According to section 4.4 in the DNV-standard *ST-0437*, a variety of water levels have to be investigated. This was checked and shown to have a negligible effect except for a slightly larger overturning moment from waves for higher water levels. The analysis was therefore carried out with only one water level set at 60 m above the seabed.

10.7 Hydro Properties

In Sesam, hydro properties include Morison's coefficients, flooding, and marine growth. Similar to Section 10.6, choices were made based on the parametric study.

Flooding of the legs was observed to do little in terms of ULS capacity. However, it was important for the dynamic properties, as the added water mass in the flooded members made a noticeable effect on the eigenfrequencies of the jackets. Therefore, the objective was to apply the most realistic case of flooding. The assembling of the joints between bracings and legs is assumed to be performed in air and to be completely sealed. Fully flooded legs and non-flooded bracings were therefore assumed in the models.

When it comes to Morison's coefficients, a jacket fully covered in marine growth led to significantly larger forces from waves and current. The ratio was observed to be almost 2 to 1 for large waves. According to *NORSOK N-003*[10], the marine growth is usually assumed to grow linearly to a maximum thickness over two years after installation. If no regular cleaning measures are planned, the jackets will spend most of their lifetime covered in marine growth. It was from these reasons deemed appropriate to choose Morison's coefficients reflecting maximum marine growth.

11 | Conclusion

Both jacket configurations showed similar trends regarding dynamic properties, design in the ultimate limit state analysis, and which details were most susceptible to damage in the fatigue limit state. From a pure performance perspective the skew-legged jacket would be the most viable configuration choice. In general, the skew jacket yielded lower utilizations in the ULS and less accumulated damage in the FLS, see Chapter 7 and Chapter 9. There were no significant differences in the dynamic properties, except for the torsional mode.

Olav Olsen suggested the straight jacket as a better option for standardization. From the analyses, the joints were shown to be the components most susceptible to fatigue damage. For these reasons standardization of a straight jacket with emphasis on X-joint optimization, could prove to be a valuable measure when establishing large scale wind turbine farms with reduced cost and climate footprint.

In the ULS, the upper part of the legs were discovered to be driven by rated conditions, where the turbine thrust is at its maximum. For the rest of the jacket, waves with a 50-year return period was the significant design factor. The FLS results suggest that sea states with large waves are critical for the fatigue life of K-joints, whereas the most probable operating conditions, where turbine loads are dominating, are decisive for the lifetime of the X-joints.

The FLS analyses revealed the importance of assessing the directions of the environmental loads, especially for the straight jacket. The maximum damage was decreased by a factor of two when imposing loads at an angle of 45° relative to the jacket. The designer is therefore recommended to place the jackets at a 45° angle relative to the mean direction of the fatigue driving environmental loads. One should note that this will lead to higher utilization of the legs in the ULS.

As this thesis aimed to serve as a concept study, the analyses performed were simplified by neglecting soil effects, turbulence, and accidental incidents, amongst others. These pose challenges in a realistic setting. Therefore, a complete design could not be definitively concluded from the results discovered. Nevertheless, many of the assumptions were investigated through parametric studies to preserve conservative modeling choices and

completeness in the reporting. For these reasons, this concept study could serve as a basis for a complete design of jacket substructures, for 15-MW wind turbines in the Southern North Sea II.

11.1 Suggestions for Further Work

This concept study was conducted by analyzing the two jacket configurations in the ultimate limit state and the fatigue limit state. However, the conditions surrounding the study required many simplifications and assumptions. The effect of the most significant simplifications was thoroughly discussed in Chapter 10. A further study of jacket substructures based on the work conducted in this thesis should involve a comprehensive analysis of the three most important simplifications: the stiffness of the transition piece, a pile-soil model, and a turbulence model. In addition, developing fatigue resistant solutions for the X-joints could improve the design significantly.

Bibliography

[1] Greenstat, Æge Energy UiB and HVL. "Optimal utnyttelse av energi fra havvind i Sørlige Nordsjø II." In: (2021). URL: https://www.uib.no/bow/145330/optimal-utnyttelse-av-energi-fra-havvind.

[2] *Informasjonsmøte om havvind*. https://www.statnett.no/contentassets/246a77003aab450387f3380212981074/masterpresentasjon-apent-mote-20220125.pdf. Accessed: 2022-03-15.

[3] *Equinor, RWE og Hydro samarbeider om havvind i Sørlige Nordsjø II*. https://www.equinor.com/no/news/20210526-team-up-offshore-wind-north-sea.html. Accessed: 2022-03-16.

[4] Wåsjø K., Bjerkås M., Søreide T. "Steel Jackets and Monotower Foundations for Offshore Wind Turbines." In: (2012). DOI: https://doi.org/10.1115/omae2012-83615.

[5] Evan Gaertner et al. *Definition of the IEA 15-Megawatt Offshore Reference Wind Turbine*. Tech. rep. International Energy Agency, 2020. URL: https://www.nrel.gov/docs/fy20osti/75698.pdf.

[6] DNV AS. *DNV-RP-C205: Environmental conditions and environmental loads*. 2021.

[7] DNV AS. *DNV-RP-C203: Fatigue design of offshore steel structures*. 2021.

[8] DNV AS. *DNV-ST-0126: Support structures for wind turbines*. 2021.

[9] DNV AS. *DNV-ST-0437: Loads and site conditions for wind turbines*. 1994.

[10] Standards Norway. *NORSOK N-003:2017: Actions and action effects*. 2020.

[11] Standards Norway. *NORSOK N-004:2013: Design of steel structures*. 2013.

[12] Musial W. "Floating Offshore Wind Turbines Explained - NREL." In: (2021). URL: https://www.linecurrents.live/reports/2021/5/28/floating-offshore-wind-turbine-tech-explained.

[13] Alexandre Mathern, Christoph von der Haar , Steffen Marx. "Concrete Support Structures for Offshore Wind Turbines: Current Status, Challenges, and Future Trends." In: (2021). DOI: https://doi.org/10.3390/en14071995.

[14] Plodpradit P., Dinh V., Kim K. "Tripod-Supported Offshore Wind Turbines: Modal and Coupled Analysis and a Parametric Study Using X-SEA and FAST." In: (2019). DOI: https://doi.org/10.3390/app9081633.

[15] Vici Ventus. "Offshore Wind Turbines: Space frame Foundations." In: (2022). URL: https://viciventus.no/global/upload/3sPPQ/files/SFT%20product%20sheet%20281111%20alt%201.pdf.

[16] *Foundation Structures*. https://www.esubsea.com/foundation-structures/. Accessed: 2022-02-14.

[17] *Our experience with suction buckets jacket*. https://orsted.com/en/our-business/offshore-wind/wind-technology/suction-bucket-jacket-foundations. Accessed: 2022-02-14.

[18] Matti Scheu et al. "Human exposure to motion during maintenance on floating offshore wind turbines." In: *Elsevier* 165 (2018), pp. 293–306. DOI: https://doi.org/10.1016/j.oceaneng.2018.07.016.

[19] Aaron Du. "Semi-Submersible, Spar and TLP – How to select floating wind foundation types?" In: (2021). URL: https://www.empireengineering.co.uk/semi-submersible-spar-and-tlp-floating-wind-foundations/.

[20] P. K. Larsen, A. H. Clausen, and A. Aalberg. *Dimensjonering av stålkonstruksjoner*. 3. utgave. Fagbokforlaget, 2020.

[21] Humar J. L. *Dynamic of Structures*. Second Edition. Balkema, 2002.

[22] Koukoura C. , Brown C. , Natarajan A. and Vesth A. "Cross-wind fatigue analysis of a full scale offshore wind turbine in the case of wind–wave misalignment." In: *Elsevier: Engineering Structures* 120 (2016), pp. 147–157. DOI: https://doi.org/10.1016/j.engstruct.2016.04.027.

[23] A. Nussbaumer, L. Borges, and L. Davaine. *Fatigue Design of Steel and Composite Structures*. 1. Edition. European Convention for Constructional Steelwork, 2011.

[24] *Fatigue verification for heavy gauge steel components*. https://resources.scia.net/en/garage/fatiguechecksteel.htm. Accessed: 2022-04-20.

[25] Almarnaess A. "Fatigue handbook: Offshore steel structures." In: (Jan. 1985). URL: https://www.osti.gov/biblio/5095889.

[26] Horn J-T. H. , Krokstad J. R., Amdahl J. "Joint Probability Distribution of Environmental Conditions for Design of Offshore Wind Turbines." In: Volume 10: Ocean Renewable Energy (2017). DOI: https://doi.org/10.1115/OMAE2017-61451.

[27] Y. Tamura and Kareem A. *Advanced Structural Wind Engineering*. Vol. 1. Springer, 2013.

[28] T. Moan. *Design of Marine Structures*. Vol. 1. 1994.

[29] Jalbi S. and Bhattacharya S. "Concept design of jacket foundations for offshore wind turbines in 10 steps." In: *Soil Dynamics and Earthquake Engineering* Vol. 139 (2020). DOI: https://doi.org/10.1016/j.soildyn.2020.106357. URL: https://www.sciencedirect.com/science/article/pii/S0267726120309623?via%3Dihub.

[30] Reistad M. Haakenstad H. Breivik Ø. and J. Aarnes O. "NORA10EI: A revised regional atmosphere-wave hindcast for the North Sea, the Norwegian Sea and the Barents Sea." In: *Royal Meteorological Society* (2020). DOI: https://doi.org/10.1002/joc.6458. URL: https://rmets.onlinelibrary.wiley.com/doi/10.1002/joc.6458.

[31] *Wind wave*. https://en.wikipedia.org/wiki/Wind_wave. Accessed: 2022-02-07.

[32] *Waves and the Concept of a Wave Spectrum*. https://wikiwaves.org/Waves_and_the_Concept_of_a_Wave_Spectrum. Accessed: 2022-03-09.

[33] *Ocean-Wave Spectra*. https://wikiwaves.org/Ocean-Wave_Spectra. Accessed: 2022-03-09.

[34] *Superelement approach in Sesam and Bladed*. https://www.dnv.com/Images/Sesam%20and%20Bladed%20-%20Efficient%20coupled%20analyses%20-%20webinar%20presentation_tcm8-102589.pdf. Accessed: 2022-05-10.

[35] Muk O. C., Bachynski E. E., Økland O. D. and Passano E. "DYNAMIC RESPONSES OF A JACKET-TYPE OFFSHORE WIND TURBINE USING DECOUPLED AND COUPLED MODELS." In: *Journal of Offshore Mechanics and Arctic Engineering* 9B (2014). DOI: https://doi.org/10.1115/OMAE2014-24246.

[36] Byoung Wan Kim; Hong Gun Sung; Sa Young Hong. "Coupled Versus Decoupled Analysis for Floating Body and Mooring Lines." In: (2017). URL: https://onepetro.org/ISOPEIOPEC/proceedings-abstract/ISOPE17/All-ISOPE17/ISOPE-I-17-146/17396.

[37] DNV. "Sesam Wind Manager: Time History Fatigue Analysis of a Jacket using a Superelement Analysis approach." In: (2021). URL: https://www.dnv.com/services/offshore-wind-analysis-software-sesam-wind-manager-2460.

[38] Horn J-T. H. , Krokstad J. R., Amdahl J. "Long-term fatigue damage sensitivity to wave directionality in extra-large monopile foundations." In: *Journal of Engineering for the Maritime Environment* 232 (2018), pp. 37–49. DOI: https://doi.org/10.1177/1475090217727136.

[39] Collier W. "A Consistent Structural Damping Model for Integrated and Superelement Modelling of Offshore Wind Turbine Support Structures in Wind Turbine Design Software Bladed." In: *Proceedings of the ASME 2019 2nd International Offshore Wind Technical Conference. ASME 2019 2nd International Offshore Wind Technical Conference* (2019). DOI: https://doi.org/10.1115/IOWTC2019-7541.

[40] F. Gonzalez-Longatt, P. Wall and V. Terzija. "Wake effect in wind farm performance: Steady-state and dynamic behavior." In: *Elsevier: Renewable Energy* 39, Issue 1 (2012), pp. 329–338. DOI: https://doi.org/10.1016/j.renene.2011.08.053.

[41] Marino E. , Giusti A. and Manuel L. "Offshore wind turbine fatigue loads: The influence of alternative wave modeling for different turbulent and mean winds." In:

Elsevier: Renewable Energy 132, part A (2017), pp. 157–169. DOI: https://doi.org/10.1016/j.renene.2016.10.023.

[42] Dong W. , Moan T. , Zhen G. "Long-term fatigue analysis of multi-planar tubular joints for jacket-type offshore wind turbine in time domain." In: *Elsevier: Engineering Structures* 33 (2011). DOI: https://doi.org/10.1016/j.engstruct.2011.02.037.

[43] *Frequently Asked Questions: IEA-15-240-RWT*. https://github.com/IEAWindTask37/IEA-15-240-RWT/wiki/Frequently-Asked-Questions-(FAQ)#i-get-a-different-rated-thrust-value-than-the-report. Accessed: 2022-05-22.

A | 15-MW RWT

A.1 Tower Properties

Table 4-2. Some Key Properties and Dimensions of the Tower and Foundation

Location	Height [m]	Outer Diameter [m]	Thickness [mm]
Monopile start	-75.000	10.000	55.341
Mud line	-30.000	10.000	55.341
	-29.999	10.000	55.341
	-25.000	10.000	55.341
	-24.999	10.000	53.449
	-20.000	10.000	53.449
	-19.999	10.000	51.509
	-15.000	10.000	51.509
	-14.999	10.000	49.527
	-10.000	10.000	49.527
	-9.999	10.000	47.517
	-5.000	10.000	47.517
	-4.999	10.000	45.517
Water line	0.000	10.000	45.517
	0.001	10.000	43.527
	5.000	10.000	43.527
	5.001	10.000	42.242
	10.000	10.000	42.242
	10.001	10.000	41.058
Tower start	15.000	10.000	41.058
	15.001	10.000	39.496
	28.000	10.000	39.496
	28.001	10.000	36.456
	41.000	9.926	36.456
	41.001	9.926	33.779
	54.000	9.443	33.779
	54.001	9.443	32.192
	67.000	8.833	32.192
	67.001	8.833	30.708
	80.000	8.151	30.708
	80.001	8.151	29.101
	93.000	7.390	29.101
	93.001	7.390	27.213
	106.000	6.909	27.213
	106.001	6.909	24.009
	119.000	6.748	24.009
	119.001	6.748	20.826
	132.000	6.572	20.826
	132.001	6.572	23.998
Tower top	144.582	6.500	23.998

Figure A.1: Tower properties [5]

A.2 Turbine Loads

The turbine loads were simulated in the aeroelastic tool Bladed. The simulated Bladed model of the IEA-15-MW turbine was originally defined in IEA Wind Task for HAWC2 and OpenFAST. DNV has written a report which verifies and compares the Bladed model with the original model developed by NREL, which can be found on DNV's websites, though it has restricted access. The report showed reasonably low discrepancies from the NREL model, and it states that these discrepancies arise from the choice of beam elements. NREL utilized a fully populated matrix for mass and stiffness, whereas Bladed used modified Timoshenko beam elements.

The loads were simulated for rated wind speeds in accordance with the choice of load combinations in the ultimate limit state analysis, see Section 5.7, and modeled as point loads in the tower top for the ULS model. The thrust at the rotor hub is plotted in Figure A.2 and can be seen to be lower than the values provided in NREL's report [5]. NREL provided an explanation for this distinction in the aftermath of the report's publication and has later supported a rated thrust value of 2,483 MN due to an error in the choice of thrust coefficients [43]. This result was reflected by the aeroelastic simulation and can be seen from the plot. Fz and Fy at the hub were neglected in the ULS analysis, though the induced eccentricities moments from the RNA are included through the moments at the yaw bearing.

The plots in Figure A.3, Figure A.4, and Figure A.5 shows the three global moments at the turbines yaw bearing. This is the part of the turbine connecting the RNA to the tower structure and is thus responsible for transferring all the rotor loads to the tower.

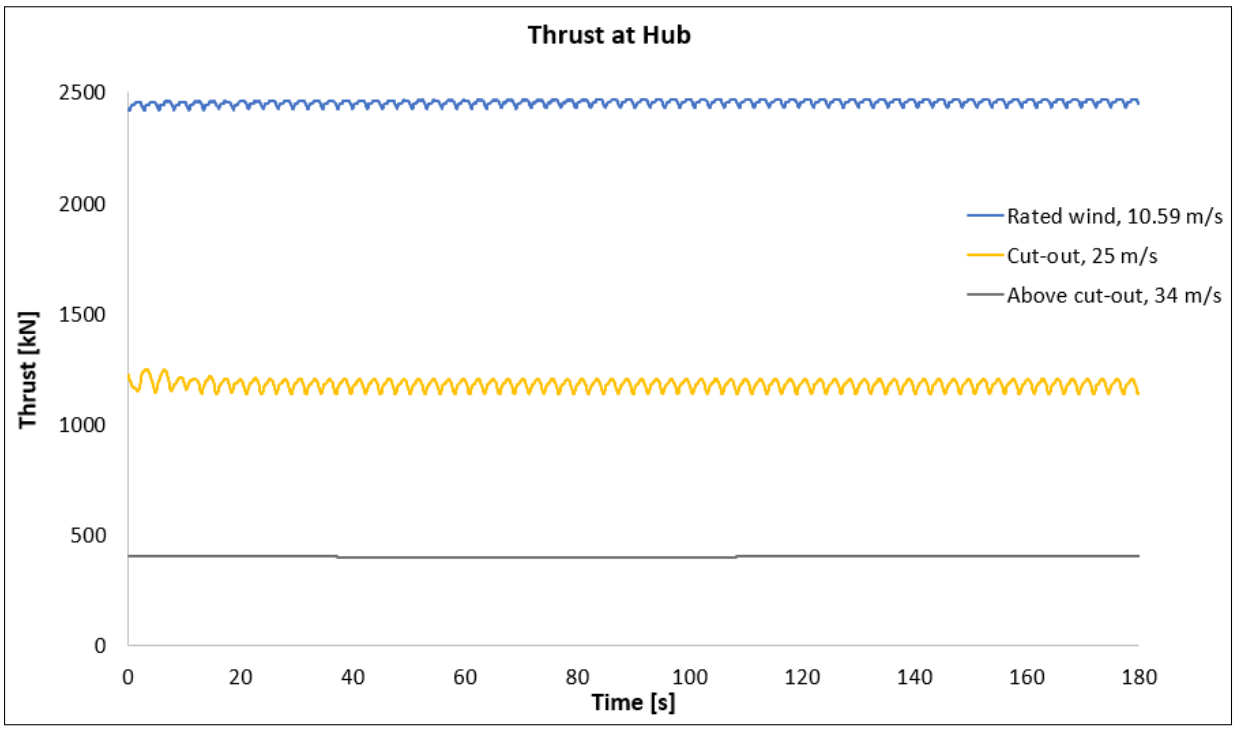

Figure A.2: Thrust at the rotor hub for rated-, cut-out- and above-rated wind speeds.

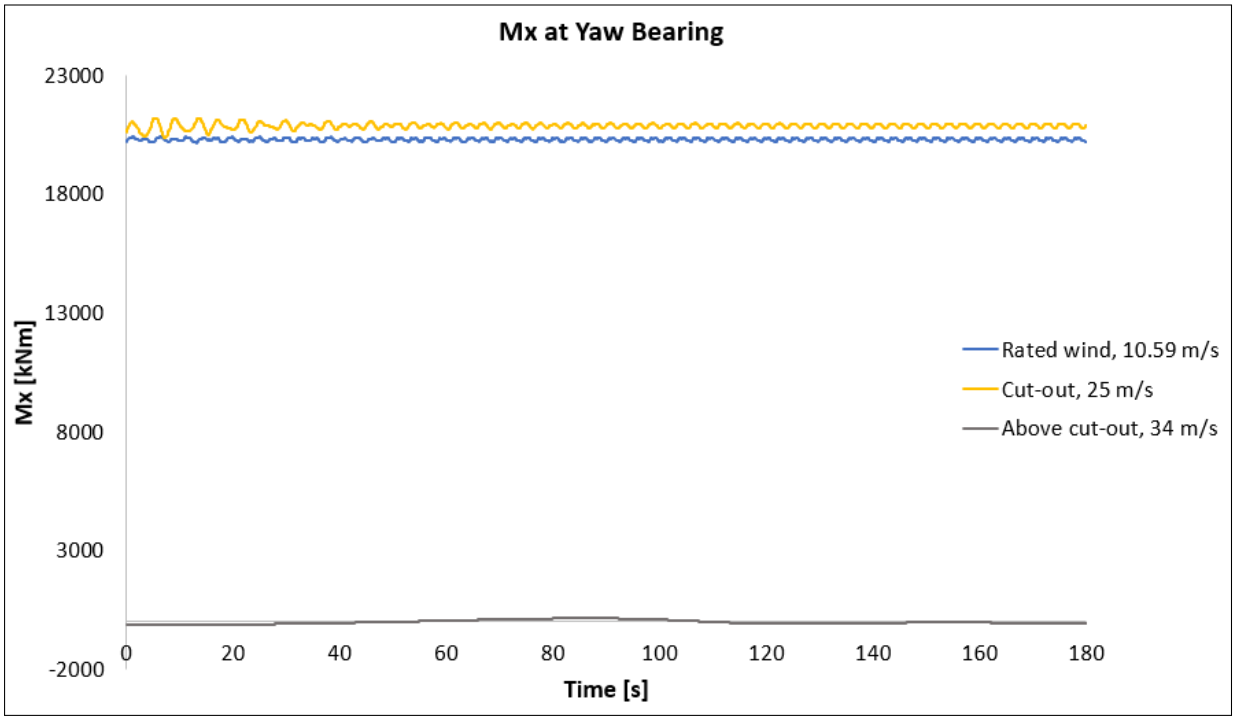

Figure A.3: Mx at yaw bearing for rated-, cut-out- and above-rated wind speeds.

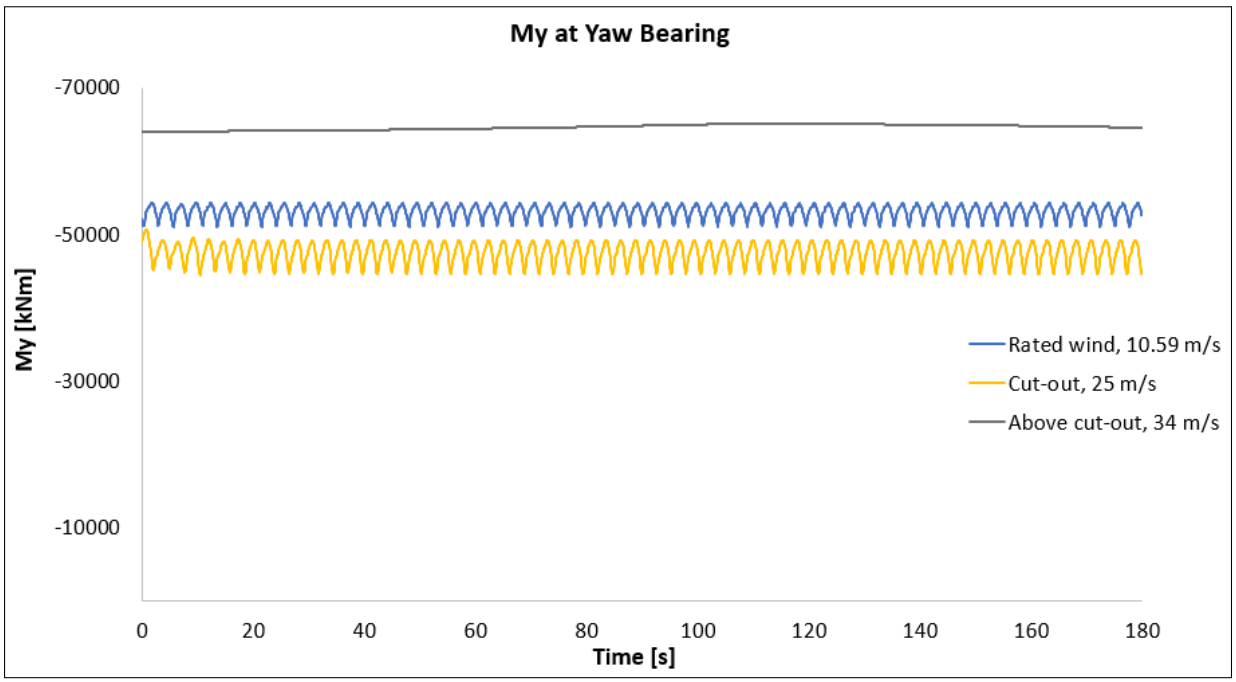

Figure A.4: My at yaw bearing for rated-, cut-out- and above-rated wind speeds.

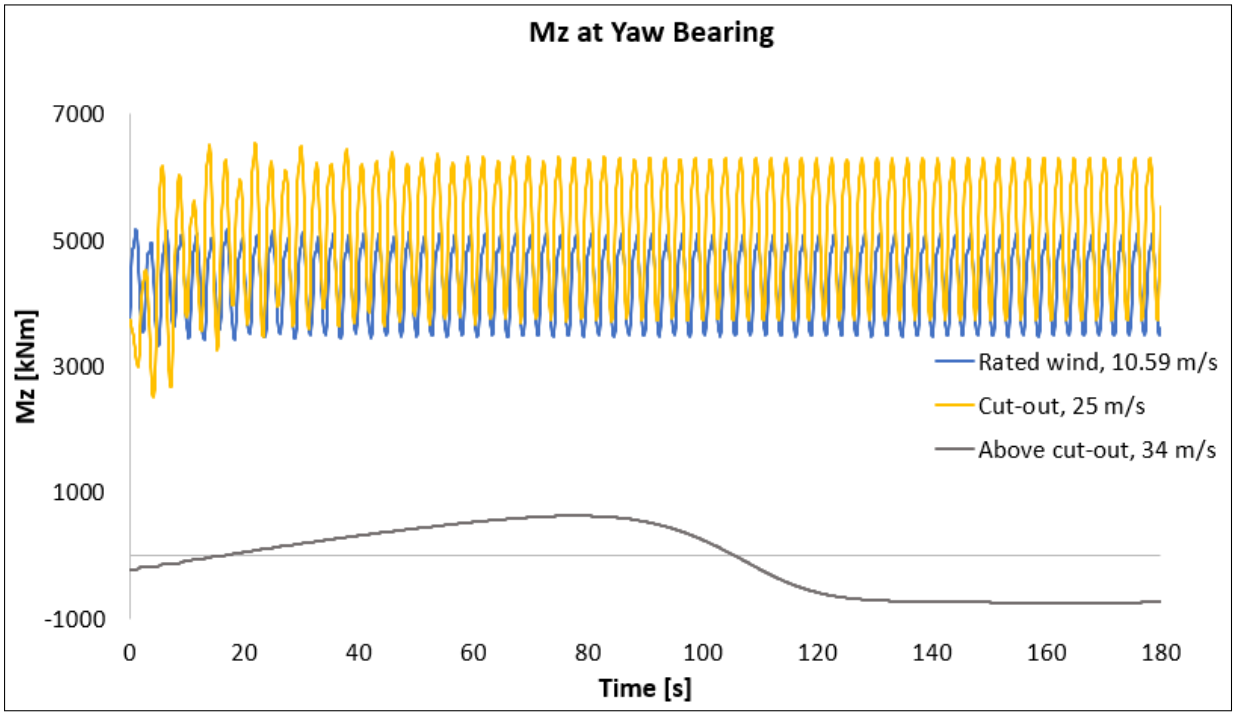

Figure A.5: Mz at yaw bearing for rated-, cut-out- and above-rated wind speeds.

B | Morison's Coefficients

Wave parameters

Wave period $T := 13s$ 13-16s sørlige nordsjø assumed

Wave height $H := 22m$ Design wave assumed

Water depth $d := 60m$

Angular frequency $\omega := \frac{2\pi}{T} = 0.483 \frac{1}{s}$

Wave length by Bob you

Deep water wave length $\lambda_0 := 1.56 \cdot T^2 \cdot \frac{m}{s^2} = 263.64\,m$

Deep water wave number $k_0 := \frac{2\pi}{\lambda_0} = 0.024 \frac{1}{m}$

$$\xi_0 := (k_0 \cdot d)^{0.5} \cdot \left[1 + \frac{k_0 \cdot d}{6} + \frac{(k_0 \cdot d)^2}{30}\right] = 1.562$$

Wave length $\lambda := \lambda_0 \cdot \tanh(\xi_0) = 241.439\,m$

Borders (shallow/intermediate/deep):

Shallow		Deep	
$\frac{1}{20} = 0.05$	$\frac{H}{\lambda} = 0.091$	$\frac{1}{2} = 0.5$	Intermediate water wave

---

Wave number (intermediate) $k_1 := \frac{2\pi}{\lambda} = 0.026 \frac{1}{m}$ $z := 0m$ (At MWL)

Max horizontal particle velocity $v_m := \omega \cdot \frac{H}{2} \cdot \frac{\cosh[k_1 \cdot (z + d)]}{\sinh(k_1 \cdot d)} = 5.806 \frac{m}{s}$

Parameters for coefficients

Diameter profile	$D_p := 1400mm$	Leg diameter
Marine growth thickness	$t := 100mm$	NORSOK N-003
Diameter	$D := D_p + 2 \cdot t$	
Roughness height	$k := 2 \cdot 10^{-2} m$	Roughness height Steel new 5x10-5 Steel painted 5x10-6 Marine growth (5x10-3 til 5x10-2)
Fluid kinematic viscosity	$\nu := 1.35 \cdot 10^{-6} \frac{m^2}{s}$	
Maximum orbital particle velocity	$v_m = 5.806 \frac{m}{s}$	
Current velocity	$v_c := 1.25 \frac{m}{s}$	
Total flow velocity	$v := v_c + v_m = 7.056 \frac{m}{s}$	

Reynolds number	$Re := \frac{v \cdot D}{\nu} = 8.363 \times 10^6$
Keulegan-Carpenter number	$K_C := \frac{v \cdot T}{D} = 57.332$
Non-dimensional roughness	$\Delta := \frac{k}{D} = 0.013$

Drag coefficient

6.7.1.5 - Dependence of drag-coefficient on roughness (for high reynolds and large Kc number)

$$C_{Ds} := \begin{cases} 0.65 \text{ if } \Delta \le 10^{-4} \\ \frac{(29 + 4\log(\Delta))}{20} \text{ if } 10^{-4} < \Delta < 10^{-2} \\ 1.05 \text{ if } \Delta \ge 10^{-2} \end{cases} = 1.05$$

$\Delta < 10^{-4}(\text{smooth})$

$10^{-4} < \Delta < 10^{-2}$

$\Delta > 10^{-2}(\text{rough})$

6.7.2.2 Wake amplification factor (For Kc smaller than 12)

$$C_\pi := 1.50 - 0.024\left(\frac{12}{C_{Ds}} - 10\right) = 1.466 \qquad K_C = 57.332$$

$$\psi := \begin{cases} C_\pi + 0.10(K_C - 12) \text{ if } 2 < K_C < 12 \\ C_\pi - 1.00 \text{ if } 0.75 < K_C < 2 \\ C_\pi - 1.00 - 2.00(K_C - 0.75) \text{ if } K_C < 0.75 \\ 1.00 \text{ if } K_C > 12 \end{cases} = 1$$

$2 \le K_C < 12$

$0.75 \le K_C < 2$

$K_C \le 0.75$

$\psi_{hor} := 1$

Drag coefficient

$C_D := C_{Ds} \cdot \psi = 1.05$

Inertia coefficients

$C_{M1} := 2$ $\qquad K_C = 57.332$

$C_{M2} := \max\left[2.0 - 0.044\left(K_C - 3\right), 1.6 - \left(C_{Ds} - 0.65\right)\right] = 1.2$

$C_M := \begin{cases} C_{M1} & \text{if } K_C < 3 \quad = 1.2 \\ C_{M2} & \text{if } K_C > 3 \end{cases}$

Coefficients marine growth

Diameter	$D_p = 1.4\,\text{m}$
Marine growth	$t = 0.1\,\text{m}$
Roughness	$k = 0.02\,\text{m}$

$C_D = 1.05$

$C_M = 1.2$

C | Jacket Responses

This section displays some of the jacket responses to certain load cases and load combinations in the ultimate limit state.

Appendix C.1 shows jacket and tower deformations due to the turbine load cases from Section 5.6.1 imposed at 0° in the tower top. As expected, rated conditions yield the largest displacements in the tower top. Another observation is that for the extreme wind condition, the tower deflects into the incoming wind. This is a consequence of the moment imposed at the tower top due to the eccentricity of the center of mass in the RNA. When the turbine is in idle mode, this moment is the dominating effect.

Appendix C.2 shows the jacket and tower deformations due to three different load combinations with loads applied at 0°. There is one combination for each of the RW, CW and EW cases. As expected, the total deformations are larger than for the load cases in Appendix C.1, as wave loads, self-weight, buoyancy and load factors are included. The inclusion of the wave loads are particularly visible for the EW load combinations.

Appendix C.3 and Appendix C.4 illustrates the axial forces in the different members for two of the load combinations that proved to be criticial in Chapter 7. Both combinations are applied 0° and 45°.

C.1 Deformations: Wind Load Cases

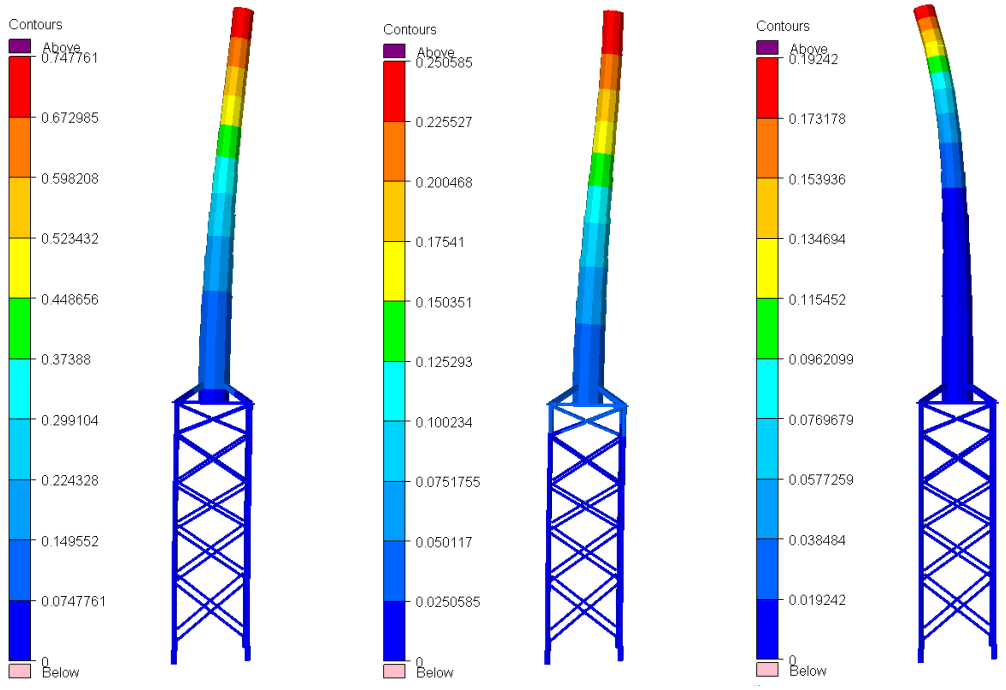

(a) Rated (10.59 m/s). (b) Cut-Out (25 m/s). (c) Extreme (34 m/s).

Figure C.1: ULS deformations in the straight-legged jacket from the applied wind load cases.

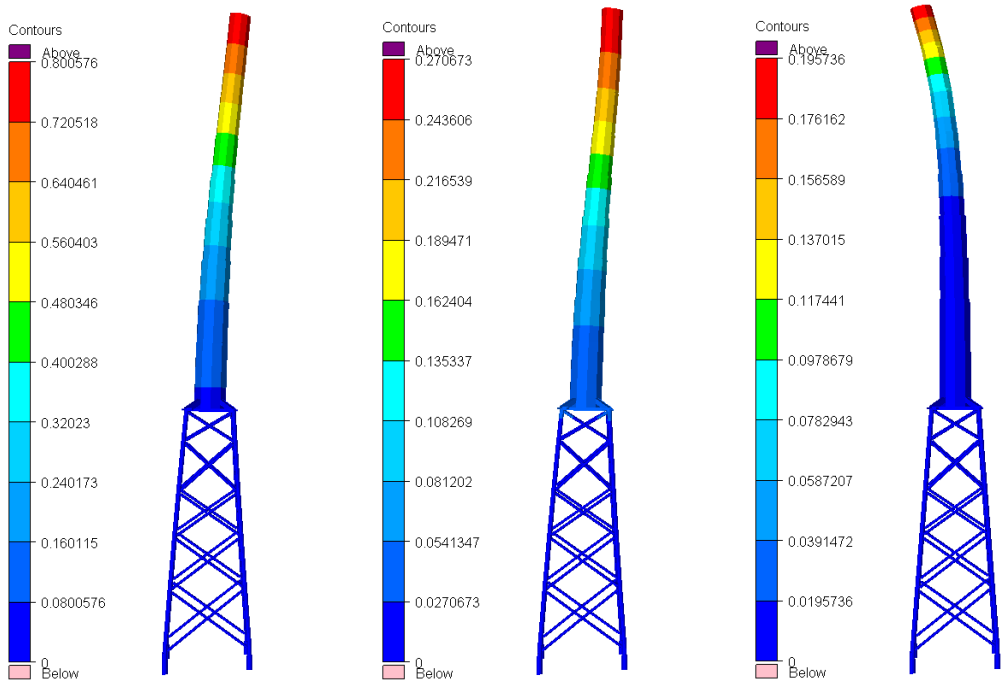

(a) Rated (10.59 m/s). (b) Cut-Out (25 m/s). (c) Extreme (34 m/s).

Figure C.2: ULS deformations in the skew-jacket from the applied wind load cases.

C.2 Deformations: Load Combinations

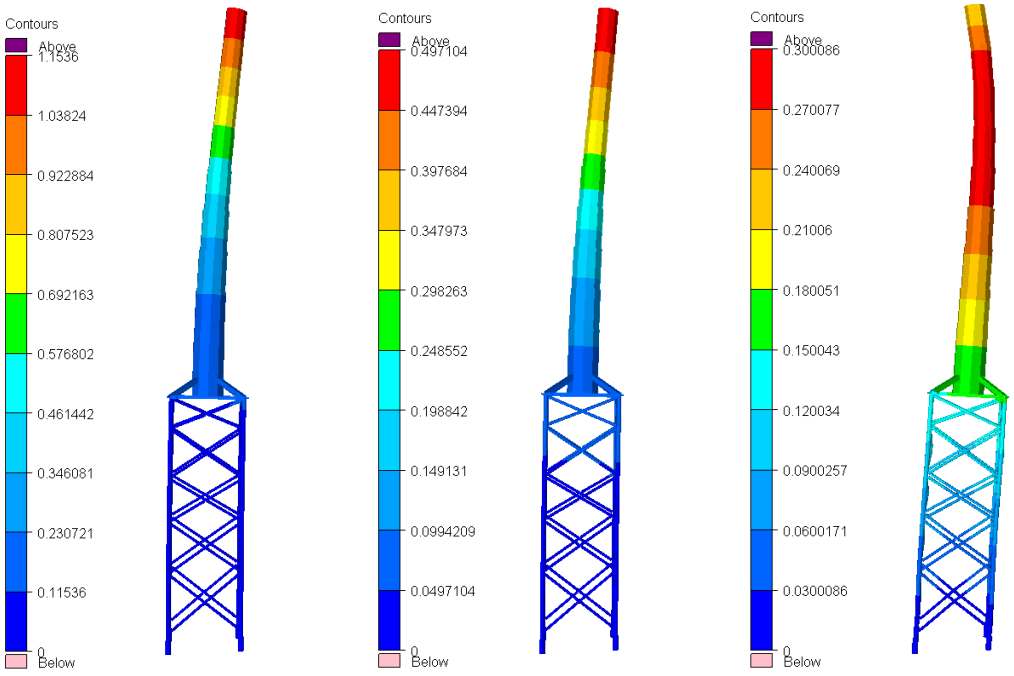

(a) RW: T7.5_H7_D0_Sh (b) CW: T9.5_H9_D0_Sh (c) EW: T13_H22_D0_Sh

Figure C.3: ULS deformations in the straight jacket for a few chosen load combinations.

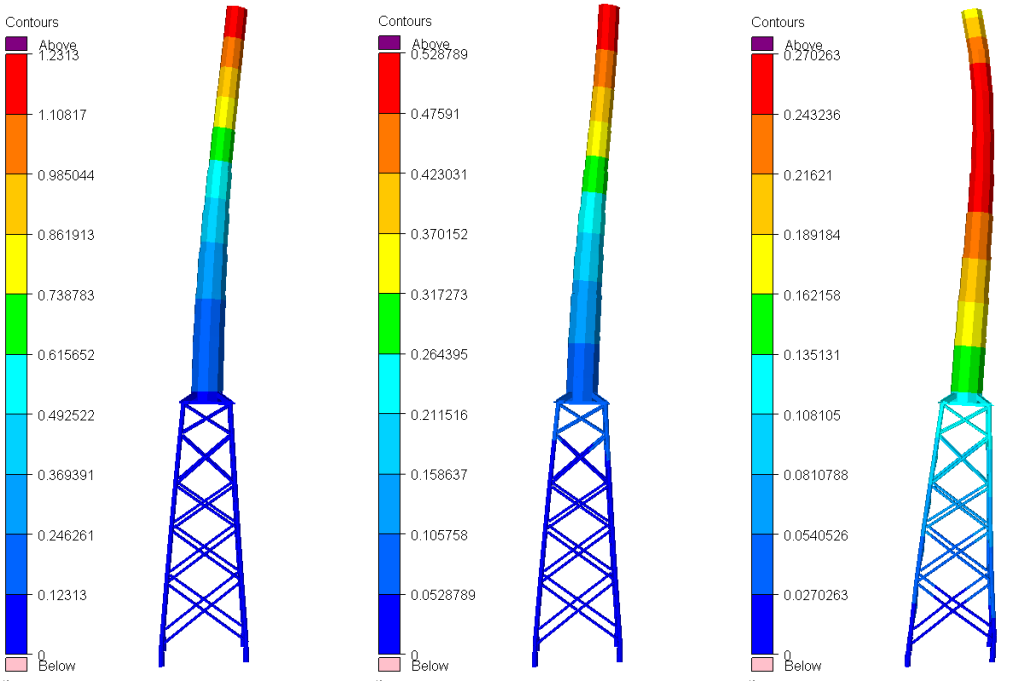

(a) RW: T7.5_H7_D0_Sh (b) CW: T9.5_H9_D0_Sh (c) EW: T13_H22_D0_Sh

Figure C.4: ULS deformations in the skew jacket for a few chosen load combinations.

C.3 Axial Forces Straight Jacket

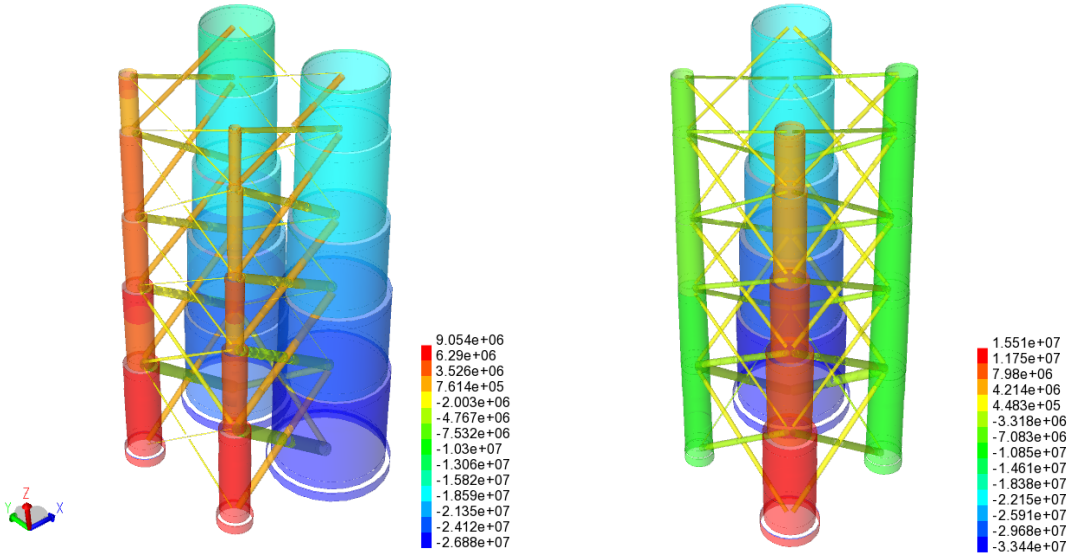

(a) T7.5H7D0Sh (b) T7.5H7D45Sh

Figure C.5: Rated wind conditions.

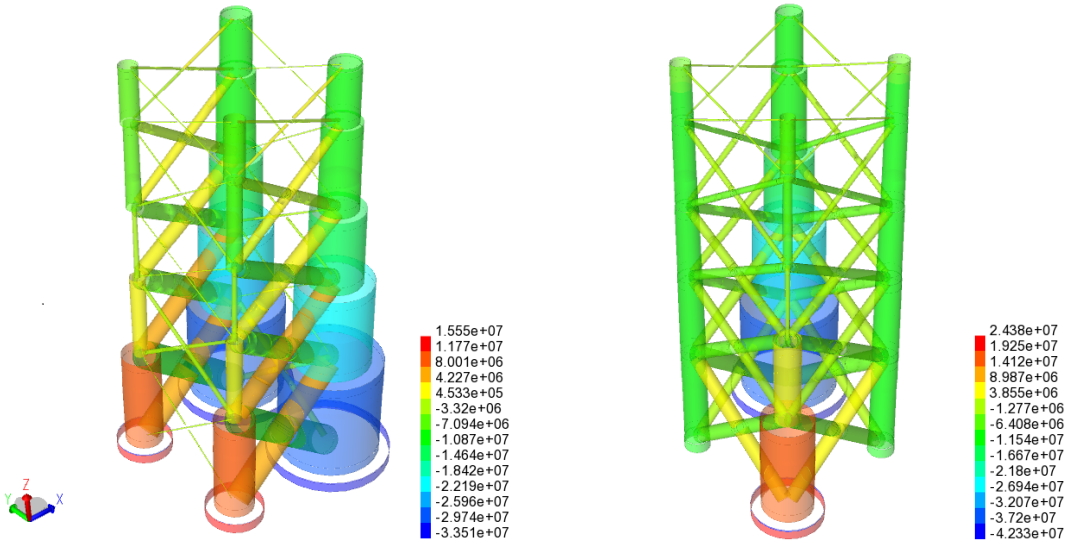

(a) T16H22D0Sh (b) T16H22D45Sh

Figure C.6: Extreme wind conditions.

C.4 Axial Forces Skew Jacket

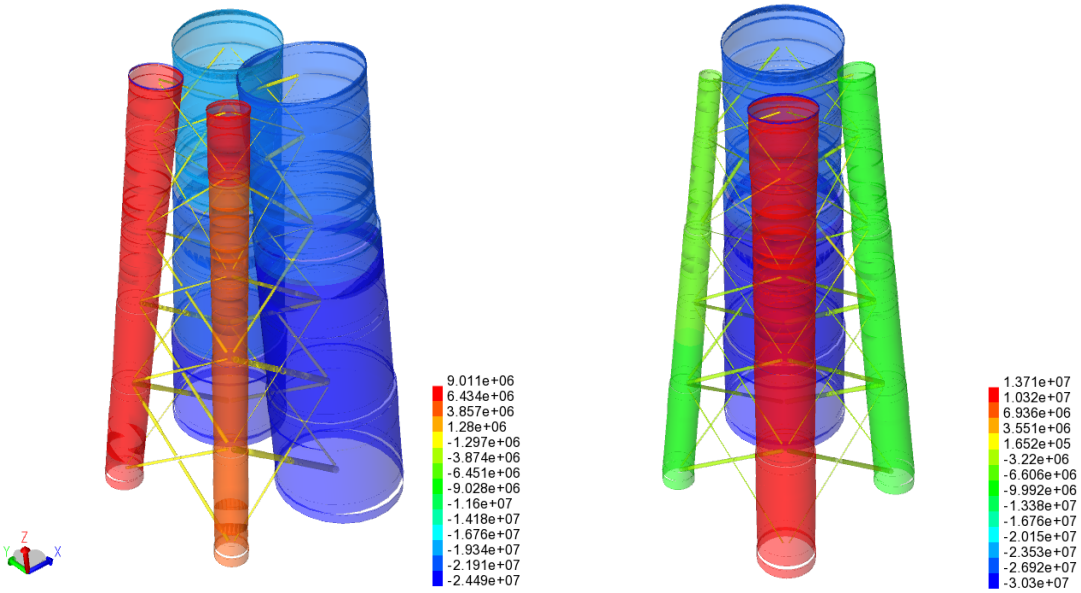

(a) T7.5H7D0Sh (b) T7.5H7D45Sh

Figure C.7: Rated wind conditions.

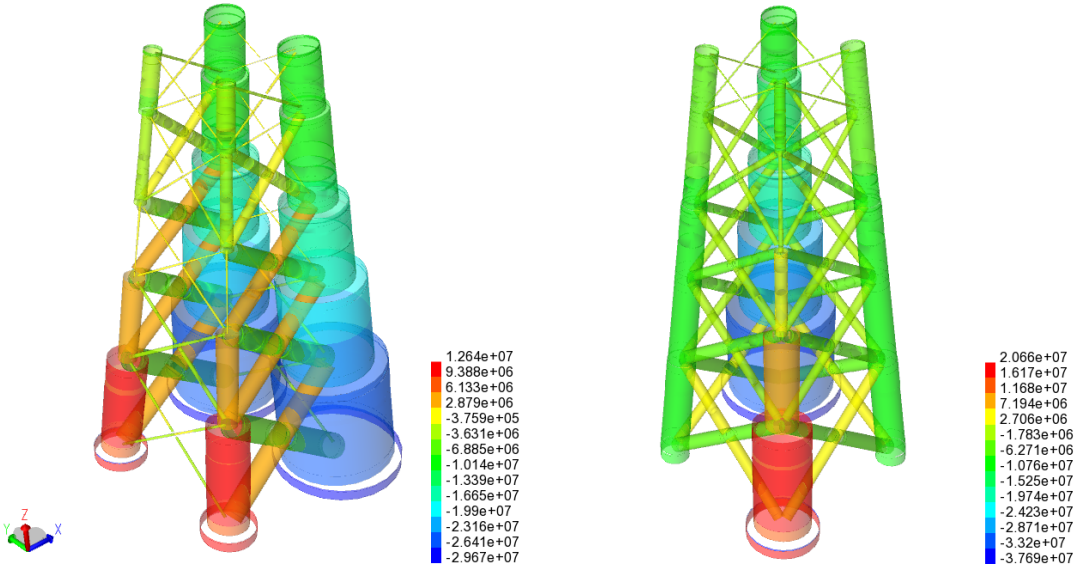

(a) T16H22D0Sh (b) T16H22D45Sh

Figure C.8: Extreme wind conditions.

D | Dogger Bank Site Statistics

Dogger Bank is an offshore site in the North Sea located off the North East coast of England and South West of Southern North Sea II. The site is currently used for the production of offshore wind energy. The report "Joint Probability Distribution of Environmental Conditions for Design of Offshore Wind Turbines" [26] provides probability distributions based on hindcast data measurements for the parameters defining sea states in the area.

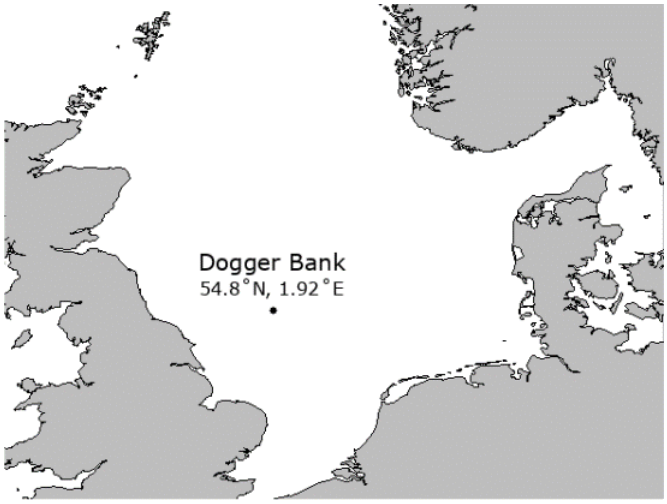

Figure D.1: Dogger Bank location.

D.1 Marginal Distributions

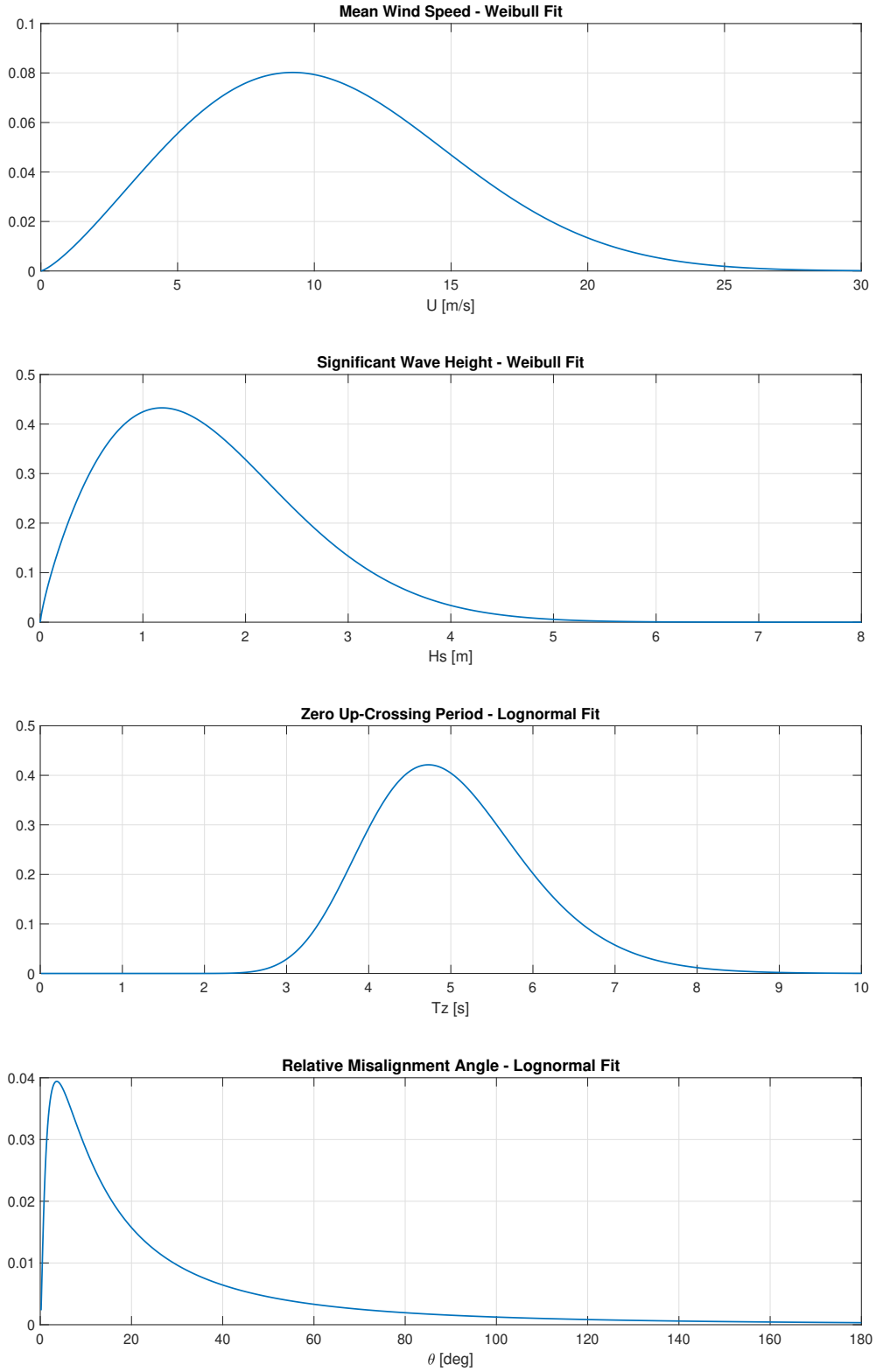

Figure D.2: Marginal distributions for the sea state parameters at Dogger Bank.

D.2 Fatigue Load Combinations

The complete list of all 80 sea states used in the coupled jacket-turbine fatigue analysis. Combinations are sorted with decreasing probability of occurrence.

No.	Name	U	H_S	T_Z	Probability
1	U7H1T4.5	7	1	4.5	0.102870
2	U9H1T4.5	9	1	4.5	0.089741
3	U11H2T5	11	2	5	0.082233
4	U5H1T4.5	5	1	4.5	0.081469
5	U13H2T5	13	2	5	0.070586
6	U9H2T5	9	2	5	0.061089
7	U11H1T4.5	11	1	4.5	0.054690
8	U3H1T4.5	3	1	4.5	0.042772
9	U15H3T6	15	3	6	0.039825
10	U15H2T5	15	2	5	0.039471
11	U17H3T6	17	3	6	0.029900
12	U7H2T5	7	2	5	0.029762
13	U13H3T6	13	3	6	0.029760
14	U13H1T4.5	13	1	4.5	0.024002
15	U5H0.25T3.5	5	0.25	3.5	0.018044
16	U3H0.25T3.5	3	0.25	3.5	0.016682
17	U17H2T5	17	2	5	0.015228
18	U19H4T7	19	4	7	0.014490
19	U17H4T7	17	4	7	0.013799
20	U19H3T6	19	3	6	0.013702
21	U7H0.25T3.5	7	0.25	3.5	0.011863
22	U11H3T6	11	3	6	0.011824
23	U5H2T5	5	2	5	0.010519
24	U1H1T4.5	1	1	4.5	0.010139
25	U21H4T7	21	4	7	0.008043
26	U15H1T4.5	15	1	4.5	0.007930
27	U15H4T7	15	4	7	0.006086
28	U1H0.25T3.5	1	0.25	3.5	0.005782
29	U9H0.25T3.5	9	0.25	3.5	0.005390
30	U21H5T7.5	21	5	7.5	0.005250
31	U19H2T5	19	2	5	0.004336
32	U21H3T6	21	3	6	0.004235
33	U23H5T7.5	23	5	7.5	0.003545
34	U19H5T7.5	19	5	7.5	0.003517
35	U3H2T5	3	2	5	0.003197
36	U23H4T7	23	4	7	0.002707
37	U9H3T6	9	3	6	0.002506
38	U17H1T4.5	17	1	4.5	0.002053
39	U11H0.25T3.5	11	0.25	3.5	0.001810

40	U23H6T8.5	23	6	8.5	0.001572
41	U25H5T7.5	25	5	7.5	0.001296
42	U25H6T8.5	25	6	8.5	0.001274
43	U13H4T7	13	4	7	0.001092
44	U23H3T6	23	3	6	0.000965
45	U21H2T5	21	2	5	0.000963
46	U17H5T7.5	17	5	7.5	0.000872
47	U21H6T8.5	21	6	8.5	0.000748
48	U1H2T5	1	2	5	0.000684
49	U25H4T7	25	4	7	0.000626
50	U27H6T8.5	27	6	8.5	0.000500
51	U13H0.25T3.5	13	0.25	3.5	0.000469
52	U19H1T4.5	19	1	4.5	0.000429
53	U25H7T9.5	25	7	9.5	0.000417
54	U27H7T9.5	27	7	9.5	0.000394
55	U7H3T6	7	3	6	0.000335
56	U27H5T7.5	27	5	7.5	0.000302
57	U23H2T5	23	2	5	0.000173
58	U25H3T6	25	3	6	0.000172
59	U29H7T9.5	29	7	9.5	0.000162
60	U23H7T9.5	23	7	9.5	0.000146
61	U29H6T8.5	29	6	8.5	0.000116
62	U29H8T10	29	8	10	0.000109
63	U27H4T7	27	4	7	0.000109
64	U19H6T8.5	19	6	8.5	0.000104
65	U27H8T10	27	8	10	0.000103
66	U15H0.25T3.5	15	0.25	3.5	0.000096
67	U21H1T4.5	21	1	4.5	0.000073
68	U11H4T7	11	4	7	0.000073
69	U15H5T7.5	15	5	7.5	0.000063
70	U29H5T7.5	29	5	7.5	0.000051
71	U31H8T10	31	8	10	0.000046
72	U5H3T6	5	3	6	0.000045
73	U31H7T9.5	31	7	9.5	0.000037
74	U25H8T10	25	8	10	0.000028
75	U31H9T11	31	9	11	0.000028
76	U25H2T5	25	2	5	0.000025
77	U27H3T6	27	3	6	0.000025
78	U29H9T11	29	9	11	0.000025
79	U31H6T8.5	31	6	8.5	0.000018
80	U17H0.25T3.5	17	0.25	3.5	0.000016

Table D.1: All 80 sea states used in the fatigue analysis.

D.3 Matlab Script: 2-Parameter Distribution

The matlab-script that was used to generate the sea states for the fatigue analysis. The scripts makes sea states based on the joint probability function of the wind speed and the wave heights at Dogger Bank. It also adds the wave period as a linear function of wave height. The initialization of the struct datatype was done so that the output data from the script is on the same format as the sea state data in Sesam Wind Manager.

Listing D.1: 2-parameter distribution for combined wind and wave probabilities at Dogger Bank.

```
clc
clear all
close all

%% General
maxWind = 40; %Maximum wind speed
maxWave = 20; %Maximum wave height

numElemWind = 10000; %200 for plotting, 10 000 for simulation
numElemWave = 10000;

[Us, Hs] = meshgrid(linspace(0, maxWind, numElemWind), linspace
    (0, maxWave, numElemWave));

%% Marginal distribution for wind
f_U = wblpdf(Us, 11.8, 2.3); %Weibull

%% Conditional probability Hs|U
% Produces a matrix with a weibull distribution for each row,
    with Alpha/Beta values varying downwards


p_a_h = [0.7669, 0.01412, 1.823]; %Fitting-parameters for the
    distribution found in the report
p_b_h = [1.673, 0.1015, 1.173];

alpha_h = pow(Us, p_a_h(1), p_a_h(2), p_a_h(3)); %Alpha/beta
    exponential fit
beta_h = pow(Us, p_b_h(1), p_b_h(2), p_b_h(3));

```

```
27 f_Hs_U = wblpdf(Hs, alpha_h, beta_h); % Conditional probability
28
29 %% Joint probability Hs,U
30 f_HsU = f_U .* f_Hs_U;
31 vol = trapz(Hs(:,1), trapz(Us(1,:), f_HsU)); %Control that V ~ 1
32
33 %% Discretization
34 divWind = 0:2:40; %Binning: 0-2m/s to 1m/s, 2-4m/s to 3m/s..
       5,7,9,...40
35 divWave = [0 0.5:1:19.5 20]; %Binning: 0-0.5m to 0.25m, 0.5-1.5m
       to 1m...
36 stepsizeU = maxWind/numElemWind;
37 stepsizeHs = maxWave/numElemWave;
38
39 %% Load combinations
40 %Initializes a data struct on Sesam wind manager format
41 LC.Name = {}; %LC name
42 LC.DR = {}; %Direct results
43 LC.IF = {}; %Interface file
44 LC.tom1 = {};
45 LC.tom2 = {};
46 LC.tom3 = {};
47 LC.RotateINT = {}; %Rotate interface load
48 LC.zero1 = {};
49 LC.U = {}; %LC wind speed
50 LC.YAW = {}; %YAW
51 LC.thetaWind = {}; %Wind dir
52 LC.SS = {}; %Sea state
53 LC.WF = {}; %Wave file
54 LC.D = {}; %Depth
55 LC.thetaWave = {}; %Wave dir
56 LC.Hs = {}; %LC significant wave height
57 LC.T = {}; %LC period
58 LC.PEF = {}; %Peak enh. factor = 1
59 LC.WS = {}; %Wave seed = 1
60 LC.CPt = {}; %Constr peak t = 0
61 LC.CPH = {}; %Constr peak H = 0
62 LC.CPT = {}; %Constr peak T = 0
63 LC.ID = {}; %Curent id
```

```
64  LC.ones1 = {}; %=1
65  LC.ones2 = {}; %=1
66  LC.ones3 = {}; %=1
67  LC.zero2 = {}; %=0
68  LC.Start = {}; %
69  LC.Stop = {}; %
70  LC.P = {}; %LC probability
71
72  % Filling up the load combinations with U, H, T, p, .....
73  i = 1;
74  P = 0;
75  for h=1:1:(maxWave+1)
76      yLimits = divWave(h:h+1);
77      H = mean(yLimits);
78      T = H_to_T(H);
79
80      for u=1:1:(maxWind/2)
81          xLimits = divWind(u:u+1);
82          U = mean(xLimits);
83          p = Int3d(xLimits, yLimits, f_HsU, stepsizeU, stepsizeHs
                );
84
85          LC(i).Name = "U"+U+"H"+H+"T"+T;
86          LC(i).U = U;
87          LC(i).Hs = H;
88          LC(i).T = T;
89          LC(i).P = p;
90
91          LC(i).RotateINT = 0;
92          LC(i).YAW = 0;
93          LC(i).SS = "NSS";
94          LC(i).WF = 0;
95          LC(i).D = 0;
96          LC(i).PEF = 1; %Peak enh. factor = 1
97          LC(i).WS = 1; %Wave seed = 1
98          LC(i).CPt = 0; %Constr peak t = 0
99          LC(i).CPH = 0; %Constr peak H = 0
100         LC(i).CPT = 0; %Constr peak T = 0
101         LC(i).ID = 0; %Curent id
```

```
102         LC(i).ones1 = 1; %=1
103         LC(i).ones2 = 1; %=1
104         LC(i).ones3 = 1; %=1
105         LC(i).zero2 = 0; %=0
106         LC(i).Start = 20;
107         LC(i).Stop = 600;
108 
109         i = i + 1;
110         P = P + p; %Check that this value converges to 1
111     end
112 end
113 %% Functions
114 
115 % Exponential function
116 function res = expo(x, p)
117     res = p(1) + p(2) .* exp(p(3).*x.^(p(4)));
118 end
119 
120 % Power function
121 function res = pow(x, p1, p2, p3)
122     res = p1 + p2 * x .^p3;
123 end
124 
125 % Lognormal distribution
126 function y = lognormal(x, mu, sig)
127     pd = makedist('Lognormal',mu,sig);
128     y = pdf(pd, x);
129 end
130 
131 % Function that finds T given Hs
132 function T = H_to_T(H)
133     t = 0.8365*H + 3.4255;
134 
135     acc = 0.5; %Rounding to closest 0.5s
136     T = round(t/acc)*acc;
137 end
138 
139 % Function that discretizes and integrates the joint probability
140 function vol = Int3d(xLim, yLim, F, stepsizeX, stepsizeY)
```

```
141     xInterval = xLim(1):stepsizeX:(xLim(2)-stepsizeX);
142     yInterval = yLim(1):stepsizeY:(yLim(2)-stepsizeY);
143
144     a = xLim(1)/stepsizeX +1;
145     b = xLim(2)/stepsizeX;
146     c = yLim(1)/stepsizeY +1;
147     d = yLim(2)/stepsizeY;
148
149     F1 = F(c:d, a:b); % OBS : M(row (Y) , col (X)
150     I = cumtrapz(yInterval, cumtrapz(xInterval, F1, 2));
151     vol = I(end);
152     if vol < 10^(-200)
153         vol = 0;
154     end
155 end
```

D.4 Matlab Script: 4-Parameter Distribution

A Matlab script for obtaining discrete values of the 4-parameter joint probability density function for sea states at Dogger Bank in the North Sea, see 8.3 based on the findings from the article [26]. There was implemented a data-structure named LC containing all the information about each load case.

Listing D.2: Obtaining discrete values of the 4-parameter probability density function, bin-sizes are defined at the top.

```
clc
clear all

%%Choosing the bin-size for the 4 parameters

tetha = [1.25 3.75 6.25 8.75 24 39 54 84 114 144];
U = [0.5 1 1.5 2 2.5 4.5 5.5 6.5 7.5 8.5 9.5 10.5 11.5 12.5 13.5
    14.5 15.5 16.5 17.5 18.5 19.5 20.5 22.5 24.5 26.5 28.5 30.5
    32.5];
Hs = [0.25 0.5 0.75 1 1.5 2 2.5 3 3.5 4 4.5 5 5.5 6 6.5 7 7.5 8
    8.5 9 10 11 12 13];
Tz = [2 2.5 3 3.5 4 4.5 5 5.5 6 7.5 8 10 12 14 16];

%The length of each parameter vector after binning
l_tetha = length(tetha);
l_u = length(U);
l_h = length(Hs);
l_t = length(Tz);

%A vector for collecting the 4-parameter probability for each
    bin
allValues_noOrder = [];


%Conditional probability parameters alpha and beta from the
    report U|theta
p_a_u = [6.458 7.827 -0.001039 1.896];
p_b_u = [2.102 0.9565 -0.008868 1.291];

% Conditional probability parameters alpha and beta from the
```

```
    report  Hs|U
26
27 p_a_h = [0.7669, 0.01412, 1.823];
28 p_b_h = [1.673, 0.1015, 1.173];
29
30
31 %% Conditional probability parameters mu and sigma from the
    report Tz|Hs
32
33 p_mu_t = [1.154 0.3389 0.5865];
34 p_sig_t = [0.07176 0.07477 -0.03705 4.347];
35
36
37 %% Load combinations
38 %Making a struct for gathering all the information for each load
    combination
39 LC.Name = {}; %LC name
40 LC.DR = {}; %Direct results
41 LC.IF = {}; %Interface file
42 LC.tom1 = {};
43 LC.tom2 = {};
44 LC.tom3 = {};
45 LC.RotateINT = {}; %Rotate int load
46 LC.zero1 = {};
47 LC.U = {}; %LC wind speed
48 LC.YAW = {}; %YAW
49 LC.thetaWind = {}; %Wind dir
50 LC.SS = {}; %Sea state
51 LC.WF = {}; %Wave file
52 LC.D = {}; %Depth
53 LC.thetaWave = {}; %Wave dir
54 LC.Hs = {}; %LC significant wave height
55 LC.T = {}; %LC period
56 LC.PEF = {}; %Peak enh. factor = 1
57 LC.WS = {}; %Wave seed = 1
58 LC.CPt = {}; %Constr peak t = 0
59 LC.CPH = {}; %Constr peak H = 0
60 LC.CPT = {}; %Constr peak T = 0
61 LC.ID = {}; %Curent id
```

```
62 LC.ones1 = {}; %=1
63 LC.ones2 = {}; %=1
64 LC.ones3 = {}; %=1
65 LC.zero2 = {}; %=0
66 LC.Start = {}; %
67 LC.Stop = {}; %
68 LC.P = {}; %LC probability
69
70 counterStruct = 1;
71
72 for i = 1:l_tetha % Counter for tetha
73     f_theta = lognormalValue(tetha(i), 2.878, 1.262);
74
75     for j = 1:l_u % Counter for U
76         alpha_u = expo(tetha(i), p_a_u);
77         beta_u = expo(tetha(i), p_b_u);
78         % Conditional f_u|tetha
79         f_U_theta = weibullValue(U(j), alpha_u, beta_u);
80
81         for k = 1:l_h % Counter for Hs
82             alpha_h = pow(U(j), p_a_h(1), p_a_h(2), p_a_h(3));
83             beta_h = pow(U(j), p_b_h(1), p_b_h(2), p_b_h(3));
84             % Conditional f_hs|u
85             f_Hs_U = weibullValue(Hs(k), alpha_h, beta_h);
86
87             for m = 1:l_t % Counter for Tz
88
89                 mu_t = pow(Hs(k), p_mu_t(1), p_mu_t(2), p_mu_t(3))
                        ;
90                 sig_t = expo(Hs(k), p_sig_t);
91                 % Conditional f_tz|hs
92                 f_Tz_Hs = lognormalValue(Tz(m), mu_t, sig_t);
93                 % The product for the 4-parameter distribution
                        according to
94                 % the report equation 14d
95                 prob = f_theta * f_U_theta * f_Hs_U * f_Tz_Hs;
96
97                 %Filling in info about each load combination in
                        the struct
```

```
98                  %for each loop
99                  LC(counterStruct).Name = "theta_"+tetha(i)+"_U_"+U
                        (j)+"_Hs_"+Hs(k)+"_T_"+Tz(m);
100                 LC(counterStruct).RotateINT = tetha(i);
101                 LC(counterStruct).U = U(j);
102                 LC(counterStruct).YAW = 0;
103                 LC(counterStruct).SS = "NSS";
104                 LC(counterStruct).WF = 0;
105                 LC(counterStruct).D = 0;
106                 LC(counterStruct).Hs = Hs(k);
107                 LC(counterStruct).T = Tz(m); %To obtain the real
                        period not the natural ln
108                 LC(counterStruct).PEF = 1; %Peak enh. factor = 1
109                 LC(counterStruct).WS = 1; %Wave seed = 1
110                 LC(counterStruct).CPt = 0; %Constr peak t = 0
111                 LC(counterStruct).CPH = 0; %Constr peak H = 0
112                 LC(counterStruct).CPT = 0; %Constr peak T = 0
113                 LC(counterStruct).ID = 0; %Curent id
114                 LC(counterStruct).ones1 = 1; %=1
115                 LC(counterStruct).ones2 = 1; %=1
116                 LC(counterStruct).ones3 = 1; %=1
117                 LC(counterStruct).zero2 = 0; %=0
118                 LC(counterStruct).Start = 20;
119                 LC(counterStruct).Stop = 600;
120                 LC(counterStruct).P = prob;
121
122                 counterStruct = counterStruct + 1;
123                 allValues_noOrder = [allValues_noOrder prob];
124             end
125         end
126
127     end
128 end
129
130 %Finding the normalizing constant to transform into natural
        probability
131 normFac = sum(allValues_noOrder);
132 %Normalizing the vector of probabilities
133 vecWithNormFac = allValues_noOrder ./ normFac;
```

```
134
135 %Normalizing all the probablities gathered in the struct(last
       data column)
136 for z = 1:length(allValues_noOrder)
137     LC(z).P = LC(z).P / normFac;
138 end
139
140 %%Functions
141 %Weibull probability for a given x
142 function res = weibullValue(x, a, b)
143
144 res = (b/a) * ((x/a)^(b-1)) * exp(-((x/a)^b));
145
146 end
147 %Lognormal probability fra given x
148 function res = lognormalValue(x, mu, sigma)
149     res = (1/(x*sigma*sqrt(2*pi))) * exp(-0.5*((log(x)-mu)^2) /
          (sigma^2));
150 end
151 %Exponential fit
152 function res = expo(x, p)
153     res = p(1) + p(2) * exp(p(3)*x^(p(4)));
154 end
155
156 %Power-law fit
157 function res = pow(x, p1, p2, p3)
158     res = p1 + p2 * x^p3;
159 end
```

E | Calibration of the Superelement

Two checks had to be performed to verify that the behaviour of the superelement closely resembled that of the original model.

E.1 Spatial Convergence

In the spatial convergence verification, the superelement displacements are compared to the original model displacements at certain timesteps, for a given load combination. For this verification, the load combination U7H1T4.5 was used, and the displacements were retrieved from the interface node.

Timestep [s]	Original Int. displacement [m]	Superelement Int. displacement [m]	Error [%]
100	0.00444363	0.00444363	0
300	0.00444365	0.00444365	0
600	0.00444617	0.00444617	0

(a) Straight jacket.

Timestep [s]	Original Int. displacement [m]	Superelement Int. displacement [m]	Error [%]
100	0.00371252	0.00371252	0
300	0.00371494	0.00371494	0
600	0.00371525	0.00371525	0

(b) Skew jacket.

Table E.1: Spatial convergence verification for the two jackets.

E.2 Spectral Convergence

The check for spectral convergence compares the eigenmodes of the superelement and the original model. With the chosen 50 calculated modes, the error was proven to be small in both jacket superelements for the majority of the modes.

Mode	Original Freq. [Hz]	Superelement Freq. [Hz]	Error [%]
1	1.567542	1.567754	-0.01
2	1.568088	1.568297	-0.01
3	3.038907	3.03968	-0.03
4	3.755026	3.747732	0.19
5	4.320448	4.311182	0.21
6	4.322495	4.313376	0.21
7	5.146894	5.11788	0.56
8	5.261095	5.258398	0.05
9	5.848265	5.817276	0.53
10	5.86582	5.83455	0.53
11	5.973373	5.951899	0.36
12	6.220122	6.170346	0.80
13	6.303847	6.303438	0.01
14	6.329461	6.328467	0.02
15	6.519493	6.544435	-0.38
16	6.714879	6.698031	0.25
17	6.71851	6.701925	0.25
18	6.983161	7.058606	-1.08
19	7.1178	7.117636	0.00
20	7.405253	7.407176	-0.03
21	7.839381	7.841881	-0.03
22	7.84142	7.843897	-0.03
23	8.265229	8.283474	-0.22
24	8.623356	8.623654	0.00
25	9.077267	9.066527	0.12
26	9.867277	9.860426	0.07
27	9.879753	9.872863	0.07
28	9.978332	9.97835	0.00
29	10.13549	10.14303	-0.07
30	10.43419	10.4313	0.03
31	10.46132	10.45836	0.03
32	10.6951	10.69564	-0.01
33	10.75954	10.78754	-0.26
34	11.11062	11.10112	0.09
35	11.11413	11.10493	0.08
36	11.30175	11.32076	-0.17
37	11.30957	11.32892	-0.17
38	11.5599	11.53517	0.21
39	11.58042	11.55779	0.20
40	11.79899	11.79442	0.04
41	11.95079	11.95099	0.00
42	12.93154	12.95421	-0.18
43	12.94328	12.9659	-0.17
44	12.97833	13.04184	-0.49
45	13.21949	13.23315	-0.10
46	13.23865	13.25237	-0.10
47	13.63341	13.67702	-0.32
48	13.69138	14.42099	-5.33
49	14.44595	14.44299	0.02
50	14.94754	14.94696	0.00

(a) Straight jacket.

Mode	Original Freq. [Hz]	Superelement Freq. [Hz]	Error [%]
1	1.865759	1.866456	-0.04
2	1.865864	1.866564	-0.04
3	3.923665	3.924619	-0.02
4	3.982199	3.982199	0.00
5	4.342918	4.345059	-0.05
6	4.345047	4.347187	-0.05
7	5.026462	5.026462	0.00
8	5.327411	5.327411	0.00
9	5.720952	5.721932	-0.02
10	5.730862	5.733309	-0.04
11	5.736748	5.739234	-0.04
12	6.575237	6.577308	-0.03
13	6.579494	6.58158	-0.03
14	6.771224	6.771225	0.00
15	6.960669	6.965816	-0.07
16	7.315699	7.450143	-1.84
17	7.946281	7.947601	-0.02
18	7.949939	7.95125	-0.02
19	8.653656	8.665761	-0.14
20	9.057602	9.058508	-0.01
21	9.165611	9.165611	0.00
22	9.479826	9.479833	0.00
23	9.984908	9.988562	-0.04
24	9.988683	9.992059	-0.03
25	10.166370	10.16671	0.00
26	10.248730	10.26343	-0.14
27	10.252700	10.26729	-0.14
28	10.923060	10.92333	0.00
29	10.928150	10.92824	0.00
30	10.985530	10.98555	0.00
31	11.127200	11.15654	-0.26
32	11.145830	11.16506	-0.17
33	11.162070	11.16736	-0.05
34	11.163220	11.17232	-0.08
35	11.237660	11.23785	0.00
36	11.820960	11.82097	0.00
37	12.418620	12.47932	-0.49
38	13.096060	13.11123	-0.12
39	13.110460	13.12562	-0.12
40	13.461470	13.46506	-0.03
41	13.474550	13.47804	-0.03
42	13.751630	13.75914	-0.05
43	14.211970	14.29681	-0.60
44	14.411080	14.70198	-2.02
45	14.701870	14.89868	-1.34
46	14.895420	14.92334	-0.19
47	14.919940	15.06927	-1.00
48	15.069180	15.31022	-1.60
49	15.767650	15.76771	0.00
50	15.915330	15.9155	0.00

(b) Skew jacket.

Table E.2: Spectral convergence verification of the two jackets.

F | Code Check FLS

The framework input file used for code checking in the FLS is primarily based on the input file from the Sesam Wind Manager tutorial: *"Time History Fatigue Analysis of a Jacket using a Superelement approach"* made by DNV.

```
% --- Read concepts and split at joints, to make sure all beam segments
%     are available individually and butt welds can be checked.
%     ================================================================
%
 DEFINE READ-CONCEPTS ON
 DEFINE BEAM-SPLIT STRUCTURE ALL-JOINTS
 DEFINE BEAM-SPLIT SECTION PIPE-ONLY


% --- Set defaults before loading structure and loads
%     ==============================================
%
 DEFINE FATIGUE-CONSTANTS DEFAULT-SN-CURVE DNV2010_F3
 DEFINE FATIGUE-CONSTANTS DEFAULT-FATIGUE-SAFETY-FACTOR 3.0
 DEFINE FATIGUE-CONSTANTS BUTTWELD-CONE-SCF-FORMULA DNVGL-RPC203-2014


% --- Open file and transfer SIN file data to Framework
%     ================================================
%
 FILE OPEN SIN-DIRECT-ACCESS #PREFIX# R#NUMBER#
 FILE TRANSFER 1 OWT #LCNAME# None


% --- Specify splash zone limits
%     =========================
```

```
%
 DEFINE FATIGUE-CONSTANTS SPLASH-ZONE-UPPER-LIMIT-ELEVATION 9.08
 DEFINE FATIGUE-CONSTANTS SPLASH-ZONE-LOWER-LIMIT-ELEVATION -3.36


% --- Assign additional SN-curves halfway legs
%     ============================================================
 SELECT MEMBERS ONLY SET LEGS

 ASSIGN POSITIONS ( ) FATIGUE-CHECK RELATIVE ( ONLY
    CHORD-SIDE     0.0
    BRACE-SIDE     0.0
    MID            0.5
    BRACE-SIDE     1.0
    CHORD-SIDE     1.0 )

 ASSIGN SN-CURVE MEMBER CURRENT INDIVIDUAL
    DNV2010_D
    DNV2010_D
    DNV2010_B1
    DNV2010_D
    DNV2010_D


% --- Assign additional SN-curves to braces
%     ========================================================
 SELECT MEMBERS ONLY SET X_BRACE

 ASSIGN POSITIONS ( ) FATIGUE-CHECK RELATIVE ( ONLY
    CHORD-SIDE     0.0
    BRACE-SIDE     0.0
    MID            0.5
    BRACE-SIDE     1.0
    CHORD-SIDE     1.0 )

 ASSIGN SN-CURVE MEMBER CURRENT INDIVIDUAL
    DNV2010_D
    DNV2010_D
    DNV2010_B1
```

```
    DNV2010_D
    DNV2010_D


% --- Assign SN-curve to tubular joints
%     ================================
 SELECT JOINTS ONLY SET JT_ALL
 ASSIGN SN-CURVE JOINT ALL CURRENT DNV2010_T


% --- Minimum (parametric) SCF values
%     ==============================
%
 DEFINE FATIGUE-CONSTANTS AXIAL-MINIMUM-SCF 1.5
 DEFINE FATIGUE-CONSTANTS IN-PLANE-MINIMUM-SCF 1.5
 DEFINE FATIGUE-CONSTANTS OUT-OF-PLANE-MINIMUM 1.5


% --- Joint data and SCFs
%     ==================
%
% --- Use loadpath to assign joint type to all joints
 SELECT JOINTS ONLY ALL
 ASSIGN JOINT-TYPE ALL ( ) LOADPATH
% --- Assign gap by automatic feature
 ASSIGN JOINT-GAP ALL ( ) AUTOMATIC
% --- Assign parametric SCFs
 ASSIGN SCF JOINT ALL ( ) None PARAMETRIC EFTHYMIOU


% --- Design Fatigue Factor (DFF)
%     ==========================
%
 DEFINE FATIGUE-SAFETY-FACTOR ON
%
% --- DFF=3
 SELECT MEMBERS ONLY ALL
 ASSIGN FATIGUE-SAFETY-FACTOR MEMBER CURRENT 3.0
```

```
% --- Verify assigned fatigue check data
%     ==================================
%
 SELECT MEMBERS ONLY SET LEGS
 SELECT MEMBERS INCLUDE SET X_BRACE
 SELECT JOINTS ONLY SET JT_ALL
 SET PRINT DESTINATION FILE
 SET PRINT PAGE-ORIENTATION LANDSCAPE
 SET PRINT PAGE-HEIGHT 6000
 SET PRINT FILE '' FatigueCheckData_Members
 PRINT MEMBER FATIGUE-CHECK-DATA ( )
 SET PRINT FILE '' FatigueCheckData_Joints
 PRINT JOINT PARAMETRIC-SCF ( )


% --- Define print of fatigue results to SIN file
%     ===========================================
 DEFINE FATIGUE-DAMAGE-TO-FILE ON #PREFIX# F#NUMBER#
    SIN-DIRECT-ACCESS


% --- Run fatigue analysis
%     ====================
%
 DEFINE TIME-HISTORY-FATIGUE-TIME UNIT-TIME #FATIGUESTART# #FATIGUEEND# 1 0.0
 RUN FATIGUE-CHECK SINFAT None ALL ( )
 DEFINE FATIGUE-SAFETY-FACTOR ON
```

G | NORSOK N-004: Design Codes

6.3.8.2 Axial compression and bending

Tubular members subjected to combined axial compression and bending should be designed to satisfy the following condition accounting for possible variations in cross-section, axial load and bending moment according to appropriate engineering principles:

$$\frac{N_{Sd}}{N_{c,Rd}} + \frac{1}{M_{Rd}} \left\{ \left[\frac{C_{my} M_{y,Sd}}{1 - \frac{N_{Sd}}{N_{Ey}}} \right]^2 + \left[\frac{C_{mz} M_{z,Sd}}{1 - \frac{N_{Sd}}{N_{Ez}}} \right]^2 \right\}^{0.5} \leq 1.0 \qquad \textbf{(6.27)}$$

Figure G.1

6.3.9.2 Axial compression, bending, and hydrostatic pressure

Tubular members subjected to combined compression, bending, and hydrostatic pressure should be proportioned to satisfy the following requirements at all cross sections along their length.

Method B ($\sigma_{ac,Sd}$ is in compression)

(a) for $\sigma_{ac,Sd} > \sigma_{q,Sd}$

$$\frac{\sigma_{ac,Sd} - \sigma_{q,Sd}}{f_{ch,Rd}} + \frac{1}{f_{mh,Rd}} \left[\left(\frac{C_{my} \sigma_{my,Sd}}{1 - \frac{\sigma_{ac,Sd} - \sigma_{q,Sd}}{f_{Ey}}} \right)^2 + \left(\frac{C_{mz} \sigma_{mz,Sd}}{1 - \frac{\sigma_{ac,Sd} - \sigma_{q,Sd}}{f_{Ez}}} \right)^2 \right]^{0.5} \leq 1.0 \qquad \textbf{(6.50)}$$

Figure G.2

6.4.3.6 Strength check

Joint resistance shall satisfy the following interaction equation for axial force and/or bending moments in the brace:

$$\frac{N_{Sd}}{N_{Rd}} + \left(\frac{M_{y,Sd}}{M_{y,Rd}} \right)^2 + \frac{M_{z,Sd}}{M_{z,Rd}} \leq 1 \qquad \textbf{(6.57)}$$

where

N_{Sd} = design axial force in the brace member
N_{Rd} = the joint design axial resistance
$M_{y,Sd}$ = design in-plane bending moment in the brace member
$M_{z,Sd}$ = design out-of-plane bending moment in the brace member
$M_{y,Rd}$ = design in-plane bending resistance
$M_{z,Rd}$ = design out-of-plane bending resistance

Figure G.3

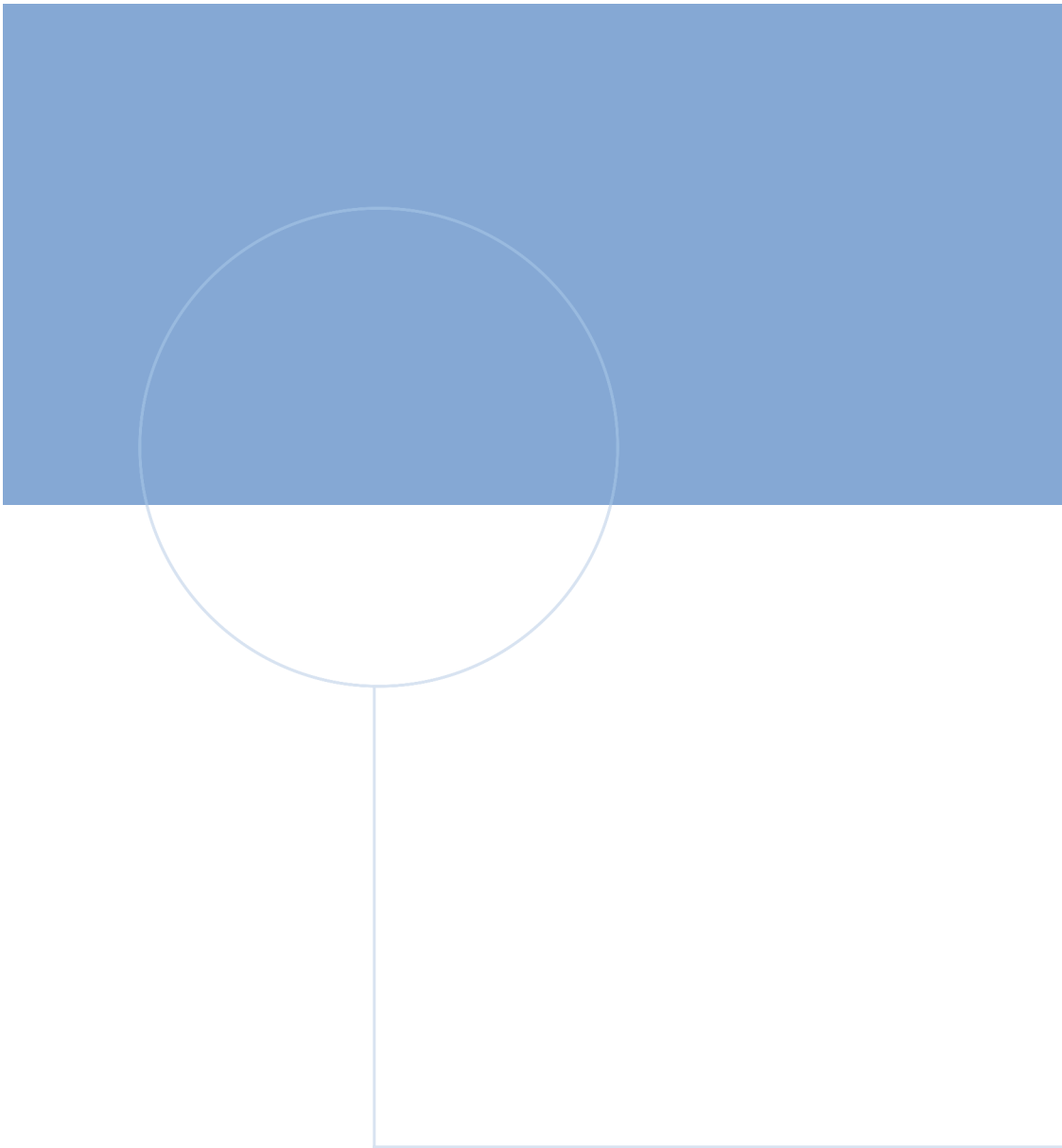

NTNU

Norwegian University of
Science and Technology